Научном већу Института за физику у Београду

Београд, 11. децембар 2020. године.

Предмет: Молба за покретање поступка за избор у звање научни сарадник
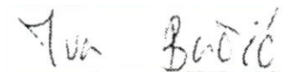
МОЛБА

Имајући у виду да испуњавам критеријуме прописане од стране Министарства просвете, науке и технолошког развоја за избор у звање научни сарадник, молим Научно веће Института за физику у Београду да покрене поступак за мој избор у звање научни сарадник.

У прилогу достављам:

1. мишљење руководиоца лабораторије са предлогом комисије за избор у звање;
2. стручну биографију;
3. преглед научне активности;
4. елементе за квалитативну и квантитативну оцену научног доприноса са доказима;
5. списак и копије објављених радова и других публикација;
6. податке о цитираности;
7. уверење о одбрањеној докторској дисертацији.

С поштовањем,

_____

Ива Бачић

Научном већу Института за физику у Београду

Предмет: Мишљење руководиоца лабораторије о избору др Иве Бачић у звање научни сарадник

Др Ива Бачић је запослена у Лабораторији за примену рачунара у науци, у оквиру Националног центра изузетних вредности за изучавање комплексних система Института за физику у Београду. У истраживачком раду се бави физиком нелинеарних динамичких система и стохастичких процеса. С обзиром да испуњава све предвиђене услове у складу са Правилником о поступку, начину вредновања и квантитативном исказивању научноистраживачких резултата истраживача МПНТР, сагласан сам са покретањем поступка за избор др Иве Бачић у звање научни сарадник.

За састав комисије за избор др Иве Бачић у звање научни сарадник предлажем:

(1) др Игор Франовић, виши научни сарадник, Институт за физику у Београду,
(2) др Антун Балаж, научни саветник, Институт за физику у Београду,
(3) проф. др Милан Кнежевић, редовни професор Физичког факултета Универзитета у Београду у пензији.

др Антун Балаж
научни саветник
руководилац Лабораторије за
примену рачунара у науци

СТРУЧНА БИОГРАФИЈА

Др Ива Бачић рођена је у Суботици 12. јуна 1992. године, где је завршила природни смер Гимназије „Светозар Марковић“. Након тога, уписала је 2010. године основне академске студије на Физичком факултету Универзитета у Београду, смер Теоријска и експериментална физика, где је дипломирала 2014. године са просечном оценом 9.44/10. Исте године је уписала мастер академске студије на Физичком факултету, смер Теоријска и експериментална физика, које је завршила 2015. године са просечном оценом 9.67/10. У току мастер студија, Ива је посетила синхротрон SOLEIL у Француској, у склопу израде мастер рада на тему *Inner-Shell Action Spectroscopy of Trapped Substance P Peptide Ions and their Nanosolvated Complexes* под менторством др Александра Милосављевића, научног саветника Института за физику у Београду. Новембра 2015. године уписала је докторске академске студије на Физичком факултету, ужа научна област Физика кондензоване материје и статистичка физика. Под менторством др Игора Франовића, вишег научног сарадника из Лабораторије за примену рачунара у науци (Scientific Computing Laboratory) Института за физику у Београду, Ива се у склопу докторских академских студија бавила коефектима шума и вишеструких временских скала у системима спрегнутих ексцитабилних јединица, одбранивши дисертацију под називом *Self-organization in Coupled Excitable Systems: Interplay Between Multiple Timescale Dynamics and Noise* новембра 2020. године.

Од марта 2016. године, Ива је запослена на Институту за физику у Београду у Лабораторији за примену рачунара у науци. Била је ангажована на пројекту основних истраживања ОН171017 *Моделирање и нумеричке симулације сложених вишечестичних система* Министарства просвете, науке и технолошког развоја Републике Србије, а поред тога је учествовала и на DAAD билатералном пројекту између Републике Србије и СР Немачке *Emergent dynamics in systems of coupled excitable units* 2017. и 2018. године. Октобра 2020. годние започела је постдокторско усавршавање при Централно-Европском Универзитету у Будимпешти, Мађарска, где учествује на ERC Synergy пројекту *Dynamics and Structure of Networks (DYNASNET)* посвећеном повезивању теорије графова и комплексних мрежа, под руководством др Алберта-Ласла Барабашија и др Мартона Пошфаија.

Др Бачић је до сада је објавила шест научних радова и неколико саопштења са међународних скупова штампана у изводу. Њен рад *Disordered configurations of the Glauber model in two-dimensional networks*, објављен у часопису *EPL (Europhysics Letters)*, истакнут је у *Research Highlights* за 2018. годину и представљен на *Europhysics News*. Своје резултате је до сада представила на више међународних конференција, и била је учесница неколико школа за усавршање младих научника. Др Бачић је руководила двама

средњошколским пројектима семинара физике у Истраживачкој станици Петница, представљеним на конференцијама „Корак у науку" 2019. и 2020. годние.

Поред матерњег, Ива говори два светска језика, енглески и немачки.

ПРЕГЛЕД НАУЧНЕ АКТИВНОСТИ

Током мастер студија, Ива се бавила интеракцијом синхротронског зрачења са наносолватисаним молекулима. Под руководством др Александра Милосављевића, научног саветника из Лабораторије за физику сударних процеса Института за физику, на синхротрону SOLEIL у Француској, користећи тандем масену X-ray спектрометрију биополимера у јонској замци, испитивала је ефекте наносолватације на акционе спектре и фрагментацију. Уочена су два различита резонантна процеса која доводе до појачаног губитка воде са наносолватисаних молекула неуропептида *Substance P*, повезана са ексцитацијом К-љуске кисеоникових атома који припадају или пептидној вези или кластеру молекула воде. Разматрање процеса фрагментације пептида као функције активационе енергије фотона у близини C, N и O К-ивице показало је да фрагментација има јаку зависност од активационе енергије.

У склопу докторских студија, под руководством др Игора Франовића, вишег научног сарадника из Лабораторије за примену рачунара у науци Института за физику, др Бачић се бавила емергентним феноменима у спрегнутим системима, насталим услед садејства шума, динамике на вишеструким временским скалама и локалне ексцитабилности. Ексцитабилност је заједничка карактеристика великог броја разнородних система, укључујући биолошке системе (неурони, ћелије миокарда, бета ћелије панкреаса, генске регулаторне мреже), моделе хемијске кинетике, ласере, моделе социјалних интеракција, климатске динамике, земљотреса и др. Са аспекта теорије нелинеарних динамичких система, особина ексцитабилности је заснована на чињеници да се систем налази у близини бифуркације између стационарног и осцилаторног режима. Манифестујући богато колективно понашање, укључујући низ феномена синхронизације и парцијалне синхронизације, патерне, таласе ексцитације, просторно локализована решења и др, системи интерагујућих ексцитабилних јединица издвојени су у посебну класу динамичких система.

Комплексна динамика у ексцитабилним системима често укључује више карактеристичних временских скала на нивоу појединачних јединица (тзв. *slow-fast* динамика) и/или услед интеракција. Један од најважнијих примера где динамика интеракција укључује вишеструке временске скале односи се на концепт адаптивности, који подразумева коеволуцију локалне динамике и динамике интеракција. При том, динамика веза (јачина интеракција, промена броја линкова) одвија се на споријој карактеристичној скали у односу на локалну динамику јединица. Међу најважнијим

примерима система са адаптивношћу истичу се неуронски системи, где се у оквиру пластичности синапси, јачина синаптичких веза повећава или смањује у складу са релативним временима опаљивања пре- и пост-синаптичког неурона.

Модели система спрегнутих екситабилних јединица типично укључују деловање шума, који потиче од интринзичних флуктуација, флуктуација у окружењу или од *coarse-grained* динамике на нижим просторним и временским скалама. Неки од извора шума у екситабилних системима укључују *quasi-random* ослобађање неуротрансмитера у неуронима или *finite-size* ефекте у хемијским реакцијама. Екситабилни системи, као изразито неравнотежни системи, показују изузетну осетљивост на пертурбације, па тако и на деловање шума. Познато је да шум у системима који се налазе у близини бифуркационог прага може да индукује тзв. резонантне феномене, који подразумевају нелинеаран одговор система на шум, као последицу тога што шум уводи нову временску скалу у систем. У случају класичних екситабилних система, добро је познат феномен резонанце кохеренције, где осцилације изазване шумом постају најрегуларније на интермедијарном интензитету шума. У случају осцилаторних система у близини бифуркације, релативно недавно уочен је феномен инверзне стохастичке резонанце, где фреквенција осцилација пертурбованих шумом има минимум на интермедијарном интензитету шума. Експериментално је потврђено да овај феномен игра значајну улогу у неуронским системима, укључујући редуковање фреквенције опаљивања у одсуству неуромодулатора, сузбијање патолошки дуге краткорочне меморије, изазивање и супресију тоничног опаљивања као и оптимизацију преноса информација.

У светлу наведеног, најважнији допринос Ивине докторске дисертације под називом *Self-organization in Coupled Excitable Systems: Interplay Between Multiple Timescale Dynamics and Noise* (Самоорганизација у спрегнутим екситабилним системима: садејство вишеструких временских скала и шума) је анализа карактеристика екситабилног понашања интерагујућих система, за разлику од класичног концепта екситабилности који се односи на појединачне јединице. У оквиру ових истраживања, др Бачић је проучавала три групе емергентних феномена у склопу комплементарних линија истраживања. Прва линија се односи на екситабилно понашање система спрегнутих екситабилних јединица. Поред испитивања екситабилног понашања мотива две адаптивно спрегнуте локално екситабилне јединице, испитан је и феномен макроскопске екситабилности, сценарија у којем се популација екситабилних јединица и сама понаша као екситабилни елемент. На примеру популације спрегнутих стохастичких неуронских мапа, развојем *mean-field* модела заснованог на гаусијанској апроксимацији, анализиране су карактеристике режима макроскопске екситабилности, као и других режима колективне динамике. Показано је да постоји висок степен квалитативне и квантитативне усаглашености између предвиђања *mean-field* модела и динамике реалног система у погледу карактеризације макроскопске екситабилности, стохастичких бифуркација, кривих фазног одговора макроскопских варијабли на пертурбацију, као и статистичких особина временских серија. У склопу

друге линије истраживања, која се односи на мотиве адаптивно спрегнутих ексцитабилних јединица, испитан је стохастички процес *switching* динамике у два система. *Switching* динамика подразумева споре стохастичке флуктуације између метастабилних стања изведених из коегзистентних атрактора одговарајућег детерминистичког система, или споре флуктуације између осцилаторних мода изазваних шумом. У систему две адаптивно купловане ексцитабилне јединице, откривене су две генеричке форме *switching* динамике, које зависе од брзине адаптације, и чија феноменологија је објашњена применом теорије сингуларних пертурбација. Поред тога, при разматрању стохастичке ексцитабилне јединице са споро адаптирајућом повратном спрегом, откривено је да се услед садејства спреге и шума може јавити, између осталог, динамички режим стохастичког бурстовања (*bursting*). При испитивању *multiscale* понашања овог система, развијен је нови метод стохастичког усредњавања (*stochastic averaging*), где је динамика споре варијабле, у оквиру тзв. *reduced* проблема, одређена коришћењем стационарних решења Фокер-Планкове једначине брзог подсистема. Трећа линија истраживања је посвећена испитивању резонантних феномена на мотивима спрегнутих ексцитабилних система. Ратматрајући парадигматски модел где је локална динамика представљена активним ротатором, представљена су два нова генеричка сценарија за феномен инверзне стохастичке резонанце. Такође је показано да споро адаптирајућа повратна спрега омогућава ефикасну контролу феномена резонанце кохеренције.

Поред наведеног испитивања емергентних феномена у спрегнутим ексцитабилним системима, др Бачић се у току докторских студија бавила и процесом уређивања кинетичког Изинговог (Глауберовог) модела на комплексним мрежама, као и анализом структуре неуређених конфигурација. Разматрани су случајеви регуларне топологије повезаности, мрежа са случајном и *small-world* топологијом добијене преповезивањем регуларне решетке, као и *multilayer* мрежа с различитом структуром повезаности између слојева. Експлицитно је показано да *small-world* топологија у термодинамичком лимесу онемогућава уређивање, при чему се неуређене конфигурације састоје од два домена који одговарају мулти-кластер структурама на почетној регуларној решетци.

Резултати ових истраживања су до сад објављени у 2 рада у часопису категорије М21а, 3 рада у часописима категорије М21 и 1 раду категорије М22, и представљени су на три међународне конференције.

ЕЛЕМЕНТИ ЗА КВАЛИТАТИВНУ ОЦЕНУ НАУЧНОГ ДОПРИНОСА

1. Квалитет научних резултата

1.1. Значај научних резултата

Др Ива Бачић се у току досадашњег рада бавила истраживањем самоорганизације у спрегнутим ексцитабилним системима са динамиком на вишеструктим временским скалама под утицајем шума, као и испитивањем зависности процеса уређивања Изинг-Глауберовог модела од структуре комплексних мрежа.

Резултати добијени истраживањем прве теме укључени су у докторску дисертацију др Бачић, при чему се корпус истражених феномена може поделити у три комплементарне линије истраживања. У склопу прве линије истраживања, концепт ексцитабилности, који је досад истраживан у случају појединачних ексцитабилних јединица, је проширен на системе спрегнутих ексцитабилних јединица, при чему је разматрана ексцитабилност мотива две спрегнуте локално ексцитабилне јединице, као и популације ексцитабилних јединица, уводећи концепт макроскопске ексцитабилности. Друга линија истраживања се тиче *switching* (алтернирајуће) динамике изазване садејством шума и вишеструких карактеристичних временских скала, и садржи анализу две врсте такве динамике, наиме спорих стохастичких флуктуација и стохастичког бурстовања (*bursting*). Трећа линија истраживања је посвећена резонантним феноменима у спрегнутим системима са локалном динамиком близу бифуркационог прага, при чему су идентификована два нова генеричка сценарија за појаву феномена инверзне стохастичке резонанце, као и нови метод контроле резонанце кохеренције. Поред наведених концептуалних доприноса, главни методолошки доприноси ових истраживања укључују проширење теорије средњег поља на стохастичке дискретне системе, екстензију теорије сингуларних пертурбација на стохастичке системе (стохастичко усредњавање), каои екстензију теорије фазног одговора на спрегнуте системе.

У склопу друге теме, експлицитно је показано да *small-world* топологија у термодинамичком лимесу онемогућава уређивање Изинг-Глауберовог модела, при чему се резултујуће неуређене конфигурације састоје од два домена, који на почетној регуларној решетци одговарају мулти-кластер структури.

1.2. Параметри квалитета часописа

Кандидаткиња др Ива Бачић је у свом досадашњем раду објавила 6 радова у међународним часописима са ISI листе, од којих је:

2 рада у категорији М21а (међународни часописи изузетних вредности):

Chaos [ISSN: 1054–1500, IF2019: 2.983, SNIP2018: 1.17],

3 рада у категорији М21 (врхунски међународни часописи),

Physical Review E [ISSN: 1539-3755, IF2016: 2.366, SNIP2015: 2.18],

EPL [ISSN: 0295-5075, IF2015: 1.963, SNIP2014: 0.97],

1 рад у категорији М22 (истакнути међународни часописи):

The European Physical Journal - Special Topics [ISSN: 1951-6355, IF2017:1.947, SNIP2015: 0.86].

Библиометријски показатељи дати су у следећој табели.

	IF	M	SNIP
Укупно	14.205	49	7.32
Усредњено по чланку	2.368	8.16	1.22
Усредњено по аутору	4.213	14.517	2.096

1. 3. Позитивна цитираност научних радова

Према подацима из базе *Web of Science*, радови др Бачић цитирани су укупно 13 пута, од чега 12 пута изузимајући аутоцитате, док је њен h-индекс 3.

1. 4. Међународна сарадња

Међународна активност др Иве Бачић обухвата:

- учешће у COST акцијама CM1204 (*XUV/X-ray light and fast ions for ultrafast chemistry (XLIC)*), 2015, и CA17120 (*Chemobrionics*), 2018 –
- учешће у српско-немачком DAAD билатералном пројекту *Emergent dynamics in systems of coupled excitable units,* 2016 – 2018
- учешће у ERC Synergy пројекту *Dynamics and Structure of Networks (DYNASNET)*, 2020 –

2. Нормирање броја коауторских радова, патената и техничких решења

Радови др Иве Бачић засновани су на аналитичким прорачунима и нумеричким симулацијама. Како сви радови имају пет или мање ко-аутора, рачунају се пуном тежином у односу на број коаутора.

3. Учешће у пројектима, потпројектима и пројектним задацима

Кандидаткиња је учествовала на следећим пројектима:

- ERC Synergy пројекат *Dynamics and Structure of Networks (DYNASNET)*, 2020 –

- пројекат основних истраживања ОН171017 *Моделирање и нумеричке симулације сложених вишечестичних система* Министарства просвете, науке и технолошког развоја Републике Србије, 2015 – 2020
- COST акција CA17120: *Chemobrionics*, 2018 –
- српско-немачки DAAD билатерални пројекат *Emergent dynamics in systems of coupled excitable units,* 2016 – 2018
- COST акција CM1204: *XUV/X-ray light and fast ions for ultrafast chemistry (XLIC)*, 2015

4. Активност у научним и научно-стручним друштвима

4. 1. Рецензије научних радова

Др Бачић је била рецезенткиња два рада у часопису *Chaos*.

4. 2. Организација научних скупова

Др Бачић је била у локалном организационом одбору конференције *COST XLIC WG2 Expert meeting on biomolecules*, одржане 2015. године на Фрушкој Гори, Србија.

5. Награде и признања за научни рад

Рад *Disordered configurations of the Glauber model in two-dimensional networks*, објављен у часопису *EPL (Europhysics Letters)*, истакнут је у *Research Highlights* тог часописа за 2018. годину и представљен на *Europhysics News*.

6. Развој услова за научни рад, образовање и формирање научних кадрова

6. 1. Кандидаткиња је стручна сарадница Семинара физике у Истраживачкој станици Петница

- одржала је у току претходне деценије низ предавања из математике и физике
- руководила је двама полазничким пројектима који су успешно завршени презентацијом полазница на годишњој петничкој конференцији „Корак у науку" и објављивањем у „Петничким свескама":
    1. *Карактеристике мреже познанства у популацији са израженим подгрупама* (2019), полазница: Исидора Мајкић, руководитељке: Александра Алорић и Ива Бачић
    2. *Испитивање Potts-овог модела на преповезаним решеткама* (2020), полазница: Нина Јаковљевић, руководитељка: Ива Бачић

7. Утицај научних резултата

Утицај научних резултата се огледа у броју цитата наведеном у тачки 4. 1. 3. овог прилога, као и прилогу о цитираности. Значај резултата је такође описан у тачки 4. 1.

8. Конкретан допринос кандидаткиње у реализацији радова у научним центрима у земљи и иностранству

Кандидаткиња је највећи део својих истраживачких делатности реализовала на Институту за физику у Београду. Поред тога, у склопу мастер рада је учествовала у мерењима на синхротрону *SOLEIL* у Француској, док је у склопу докторских студија провела око три месеца на институту *Weierstrass* (*WIAS*) у Берлину, Немачка. Допринос др Бачић се огледа у изради нумеричких симулација, добијању, интерпретацији и презентацији нумеричких резултата, као и писању радова.

ЕЛЕМЕНТИ ЗА КВАЛИТАТИВНУ ОЦЕНУ НАУЧНОГ ДОПРИНОСА

Остварени М-бодови по категоријама публикација

Категорија	М-бодова по публикацији	Број публикација	Укупно М-бодова (нормирано)
М21а	10	2	20 (20)
М21	8	3	24 (24)
М22	5	1	5 (5)
М34	0.5	3	1.5 (1.36)
М70	6	1	6 (6)

Поређење оствареног броја М-бодова са минималним условима потребним за избор у звање научног сарадника

	Потребно	Остварено (нормирано)
Укупно	16	56.5 (56.36)
М10+М20+М31+М32+М33+М41+М42	10	49
М11+М12+М21+М22+М23	6	49

Списак публикација

Радови објављени у међународним часописима изузетних вредности (категорија M21a):

1. **Вачић**, and I. Franović, Two Paradigmatic Scenarios for Inverse Stochastic Resonance, Chaos **30**, 033123 (2020) [ISSN: 1054–1500, IF2019: 2.983]
2. Franović, S. Yanchuk, S. R. Eydam, **I. Вачић**, and M. Wolfrum, *Dynamics of a Stochastic Excitable System with Slowly Adapting Feedback*, Chaos **30**, 083109 (2020) [ISSN: 1054–1500, IF2019: 2.983]

Радови објављени у врхунским међународним часописима (категорија M21):

1. **I. Вачић**, V. Klinshov, V. Nekorkin, M. Perc, and I. Franović, *Inverse stochastic resonance in a system of excitable active rotators with adaptive coupling*, Europhys. Lett. 124, 40004 (2018) [ISSN: 0295-5075, IF2015: 1.963]
2. I. Franović, O. V. Maslennikov, **I. Вачић**, and V. I. Nekorkin, *Mean-field dynamics of a population of stochastic map neurons*, Phys. Rev. E 96, 012226 (2017) [ISSN: 1539-3755, IF2016: 2.366]
3. **I. Вачић,** I. Franović, and M. Perc, *Disordered Confgurations of the Glauber Model in Two-dimensional Networks*, Europhys. Lett. 120, 68001 (2017) [ISSN: 0295-5075, IF2015: 1.963]

Радови објављени у истакнутим међународним часописима (категорија M22):

1. **I. Вачић**, S. Yanchuk, M. Wolfrum, and I. Franović, *Noise-induced switching in two adaptively coupled excitable systems*, Eur. Phys. J. - Spec. Top. 227, 1077 (2018) [ISSN: 1951-6355, IF2017: 1.947]

Саопштења са међународног скупа штампана у изводу (категорија M34):

1. **I. Вачић**, M. Lj. Ranković, F. Canon, V. Cerovski, C. Nicolas, A. Giuliani, and A. R. Milosavljević, *Gas-phase X-ray action spectroscopy of protonated nanosolvated substance P peptide around O K-edge,* WG2 Expert Meeting on Biomolecules, 27-30 April 2015, Fruška gora, Serbia.
2. **I. Вачић,** *Inverse stochastic resonance in a system of active rotators with adaptive coupling*, Dynamics of Coupled Oscillator Systems, 19-21 November 2018, WIAS Berlin, Germany.
3. **I. Вачић**, I. Franović, and M. Perc, *Disordered Configurations Of The Glauber Model On Two-Dimensional Networks*, The 20th Symposium on Condensed Matter Physics - SFKM 2019, 7-11 October 2019, Belgrade, Serbia.

Mean-field dynamics of a population of stochastic map neurons

Igor Franović,[1,*] Oleg V. Maslennikov,[2,†] Iva Bačić,[1] and Vladimir I. Nekorkin[2]

[1]*Scientific Computing Laboratory, Center for the Study of Complex Systems, Institute of Physics Belgrade,*
University of Belgrade, Pregrevica 118, 11080 Belgrade, Serbia
[2]*Institute of Applied Physics of the Russian Academy of Sciences, 46 Ulyanov Street, 603950 Nizhny Novgorod, Russia*

We analyze the emergent regimes and the stimulus-response relationship of a population of noisy map neurons by means of a mean-field model, derived within the framework of cumulant approach complemented by the Gaussian closure hypothesis. It is demonstrated that the mean-field model can qualitatively account for stability and bifurcations of the exact system, capturing all the generic forms of collective behavior, including macroscopic excitability, subthreshold oscillations, periodic or chaotic spiking, and chaotic bursting dynamics. Apart from qualitative analogies, we find a substantial quantitative agreement between the exact and the approximate system, as reflected in matching of the parameter domains admitting the different dynamical regimes, as well as the characteristic properties of the associated time series. The effective model is further shown to reproduce with sufficient accuracy the phase response curves of the exact system and the assembly's response to external stimulation of finite amplitude and duration.

I. INTRODUCTION

Gaining a comprehensive understanding of the emergent dynamics of neuronal populations and their interactions is a topical issue in neuroscience [1,2]. The acquired neurobiological data corroborate that the operational tasks at different levels of the brain's multiscale hierarchical organization are distributed across anatomically segregated, but functionally integrated, moduli [3–5]. Within theoretical studies, substantial attention have received the phenomena unfolding on the intermediate (mesoscopic) scale [6], whereby the considered models are supposed to reflect the behavior of assemblies comprising microcolumns or cortical columns [7–9]. The mesoscopic dynamics typically consists of oscillations of different frequencies and amplitudes, which may be interspersed by episodes of chaotic or pseudo-chaotic irregular behavior [7]. This can further be modulated via interplay with activity generated at other scales, primarily the stochastic fluctuations from the microscopic level and the slow rhythms derived from the macroscopic structures.

Conceptually, the given phenomena are often addressed by invoking a paradigm where each population exhibiting a collective mode is regarded as a large-scale oscillator, such that the assembly's response to external stimuli, noise, or collective oscillations from afferent populations may be examined using the methods of nonlinear dynamics [10]. The ensuing models of collective motion are developed using different forms of mean-field (MF) approximation, which mainly apply the bottom-up strategy [11] to build reduced and analytically tractable description of population behavior starting from the high-dimensional system of (stochastic) differential equations for the local neuron dynamics. An additional point that makes the mesoscopic circuits particularly suitable for the MF treatment is that the often used assumption on assembly homogeneity approximately holds at this scale

[12]. In terms of fashion by which the population dynamics is statistically characterized, one may classify the effective systems into neural mass or probability density models [8,13]. The former rely on the large coherence approximation and yield the mean-rate dynamics [14], whereas the latter involve the diffusion approximation, providing for the evolution of the assembly-averaged dynamics and the corresponding variance [15,16]. The MF approach and its generalization to spatially extended systems have become a standard tool for analyzing diverse problems in neuroscience and other fields [17–23].

Nevertheless, one should emphasize that the MF analysis has so far exclusively been applied to the class of continuous-time systems, while the effective models for assemblies of coupled maps have been lacking. In particular, the collective motion of spiking or bursting neurons influenced by noise has been extensively studied using different models of coupled discrete systems, such as Rulkov [24–31] or Izhikevich neuron maps [32,33], but this has not been complemented by an appropriate MF theory. The latter has likely been the consequence of inability to implement the Fokker-Planck formalism to discrete-time systems. In the present paper, we obtain for the first time the MF theory for a population of coupled stochastic neuronal maps. The derivation relies on Gaussian approximation, which is introduced within the framework of Gaussian closure hypothesis [34–40].

We apply the MF approach to systematically analyze the emergent behavior and the stimulus-response relationship of a population of stochastic map neurons, where the local dynamics can exhibit a variety of regimes, including excitability, subthreshold oscillations, regular and chaotic spiking or bursting, as well as mixed spiking-bursting oscillations [41–44]. The particular set of issues we address consists in establishing whether and how the MF model can be used to (i) qualitatively analyze the network stability and bifurcations of the exact system associated to emergence of generic collective regimes; (ii) provide adequate quantitative predictions in terms of bifurcation thresholds, and the average interspike intervals or bursting cycles of the exact system; as well as (iii) accurately anticipate the population's response
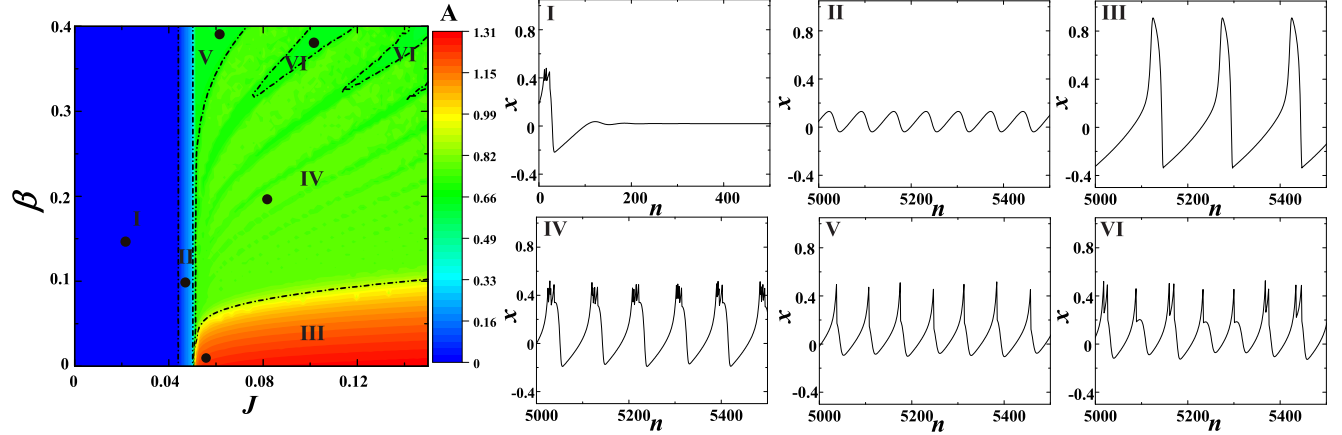
*franovic@ipb.ac.rs
†olmaov@ipfran.ru

FIG. 1. Dynamical regimes exhibited by model (1). The heat map refers to variation of the amplitude of oscillations A of the x time series in the J-β plane. The wave forms shown in subfigures I–VI illustrate the different forms of neuron's behavior, including excitability (I), subthreshold oscillations (II), regular spiking (III), chaotic bursting (IV), chaotic spiking (V), as well as the mixed spike-burst activity (VI). The dots in the heat map indicate the particular (J,β) values where the representative wave forms are obtained.

to different forms of external stimuli. Within this context, it will be examined whether the effective model is capable of reproducing the properties of noise-activated, noise-induced, and noise-perturbed modes of collective behavior.

The paper is organized as follows. In Sec. II, we make an overview of the local map dynamics and introduce the population model. Section III outlines the ingredients most relevant for the derivation of the MF system, with the remaining technical details left for the Appendix. In Sec. IV, the qualitative and quantitative agreement between the dynamics of the exact and the MF model is illustrated by the appropriate bifurcation diagrams, as well as by comparing the characteristic features of the associated regimes. Section V concerns the assembly's stimulus-response relationship, first investigating the analogy between the respective phase-response curves (PRCs) of the exact system and the effective model in spiking and bursting regimes and then considering the extent to which the MF model reproduces the population's response to rectangular pulses of finite amplitude and duration. In Sec. VI, we provide a summary of our main results.

II. MAP NEURON DYNAMICS AND THE POPULATION MODEL

The dynamics of an isolated neuron conforms to a map model first introduced in Refs. [45,46], which is given by

$$
\begin{aligned}
x_{n+1} &= x_n + G(x_n) - \beta H(x_n - d) - y_n, \\
y_{n+1} &= y_n + \epsilon(x_n - J),
\end{aligned}
\tag{1}
$$

where n denotes the iteration step. The variable x_n qualitatively accounts for the membrane potential, whereas the recovery variable y_n, whose rate of change is set by a small parameter $\epsilon = 10^{-2}$, mimics the behavior of ion-gating channels. The parameters a, β, and d modify the profile of the ensuing oscillations, while J crucially influences the neural excitability, viz. the transitions from silence to active regimes.

The x_n evolution features two nonlinear terms, one being a FitzHugh-Nagumo-like cubic nonlinearity

$G(x_n) = x_n(x_n - a)(1 - x_n)$, which is complemented by a discontinuity term $-\beta H(x_n - d)$, where H stands for the Heaviside step function. The parameters $a = 0.1$ and $d = 0.45$ are kept fixed throughout the paper. The impact of discontinuity consists in making the fast subsystem [Eq. (1) with $\epsilon = 0$] a Lorenz-type map within certain parameter domains [46,47], which endows the model with the ability to generate chaotic spike or burst oscillations, otherwise lacking in the Fitzhugh-Nagumo type of systems.

Under variation of J and β, the map (1) may reproduce a rich repertoire of generic regimes displayed by the real neurons, as demonstrated in Fig. 1. In particular, the main frame shows amplitudes of the corresponding x time series for the given (J,β), while the remaining subfigures illustrate the characteristic wave forms pertaining to excitable regime (region I), subthreshold oscillations II), regular (III) or chaotic spiking (I), chaotic bursting (V), as well as the mixed chaotic spike-burst activity (VI). Some of the indicated boundaries, such as those involving domains IV, V, and VI should be understood as tentative, since the associated transitions are smooth and therefore difficult to discern.

The detailed phase plane analysis concerning the relevant unstable invariant curves and the mechanisms underlying transitions between the different dynamical regimes can be found in Ref. [48]. Here we briefly mention that under increasing J, the equilibrium loses stability via the Neimarck-Sacker bifurcation, which gives rise to subthreshold oscillations. Note that the latter may be considered an excitable state, in the sense that a strong-enough perturbation can elicit genuine spike, though the phase point does not relax to the equilibrium but rather to a closed invariant curve.

Adopting model (1) for local dynamics, we focus on an assembly of N stochastic neurons coupled in the all-to-all fashion via electrical synapses (diffusive couplings). Each neuron receives input from the units within the assembly and is further influenced by synaptic noise from the embedding environment. Note that it is quite common in two-dimensional neuron models with sharp separation of characteristic time scales to interpret the stochastic perturbation acting on the fast
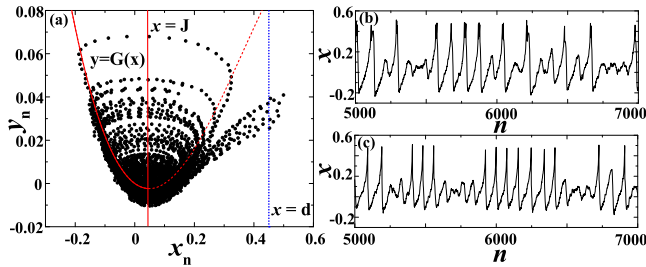
FIG. 2. Impact of noise on a single map neuron in the excitable regime. (a) The mechanism behind noise-induced spiking. The data are obtained for $J = 0.046$, $\beta = 0.4$, $\sigma = 0.005$. The equilibrium is deterministically stable given that the line $x = J$ intersects the invariant curve $y = G(x)$ below the curve's minimum. (b) The x_n series corresponding to noise-induced bursting ($J = 0.042$, $\beta = 0.2$, $\sigma = 0.008$), whereas (c) demonstrates stochastic spiking superimposed on subthreshold oscillations ($J = 0.048$, $\beta = 0.4$, $\sigma = 0.008$).

(slow) time scale as synaptic (intrinsic) noise [49–51]. The population activity is then described by the following system:

$$x_{i,n+1} = x_{i,n} + G(x_{i,n}) - \beta H(x_{i,n} - d) - y_{i,n} + I_{i,n}^{\text{syn}},$$
$$y_{i,n+1} = y_{i,n} + \epsilon(x_{i,n} - J), \qquad (2)$$
$$I_{i,n}^{\text{syn}} = I_{i,n}^{\text{coup}} + I_{i,n}^{\text{rand}} = \frac{c}{N} \sum_{j=1, j \neq i}^{N} (x_{j,n} - x_{i,n}) + \sigma \xi_{i,n},$$

where i specifies the particular neuron. The synaptic currents $I_{i,n}^{\text{syn}}$ comprise two types of terms. The diffusive couplings $I_{i,n}^{\text{coup}}$ are characterized by the strength c, which is assumed to be uniform over the network and is set to $c = 1$ in the remainder of the paper. The random inputs $I_{i,n}^{\text{rand}}$ involve uncorrelated white noise $[E[\xi_{i,n}] = 0, E[\xi_{i,n}\xi_{j,n'}] = \delta_{ij}\delta(n - n')]$ of intensity σ.

Confined to a single unit, the stochastic component may influence its dynamics either by perturbing the deterministic oscillatory regimes or by inducing oscillations in the excitable regime, cf. Fig. 2(b). The onset of noise-induced spiking or bursting within the parameter domain where the fixed point is deterministically stable (domain I in Fig. 1) corresponds to a phenomenon of stochastic bifurcation [39,52–55]. The latter are typically described phenomenologically, in a sense that certain time-averaged quantities, such as the asymptotic probability distributions of relevant variables or the associated power spectra, exhibit a qualitative change under variation of noise intensity. For instance, in continuous-time systems, it has been shown that the stochastic Hopf bifurcation from a stochastically stable fixed point to a stochastically stable limit cycle is accompanied by the loss of Gaussian property for the asymptotic distributions of the appropriate variables [56]. At variance with standard deterministic bifurcations, where one clearly observes a critical value of the control parameter, the change of system's behavior in noise-induced transitions is gradual [39]. Note that noise can also play an important part in the (J,β) region II where the deterministic map shows subthreshold oscillations. Here noise can give rise to a form of dynamics reminiscent of mixed-mode oscillations, cf. Fig. 2(c).

So far, models similar to (2) have been applied to address a number of problems associated to collective phenomena in networks of coupled neurons, including synchronization of electrically coupled units with spike-burst activity [57,58], pattern formation in complex networks with modular architecture [41,42,59], transient cluster activity in evolving dynamical networks [44], as well as the basin stability of synchronization regimes in small-world networks [43]. Within this paper, the collective motion will be described in terms of the global variables $X_n = \frac{1}{N} \sum_{i=1}^{N} x_{i,n}$ and $Y_n = \frac{1}{N} \sum_{i=1}^{N} y_{i,n}$.

III. DERIVATION OF THE MEAN-FIELD MODEL

Considering a MF approximation, our main goal lies in deriving a reduced low-dimensional deterministic set of nonlinear difference equations whose dynamics is qualitatively analogous to the collective motion of the original system (2) composed of $2N$ coupled stochastic maps. In particular, the MF model should be able to generate all the regimes exhibited by the exact system, qualitatively reproducing the bifurcations that the latter undergoes. Also, applying the effective model, one should be capable of inferring with sufficient accuracy the parameter domains which admit the different collective states of the exact system, with the corresponding time series exhibiting similar characteristic quantitative features. Regarding the explicit effects of noise, the MF model is expected to account for the onset or suppression of different types of collective modes associated to macroscopic spiking or bursting activity, which are mediated by synchronization or desynchronization of individual neuron dynamics, respectively. The synchronization processes may be influenced by noise in a variety of ways, including the scenarios where noise acts as a perturbation to mainly deterministic (and chaotic) local oscillations, or the ones where noise plays a facilitatory role, in the sense that the collective mode emerges via synchronization of noise-induced local dynamics.

Given that we consider a system of discrete-time equations, one cannot adopt the usual method of deriving the MF model via Fokker-Planck formalism [40]. Nevertheless, an analytically tractable MF model may still be built by focusing on the evolution of cumulants [34–36,39], whereby the full density of states is factorized into a series of marginal densities. The advantage of such an approach is that the simplifying approximations aimed at truncating the underlying cumulant series can be introduced in a controlled fashion. Such approximations, stated in a form of closure hypothesis [34], are required due to nonlinearity of the original system, which causes the dynamics of cumulants of the given order to be coupled to those of the higher order.

In our case, the derivation of the effective model incorporates an explicit Gaussian closure hypothesis [34–36,39], by which all the cumulants above second order are assumed to vanish. The collective dynamics is then described by a set of five variables (the first- and second-order cumulants), including

(i) the means, given by $m_{x,n} = \lim_{N\to\infty} \frac{1}{N} \sum_{i=1}^{N} x_{i,n} \equiv \langle x_{i,n} \rangle$, $m_{y,n} = \lim_{N\to\infty} \frac{1}{N} \sum_{i=1}^{N} y_{i,n} \equiv \langle y_{i,n} \rangle$;

(ii) the variances, defined as $S_{x,n} = \langle x_{i,n}^2 \rangle - \langle x_{i,n} \rangle^2 = \langle x_{i,n}^2 \rangle - m_{x,n}^2$ and $S_{y,n} = \langle y_{i,n}^2 \rangle - \langle y_{i,n} \rangle^2 = \langle y_{i,n}^2 \rangle - m_{y,n}^2$;

(iii) the covariance $U_n = \langle x_{i,n} y_{i,n} \rangle - m_{x,n} m_{y,n}$.

The expressions for higher-order moments $\langle x_{i,n}^k \rangle$ in terms of the first- and second-order cumulants [60], such as

$$\langle x_i^3 \rangle = m_x^3 + 3m_x S_x$$

$$\langle x_i^4 \rangle = m_x^4 + 6m_x^2 S_x + 3S_x^2$$

$$\langle x_i^2 y_i \rangle = m_y S_x + m_y m_x^2 + 2m_x U$$

$$\langle x_i^3 y_i \rangle = 3S_x U + 3S_x m_x m_y + 3m_x^2 U + m_y m_x^3 \qquad (3)$$

$$\langle x_i^5 \rangle = m_x^5 + 15m_x S_x^2 + 10m_x^3 S_x$$

$$\langle x_i^6 \rangle = m_x^6 + 15S_x^3 + 15m_x^4 S_x + 45m_x^2 S_x^2,$$

can be derived using the closure hypothesis.

The Gaussian approximation effectively amounts to an assumption that the relation

$$\lim_{N \to \infty} \frac{1}{N} \sum_{i=1}^{N} x_{i,n}^k \approx E\big[x_{i,n}^k\big], \qquad (4)$$

holds, whereby E refers to expectation value obtained by averaging over an ensemble of different stochastic realizations. In other words, one supposes that the local variables are independent and are drawn from a normal distribution $\mathcal{N}(m_x, S_x)$. We do not know *a priori* whether such an assumption is fulfilled but can only judge on its validity by verifying the correctness of the predictions on the population dynamics provided by the MF model. Also note that the effective model concerns the assembly dynamics in the thermodynamic limit

$N \to \infty$. The stochastic terms in this case can be neglected, as one may show them to contribute to finite-size effects which scale as $1/N$. This means that the influence of noise in our MF model is felt only via the noise intensity, which assumes the role of an additional bifurcation parameter.

Let us illustrate the main technical points required for the derivation of the MF model. Our focus will lie with a couple of relevant examples, whereas the remaining details are provided in the Appendix. We begin by considering the dynamics of m_x, which is given by

$$m_{x,n+1} = m_{x,n} - m_{y,n} + \langle G(x_{i,n}) \rangle - \beta \langle H(x_{j,n} - d) \rangle. \quad (5)$$

It is easy to see that there is no contribution from the coupling term. As far as the third term on the right-hand side of Eq. (5) is concerned, using Eq. (3), one arrives at

$$\langle G(x_i) \rangle = \langle -x_i^3 + (1+a)x_i^2 - ax_i \rangle$$
$$= G(m_x) + S_x(1 + a - 3m_x). \qquad (6)$$

In the last expression, we have dropped the time index for simplicity and have introduced the shorthand notation $G(m_x) \equiv -m_x^3 + (1+a)(m_x^2 + S_x)$.

The key problem is how to treat the final term in the right-hand side of Eq. (5). Our approach consists in replacing the assembly average by the expectation value ($\langle H(x_i - d) \rangle \approx E[H(x_i - d)]$), obtained by assuming that the local variables at an arbitrary time moment are normally distributed according to $P(x_i) \sim \mathcal{N}(m_x, S_x)$. The expectation may then be evaluated as

$$E[-\beta \langle H(x_i - d) \rangle] = \int dx_1 \int dx_2 ... \int dx_N \left(-\frac{\beta}{N} \sum_i H(x_i - d) \right) p(x_1, x_2, ..., x_N)$$

$$= -\beta \int_{-\infty}^{\infty} dx_1 H(x_1 - d) p(x_1) = -\beta \int_d^{\infty} \frac{1}{\sqrt{2\pi S_x}} e^{-\frac{(x_1 - m_x)^2}{2S_x}} = -\frac{\beta}{2} \left(1 - \text{Erf}\left[\frac{d - m_x}{\sqrt{2S_x}} \right] \right), \qquad (7)$$

with the error function $\text{Erf}(x) = \frac{2}{\sqrt{\pi}} \int_0^x e^{-t^2} dt$. In the above calculation, we have explicitly used the assumption on the independence of distributions of local variables at any given moment of time.

In a similar fashion, one may consider the S_x dynamics, which constitutes the most demanding part of the derivation. In particular, proceeding from the S_x definition, we obtain

$$S_{x,n+1} = \langle x_{i,n+1}^2 \rangle - \langle x_{i,n+1} \rangle^2$$

$$= \langle [(1-c)x_{i,n} + G(x_{i,n}) - \beta H(x_{i,n} - d) - y_{i,n} + \xi_{i,n} + cm_{x,n}]^2 \rangle - [m_{x,n} - m_{y,n} + G(m_{x,n}) + S_{x,n}(1 + a - 3m_{x,n})$$

$$- \beta \langle H(x_{i,n} - d) \rangle]^2. \qquad (8)$$

As an illustration, let us evaluate one of the terms containing an average over the threshold function:

$$-2\beta E[\langle G(x_i)H(x_i - d) \rangle] = -2\beta \left[\int dx_1 G(x_1)H(x_1 - d)p(x_1) - \int dx_1 H(x_1 - d)p(x_1)[G(m_x) + S_x(1 + a - 3m_x)] \right]$$

$$\approx -2\beta \left[\int dx_1 [G(m_x) + G'(m_x)(x_1 - m_x) + \frac{1}{2}G''(m_x)(x_1 - m_x)^2]H(x_1 - d)p(x_1) \right.$$

$$\left. - \int dx_1 H(x_1 - d)p(x_1)[G(m_x) + S_x(1 + a - 3m_x)] \right] = ...$$

$$= -2\beta[(1+a)(m_x + d) - a - 3m_x d]\sqrt{\frac{S_x}{2\pi}} \exp\left[-\frac{(d - m_x)^2}{2S_x} \right]. \qquad (9)$$

Again, the time indexes have been suppressed to simplify the notation.

Leaving the remaining elements of the derivation for the Appendix, we now state the final equations of the MF model in the thermodynamic limit

$$m_{x,n+1} = m_{x,n} - m_{y,n} + G(m_{x,n}) + S_{x,n}(1 + a - 3m_{x,n}) - \frac{\beta}{2}\left(1 - \text{Erf}\left[\frac{d - m_{x,n}}{\sqrt{2S_{x,n}}}\right]\right)$$

$$m_{y,n+1} = m_{y,n} + \epsilon(m_{x,n} - J)$$

$$S_{x,n+1} = (1-c)^2 S_{x,n} + S_{y,n} + \sigma^2 - 2(1-c)U_n + S_{x,n}\left(-3m_{x,n}^2 + 2(1+a)m_{x,n} - a\right)^2$$

$$- 2(1-c)\left(3m_{x,n}^2 S_{x,n} + 3S_{x,n}^2 - 2(1+a)m_{x,n}S_{x,n} + aS_{x,n}\right) + 2(3S_{x,n}U_n + 3m_{x,n}^2 U_n - 2(1+a)m_{x,n}U_n)$$

$$- 2\beta[(1+a)(m_{x,n} + d) - a - 3dm_{x,n}]\sqrt{\frac{S_{x,n}}{2\pi}}\exp\left[-\frac{(d-m_{x,n})^2}{2S_{x,n}}\right] - 2\beta(1-c)\sqrt{\frac{S_{x,n}}{2\pi}}\exp\left[-\frac{(d-m_{x,n})^2}{2S_{x,n}}\right]$$

$$+ S_{x,n}^2\left[36m_{x,n}^2 - 24(1+a)m_{x,n} + 2(1+a)^2 + 6a\right] + 15S_{x,n}^3$$

$$S_{y,n+1} = S_{y,n} + \epsilon^2 S_{x,n} + 2\epsilon U_n$$

$$U_{n+1} = U_n - (a + c + \epsilon)U_n + \epsilon(1 - c - a)S_{x,n} - S_{y,n} - (U_n + \epsilon S_{x,n})[3S_{x,n} + 3m_{x,n}^2 - 2(1+a)m_{x,n}]$$

$$- \beta\epsilon\sqrt{\frac{S_{x,n}}{2\pi}}\exp\left[-\frac{(d-m_{x,n})^2}{2S_{x,n}}\right]. \tag{10}$$

IV. ANALYSIS OF STABILITY AND BIFURCATIONS

In this section, our goal is to demonstrate the qualitative and quantitative analogies between the dynamics of the exact system and the MF model. To this end, we first examine the succession of macroscopic regimes in the J-β parameter plane for σ fixed at an intermediate value $\sigma = 0.002$, see Fig. 3. As in case of a single unit, changing J is relevant for the system's excitability, viz. the transitions from silent to active regimes, while β influences the wave forms of the active states (spiking, bursting, or mixed spike-bursting activity). The assembly is found to exhibit the collective modes which qualitatively correspond to the dynamics of a single unit illustrated in plates
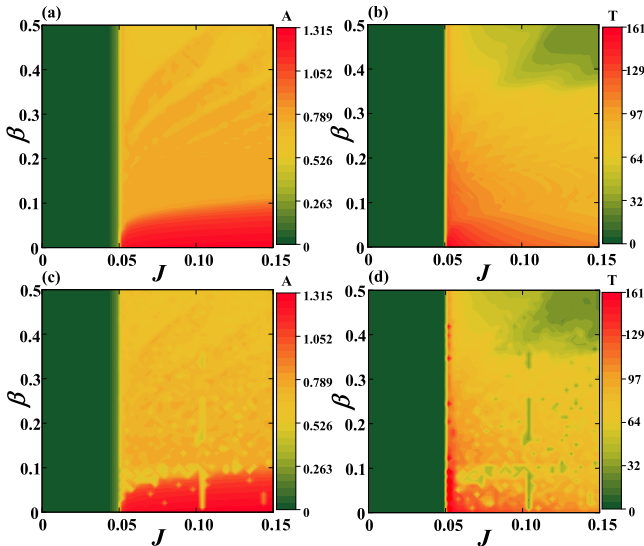
III and VI of Fig. 1. The heat maps in the left column of Fig. 3 provide a comparison between the oscillation amplitudes A of the global variable X (top row) and the MF variable m_x (bottom row) for the given (J, β). The right column indicates how well are matched the average interspike interval (or the average bursting cycle) T of the exact system with the corresponding characteristics of the dynamics of the MF model (A1). In the given instances, exact system comprises an assembly of $N = 100$ neurons, having obtained A by averaging over a
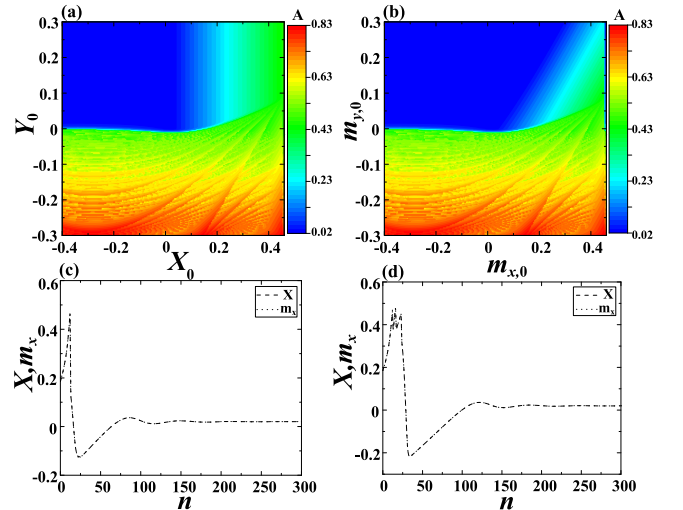

FIG. 3. Heat maps in (a) and (b) show the dependencies $A(J,\beta)$ and $T(J,\beta)$ obtained by stochastic averaging for a network of $N = 100$ neurons, respectively. Panels (c) and (d) illustrate the analogous results for the MF model. The noise intensity in all instances is $\sigma = 0.001$.

FIG. 4. Macroscopic excitability feature. In (a) and (b) are shown the maximum values of X and m_x reached within the time series of the exact and the MF system, starting from the analogous initial conditions (X_0, Y_0) and $(m_{x,0}, m_{y,0})$, respectively. The parameters are $J = 0.02, \beta = 0.4$. (c) Illustrates the case where a strong-enough perturbation elicits a single-spike response $(J = 0.02, \beta = 0.4)$, whereas (d) corresponds to a bursting response made up of three spikes $(J = 0.02, \beta = 0.15)$. In both instances, the time series of the MF model (dotted line) is indistinguishable from that of the exact system (dashed line).
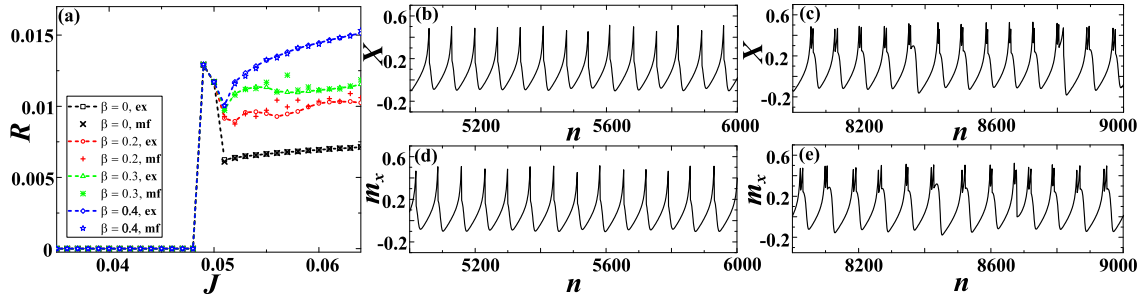
FIG. 5. (a) A family of $R(J)$ curves over β for a network of size $N = 100$ under fixed $\sigma = 0.001$. Superimposed are the results for the MF model, whereby the symbols $\times, +, *, \star$ correspond to cases $\beta = 0, 0.2, 0.3$, and 0.4, respectively. Panels (b) and (c) illustrate the X series associated to the spiking and the bursting collective modes. The considered network is made up of $N = 100$ neurons, with the parameters set to $J = 0.06$, $\beta = 0.4$, $\sigma = 0.001$ in (b), and $J = 0.08$, $\beta = 0.2$, $\sigma = 0.001$ in (c). In (d) and (e) are provided the m_x series obtained for parameters from (b) and (c).

sufficiently long time series, whereas T is determined by taking average over an ensemble of 20 different stochastic realizations. With regard to T, we have selected a convenient threshold $\theta = 0.2$, which allows a clear detection of individual spikes and enables one to unambiguously discern the initiation stage of bursts, as required for calculating the length of the bursting cycle.

Let us begin the analysis by focusing on the domain of J values where the exact system exhibits the stochastically stable equilibrium, while the MF model has a stable stationary state. The stochastic stability physically implies that fluctuations around the deterministic fixed point are typically of the order of noise, though some rare spikes may still be evoked. For J sufficiently close to the region admitting the sub-threshold oscillations, the population manifests macroscopic excitability. The term "macroscopic" here refers to a form of emergent assembly behavior rather than the characteristic spatial scale. To properly illustrate this feature, we have analyzed the assembly dynamics in the limit $\sigma = 0$, cf. Fig. 4. In particular, Figs. 4(a) and 4(b) show the maximum X and m_x values reached in the corresponding time series obtained for sets of different initial conditions (X_0, Y_0) and $(m_{x,0}, m_{y,0})$, respectively. The comparison between the two plots clearly corroborates that the boundary defining the domain of spiking response is appropriately anticipated by the MF model. An important remark is that for the given J, the assembly may exhibit different forms of macroscopic excitability, generating a single spike or a burst of spikes, as dependent on the value of β. This is demonstrated by the time series in Figs. 4(c) and 4(d). The former refers to a one-spike response in case of $\beta = 0.4$. For smaller β, one observes responses comprising two or more closely packed spikes, with Fig. 4(d) illustrating a three-spike burst encountered for $\beta = 0.25$. Note that the time series of the full system and the MF model are exactly matched in the limit $\sigma = 0$.

Next we address the noise-influenced transitions from silence to active regimes observed under increasing J. To do so, in Fig. 5(a) we have plotted the change of the firing (spiking or bursting) frequency R for an assembly consisting of $N = 100$ neurons. The average frequency is determined by considering an ensemble of 20 different stochastic realizations, having σ fixed to the moderate value from Fig. 4. The results from simulations of the full system (2) are compared against

the data obtained for the MF model. In this context, two points should be stressed. First, for moderate σ, note that the firing frequencies of the MF model lie in close agreement to those of the exact system. As a second point, one finds that such quantitative agreement extends to different forms of collective behavior, viz. it holds for different types of transitions from silent to active regimes. As already indicated, the wave forms pertaining to the active states depend on β, such that the associated transitions are mediated by the distinct synchronization processes. For instance, at $\beta = 0$, synchronization involves time series of single units that conform to spiking activity of type III from Fig. 1, which are quite resilient to impact of noise. On the other hand, for $\beta = 0.3$ or $\beta = 0.4$, the individual units exhibit chaotic bursting or spiking activity, respectively, such that the underlying synchronization process may be more susceptible to stochastic effects. The typical X time series illustrating the different collective modes are compared to the corresponding m_x series in Figs. 5(b)–5(e). The top (bottom) row concerns the data for the exact system (MF model).
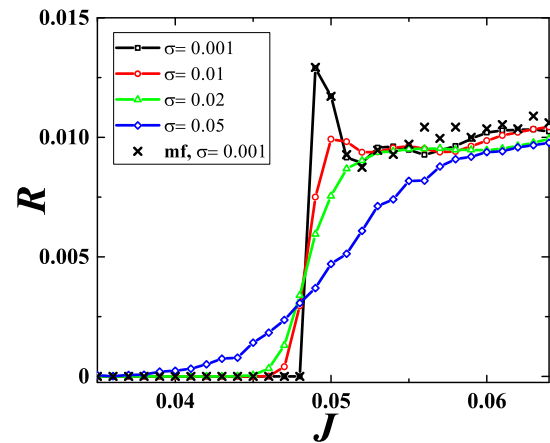

FIG. 6. Family of $R(J)$ curves over σ obtained for a network of $N = 100$ neurons under fixed $\beta = 0.2$. The different symbols correspond to cases $\sigma = 0.001$ (squares), $\sigma = 0.01$ (circles), $\sigma = 0.02$ (triangles), and $\sigma = 0.05$ (diamonds). The crosses connected by the dashed line highlight the $R(J)$ curve for the MF model at $\sigma = 0.001$.
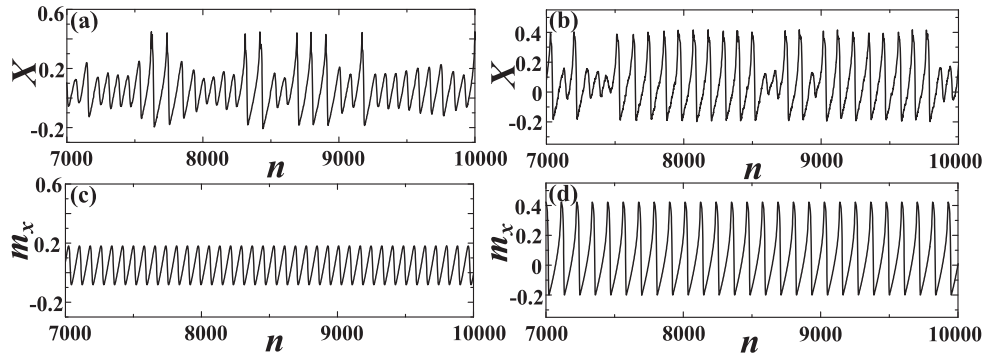
FIG. 7. Noise-induced phenomena within the J interval in vicinity of the deterministic threshold. X series in (a) shows the noise-induced spike-bursting activity on top of subthreshold oscillations ($J = 0.047$, $\beta = 0.2$, $\sigma = 0.02$). (b) Illustrates the "skipping" phenomenon where the stochastic effects occasionally suppress the large-amplitude oscillations of the X variable ($J = 0.058$, $\beta = 0.2$, $\sigma = 0.01$). In (c) and (d) are provided the m_x series corresponding to parameter sets from (a) and (b), respectively.

In order to investigate more closely the influence of noise for J interval in vicinity of the transition from silence to active regimes, we examine how the profiles of $R(J)$ curves change under increasing σ. The results shown in Fig. 6 refer to $\beta = 0.2$ and a population comprised of $N = 100$ neurons. As expected, the transition appears quite sharp for moderate noise $\sigma = 0.001$ but is considerably flattened for larger σ, e.g., $\sigma = 0.05$. The crosses indicate the firing frequencies predicted by the MF model for $\sigma = 0.001$.

For larger σ, the MF model fails to reproduce the behavior of the exact system in vicinity of threshold J, in the sense that it overestimates the maximal R value, as well as the actual critical J characterizing the transition. Viewed from another angle, one may infer that for sufficiently large σ and J below the threshold given by the MF model, the latter fails to capture the impact of synchronization processes taking place between the noise-induced oscillations of individual units. This especially refers to J interval where the spikes or bursts (depending on the given β) are superimposed on the background of subthreshold oscillations. An example of such a discrepancy between the behavior of the exact and the effective system is provided in Fig. 7, cf. Fig. 7(a) and Fig. 7(c). Also, for strong σ and J values above the transition, the firing frequencies anticipated by the effective model are typically higher than those of the exact system (not shown). Within this region, the stochastic effects suppress synchronization between the chaotic oscillations of single neurons, thereby reducing the corresponding R value. This is not accounted for with sufficient accuracy by the MF system. Note that such suppression of synchronization is reflected in the corresponding X series by the spike (burst) "skipping" mechanism, where the large-amplitude oscillations are occasionally replaced with subthreshold oscillations. For the associated J and σ values, such a phenomenon is absent in the dynamics of the effective model, cf. Fig. 7(b) and Fig. 7(d). In both of the scenarios illustrated in Fig. 7, the reason for the failure of MF model is that the Gaussian approximation breaks down due to large stochastic fluctuations.

The fashion in which the validity of the effective model's predictions deteriorates with increasing σ is made more explicit in Fig. 8, which shows the $A(J,\sigma)$ and $T(J,\sigma)$ dependencies for the exact and the approximate system at fixed $\beta = 0.4$. The considered size of the network is $N = 100$. Comparison between the respective A (left column) and T plots (right column) suggests that the range of σ values where the MF approximation applies is contingent on J. For instance, in the J region below the deterministic threshold, one may estimate this range by noting that the effective bifurcation diagram in Fig. 8(a) indicates that noise-induced macroscopic oscillations emerge for $\sigma \approx 0.003$. Since this point is not adequately represented by the effective model, cf. Fig. 8(c), one may state that the Gaussian approximation breaks down around $\sigma \approx 0.003$ within the given J region. Nevertheless, for J above the deterministic threshold, the validity of the MF model appears to depend rather strongly on particular J, with the σ values where the Gaussian approximation effectively fails spanning the range $\sigma \in (0.002, 0.006)$.
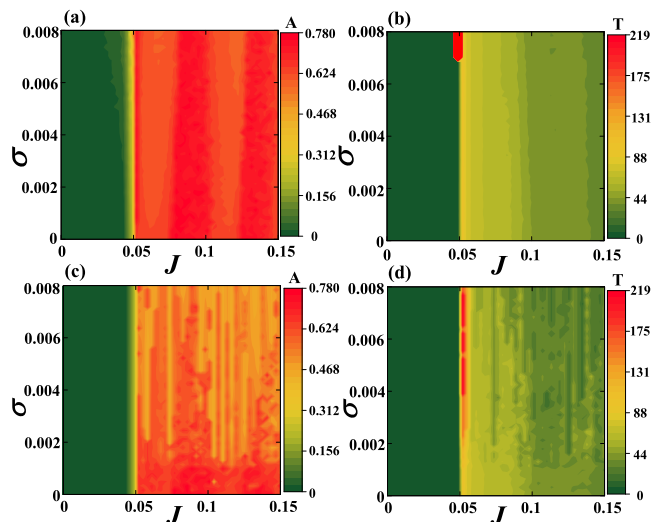

FIG. 8. Panels (a) and (b), respectively, refer to $A(J,\sigma)$ and $T(J,\sigma)$ dependencies for the network of $N = 100$ neurons under fixed $\beta = 0.4$. The results in (a) are obtained by averaging over a sufficiently long time series, whereas data in (b) derive from averaging over an ensemble of 20 different stochastic realizations. In (c) and (d) are provided the $A(J,\sigma)$ and $T(J,\sigma)$ dependencies determined by numerical simulations of the MF model.
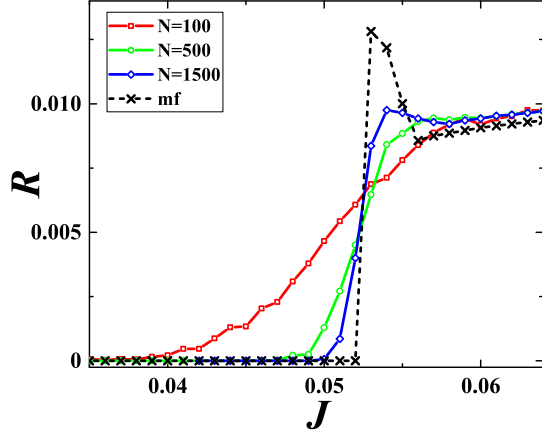
FIG. 9. $R(J)$ dependencies for increasing N under fixed $(\beta,\sigma) = (0.2,0.05)$. The squares, circles, and diamonds correspond to cases $N = 100$, $N = 500$, and $N = 1500$, respectively. The results predicted by the MF model are indicated by crosses connected via dashed line.

So far, we have investigated the impact of noise by comparing the results for the network of size $N = 100$ to those obtained for the effective system. Nevertheless, within Sec. III, it has already been emphasized that the MF model, deterministic in character, refers to the system's behavior in the thermodynamic limit $N \to \infty$, whereas the explicitly stochastic terms could only be incorporated as finite-size effects. This makes it relevant to examine how the behavior of the exact system within the J domain around deterministic threshold changes for large and fixed σ under increasing N. To this end, we have plotted in Fig. 9 the $R(J)$ curves calculated for $N = 100$ (squares), $N = 500$ (circles), and $N = 1500$ (diamonds) at fixed $\beta = 0.2, \sigma = 0.05$. The curve for $N = 100$ evinces that the given σ value is quite large in a sense of being sufficient to induce collective oscillations within the excitable regime. Apart from the dependencies for the full system, we also show the $R(J)$ curve associated to the MF model (dashed line with crosses). An interesting point regarding the latter is that the J threshold for the emergence of the collective mode is shifted toward a larger value compared to the case $\sigma \approx 0.01$. While the given transition itself appears quite sharp, the curves corresponding to the exact system approach it with increasing N, both in terms of the J threshold and the R values above the transition. This corroborates that the (J,σ) domain where the Gaussian approximation behind the MF model fails expectedly reduces with the increasing system size.

V. RESPONSE TO EXTERNAL STIMULI

The aim of this section is to investigate the extent to which the MF model can be used to predict the stimulus-response relationship of an assembly exhibiting different macroscopic regimes, including the excitable state, as well as the spiking and bursting collective modes. Let us first focus on the two latter instances and examine the sensitivity of a population to an external pulse perturbation within the framework of phase resetting theory [61–64]. In order to compare the behavior of the exact system and the effective model, we determine
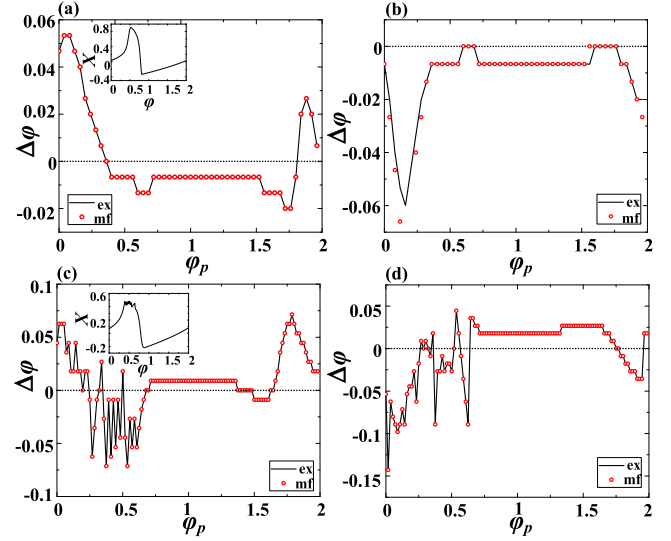

FIG. 10. Assembly phase resetting. Panels (a) and (b) show the PRCs for a population in spiking regime ($J = 0.055$, $\beta = 0$) under excitatory ($a = 0.008$) and inhibitory stimulation ($a = -0.008$), respectively. Results for the exact system ($N = 500$) are indicated by the solid line, whereas the data for the MF model are denoted by circles. The bottom row illustrates the PRCs for an assembly exhibiting macroscopic bursting ($J = 0.06$, $\beta = 0.1$), whereby (c) describes the effect of an excitatory ($a = 0.01$) and (d) of an inhibitory pulse perturbation ($a = -0.01$). The insets in (a) and (c) demonstrate how the phases are assigned to the points within the spiking and bursting cycles, respectively. Phase is expressed in units of π.

the corresponding PRCs, which describe the phase shift $\Delta\phi$, induced by the perturbation, in terms of the phase ϕ_p when the perturbation is applied. The considered stimulus has a form of a short pulse current $I_p = a_p H(n - n_i)H(n - n_f)$, whose magnitude a_p and width $\Delta = n_i - n_f$ are small compared to the amplitude and duration of the spiking (or bursting) cycle T_0, respectively. In case of the exact system, the same pulse current is delivered to each neuron i, adding the term I_p to x_i dynamics, whereas in the effective model, stimulation is administered via the m_x variable. The phase φ_p is defined in reference to T_0 by $\varphi_p = n_p/T_0$. The associated phase difference following the reset is calculated as $\Delta\varphi = 1 - T_1/T_0$, where T_1 denotes the duration of the perturbed spiking or bursting cycle.

The PRCs characterizing the assembly response in the spiking regime are provided in Fig. 10(a) and Fig. 10(b), whereby the former is obtained under the action of an excitatory ($a_p > 0$), and the latter under the influence of inhibitory stimulation ($a_p < 0$). We stress that, in both instances, the results derived from the effective model, denoted by circles, show excellent agreement with the data for the exact system (solid lines). In qualitative terms, one observes that excitatory stimulation may advance the phase of the spiking cycle if it arrives sufficiently close to the spike but still before the sharp rising stage. However, an excitatory perturbation acting during the spike or within the effective refractory period has a suppression effect, reflected in delaying of the next spike. In contrast to excitatory stimulation, the inhibitory pulse postpones the next firing time if it is introduced within the interval close to the rising stage of spike.
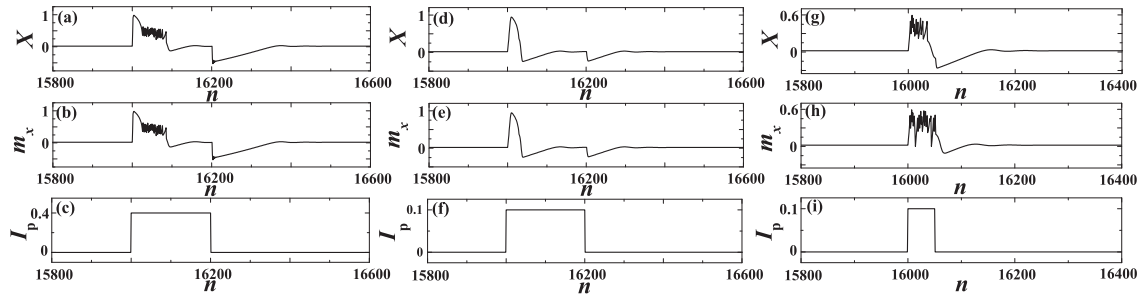
FIG. 11. Stimulus-response relationship in the excitable regime ($J = 0.02$). The top (middle) row refers to the response of the full system (MF model), whereas the bottom row shows the profile of the external stimulation. In panels (a)–(c), the system parameters are $\beta = 0.4$, $\sigma = 0$, while the perturbation is characterized by $a_p = 0.4, \Delta = 200$. Panels (d)–(f) concern the response of an assembly ($\beta = 0.1$, $\sigma = 0.001$) subjected to a rectangular pulse $a_p = 0.4$, $\Delta = 200$. Panels (g)–(i) illustrate the response of a population ($\beta = 0.4$, $\sigma = 0.001$) influenced by the external stimulation $a_p = 0.1, \Delta = 50$. The considered network is of size $N = 500$.

The PRCs determined for an assembly exhibiting collective bursting show qualitatively analogous effects to those described so far, see Fig. 10(c) and Fig. 10(d). This especially refers to impact of perturbation delivered sufficiently close to a moment of burst initiation. An apparent difference compared to Fig. 10(a) and Fig. 10(b) emerges during the bursting stage itself, where the associated PRCs expectedly exhibit strong fluctuations. Apart from that, one finds an interesting effect that both the excitatory and the inhibitory stimulation have a facilitatory role, i.e., cause phase advancement during the relaxation stage of the bursting cycle.

For a population in the excitable state, we consider scenarios where the system is influenced by a rectangular pulse perturbation of finite magnitude and duration, in a sense that the latter are comparable to corresponding features of typical spiking or bursting cycles. Note that the selected J value $J = 0.02$ lies sufficiently away from the interval admitting the subthreshold oscillations. Again, our objective is to determine whether the MF model correctly anticipates the response of the exact system, now in the presence of small to moderate noise. Some of the illustrative examples concerning the stimulus-response relationship under the finite perturbation are provided in Fig. 11. The top and the middle rows refer to X and corresponding m_x time series, respectively, while the bottom row shows the profile of the applied stimulus. We find that in the absence of noise or for sufficiently small σ, the effective model reproduces the evoked behavior of the full system quite accurately. This also refers to some highly complex forms of responses, as corroborated in Figs. 11(a)–11(c), which concern relatively large a_p and Δ. Under increasing σ, the ability of the MF model to predict the dynamics of the exact system gradually reduces but in a fashion that involves a nontrivial dependence on β. In particular, for smaller $\beta \approx 0.1$, which would facilitate macroscopic spiking mode for supercritical J, it turns out that the dynamics of the MF model lies in close agreement to the one of the exact system even for moderate noise $\sigma = 0.001$, cf. Figs. 11(d)–11(f). However, for higher β, such an analogy between the responses of the exact and the MF system is lost, see Figs. 11(g)–11(i). Naturally, the validity of the predictions given by the MF model deteriorates if the stimulation amplitude a_p and the duration Δ are large, especially in the presence of non-negligible noise.

VI. SUMMARY AND DISCUSSION

We have developed an MF approach in order to systematically analyze the emergent dynamics and the input-output relationship of a population of stochastic map neurons. The reduced low-dimensional model has been derived within the framework of Gaussian approximation, formally introduced in a form of a closure hypothesis. In physical terms, such an approximation suggests that the local variables at an arbitrary moment of time are independent and conform to a normal distribution centered about the assembly mean and characterized by the associated assembly variance. Validity of such an approximation cannot be established *a priori*, but has been systematically verified by numerically corroborating that the MF model reproduces the behavior of the exact system with sufficient accuracy.

In particular, we have first demonstrated that the effective model can qualitatively capture all the bifurcations of the exact system leading to the onset of different generic regimes of collective behavior. As far as the quantitative agreement is concerned, we have established substantial matching between the parameter domains admitting the respective dynamical regimes for the exact and the approximate system. Moreover, the typical features of the associated regimes, such as the average interspike interval or the average bursting cycle, exhibit analogous changes with parameter variation and in many parameter domains display numerically similar values.

An important issue has been to explicitly examine how the effects of noise are reflected in the behavior of the MF model. For the noise-perturbed activity, where the sufficiently small noise weakly influences the deterministic attractors of the system, the obtained results indicate that the Gaussian approximation holds. Nevertheless, the physical picture changes in case of noise-induced collective behavior. In particular, for different scenarios of stochastic bifurcations, typically corresponding to transitions from subthreshold oscillations, which involve generalized excitability feature, to spiking or bursting regimes, the exact system undergoes a gradual (smooth) change of collective dynamics, whereas the MF model exhibits a standard deterministic bifurcation with a sharp bifurcation threshold. In such instances, the collective variables of exact system manifest large fluctuations, which

explicitly violate the Gaussian approximation behind the effective model. Note that the loss of Gaussianity property for asymptotic distribution of relevant variables, which accompanies the described stochastic bifurcations, does not imply per se that our Gaussian approximation fails in the supercritical state. This point is evinced by the fact that the dynamics of the effective model shows qualitatively and quantitatively similar features to those of the exact system if the considered parameters lie sufficiently above the stochastic bifurcation. In fact, the Gaussian approximation applied in the derivation of the MF model breaks down only in vicinity of such transitions, where the finite-size effects neglected in Eq. (A1) become most prominent. We have numerically verified the prevalence of finite-size effects in these parameter domains, showing that the change of the appropriate order parameter, such as the spiking frequency, becomes sharper as the size of the neural assembly is increased. Nevertheless, the validity of Gaussian approximation is regained once the system is sufficiently above the bifurcation.

Apart from considering asymptotic dynamics, we have verified that the MF model is capable of capturing the stimulus-response features of the exact system. For short pulse-like perturbations, it has been found that the approximate system reproduces the PRCs of the exact system for both the spiking and bursting regimes of collective activity with high accuracy. Substantial analogies have also been observed in case of macroscopic excitable regime for scenarios where the assembly is stimulated by rectangular pulse perturbations of finite amplitude and duration.

Having developed a viable MF approach, the present research has set the stage for a more systematic exploration of collective dynamics of assemblies of map neurons by analytical means. We believe that the introduced techniques can be successfully applied for treating the emergent behavior of populations in case of chemically and delay-coupled neurons [41]. Moreover, the method may likely be used to explore the effects of parameter inhomogeneity, as well as to study the impact of complex network topologies [41,43]. Our ultimate goal will be to extend the MF approach to account for collective behavior of interacting populations of map neurons [41,42].

APPENDIX

In the following, we provide the remaining details concerning the calculation of the S_x dynamics, which is the most complex part of the derivation of the effective model. Following some algebra, Eq. (9) can be transformed to

$$S_{x,n+1} = (1-c)^2 S_{x,n} + S_{y,n} + \sigma^2 - 2(1-c)U_n + \underbrace{(\langle G(x_{i,n})^2 \rangle - \langle G(x_{i,n}) \rangle^2)}_{\text{Var}(G(x_{i,n}))} + 2(1-c)(\langle x_{i,n} G(x_{i,n}) \rangle - m_{x,n} \langle G(x_{i,n}) \rangle)$$

$$- 2(\langle y_{i,n} G(x_{i,n}) \rangle - m_{y,n} \langle G(x_{i,n}) \rangle) - 2\beta(1-c)[\langle x_{i,n} H(x_{i,n}-d) \rangle - m_{x,n} \langle H(x_{i,n}-d) \rangle] - 2\beta(\langle G(x_{i,n}) H(x_{i,n}-d) \rangle$$

$$- \langle G(x_{i,n}) \rangle \langle H(x_{i,n}-d) \rangle) + \beta^2 \underbrace{(\langle H(x_{i,n}-d)^2 \rangle - \langle H(x_{i,n}-d) \rangle^2)}_{\text{Var}(H(x_{i,n}-d)))}. \tag{A1}$$

The partial results required for completing the calculation are given by

$$\langle x_i G(x_i) \rangle - m_x \langle G(x_i) \rangle = G'(m_x)S_x - 3S_x^2$$
$$\langle y_i G(x_i) \rangle - m_y \langle G(x_i) \rangle = -3S_x U_{xy} - 3m_x^2 U_{xy} + 2(1+a)m_x U_{xy}, \tag{A2}$$

where $G'(m_x) \equiv -3m_x^2 + 2(1+a)m_x - a$. Note that the time indexes have been omitted for simplicity. After some tedious work, it may also be shown that the expression for variance $\text{Var}(G(x_i))$ reads

$$\text{Var}(G(x_i)) = G'^2(m_x)S_x + S_x^2 \left[36m_x^2 - 24(1+a)m_x + 2(1+a)^2 + 6a \right] + 15S_x^3. \tag{A3}$$

Let us now explicitly calculate the terms containing the threshold function. First, we have

$$-2\beta(1-c)[\langle x_i H(x_i-d) \rangle - \langle x_i \rangle \langle H(x_i-d) \rangle]$$

$$= -2\beta(1-c)\left[\int dx_1 dx_2 ... dx_N \frac{1}{N} \sum_i x_i H(x_i-d) p(x_1,...,x_N) - m_x \int dx_1 dx_2 ... dx_N \frac{1}{N} \sum_i H(x_i-d) p(x_1,...,x_N) \right] = ...$$

$$= -2\beta(1-c)\left[\int dx_1(x_1 - m_x) H(x_1-d) p(x_1) \right] = -2\beta(1-c)\sqrt{\frac{S_x}{2\pi}} \exp\left[-\frac{(d-m_x)^2}{2S_x} \right]. \tag{A4}$$

Note that the second term containing the threshold function has been evaluated in the main text, cf. Eq. (10).

Finally, let us address the term $\beta^2 \text{Var}[H(x_i - d)]$, which can be estimated by considering the associated expectation $\beta^2 \text{Var}[H(x_i - d)] \approx \beta^2 [\langle H(x_i - d)^2 \rangle - \langle H(x_i - d) \rangle^2]$. Applying the technique introduced in Sec. III, we obtain

$$E[\beta^2 H(x_i - d)^2] = \beta^2 \int dx_1 \int dx_2 ... \int dx_N \left[\frac{1}{N^2} \sum_i \sum_j H(x_i - d) H(x_j - d) \right] p(x_1, x_2, ..., x_N)$$

$$= \underbrace{\frac{\beta^2}{N^2} N \int dx_1 H(x_1 - d) p(x_1)}_{N \text{ cases where } i=j} + \underbrace{\frac{\beta^2}{N^2} N(N-1) \int dx_1 \int dx_2 H(x_1 - d) H(x_2 - d) p(x_1) p(x_2)}_{N(N-1) \text{ cases where } i \neq j}$$

$$= \frac{\beta^2}{2N} \left[1 - \text{Erf}\left(\frac{d - m_x}{\sqrt{2S_x}} \right) \right] + \frac{\beta^2}{4N^2} N(N-1) \left[1 - \text{Erf}\left(\frac{d - m_x}{\sqrt{2S_x}} \right) \right]^2 . \tag{A5}$$

Given that $\beta^2 \langle H(x_i - d) \rangle^2 = \frac{\beta^2}{4} [1 - \text{Erf}(\frac{d-m_x}{\sqrt{2S_x}})]^2$, one arrives at

$$\beta^2 \text{Var}[H(x_i - d)] = \frac{\beta^2}{4N} \left[1 - \text{Erf}\left(\frac{d - m_x}{\sqrt{2S_x}} \right) \right] \left[1 + \text{Erf}\left(\frac{d - m_x}{\sqrt{2S_x}} \right) \right] . \tag{A6}$$

This shows that the variance of the threshold function ultimately contributes to a finite-size effect which can be neglected in the thermodynamic limit.

[1] G. Buzsáki, *Rhythms of the Brain* (Oxford University Press, Oxford, 2009).
[2] A. Destexhe and D. Contreras, Science **314**, 85 (2006).
[3] C. Zhou, L. Zemanová, G. Zamora, C. C. Hilgetag, and J. Kurths, Phys. Rev. Lett. **97**, 238103 (2006).
[4] E. Bullmore and O. Sporns, Nat. Rev. Neurosci. **10**, 186 (2009).
[5] O. Sporns, D. Chialvo, M. Kaiser, and C. C. Hilgetag, Trends Cogn. Sci. **8**, 418 (2004).
[6] W. J. Freeman, *Neurodynamics: An Exploration in Mesoscopic Brain Dynamics* (Springer-Verlag, London, 2000).
[7] H. Liljenström, Scholarpedia **7**, 4601 (2012).
[8] G. Deco, V. K. Jirsa, P. A. Robinson, M. Breakspear, and K. Friston, PLoS Comput. Biol. **4**, e1000092 (2008).
[9] J. L. P. Velazquez and R. Wennberg, *Coordinated Activity in the Brain: Measurements and Relevance to Brain Function and Behavior* (Springer, New York, 2009).
[10] Y. Baibolatov, M. Rosenblum, Z. Z. Zhanabaev, M. Kyzgarina, and A. Pikovsky, Phys. Rev. E **80**, 046211 (2009).
[11] W. Gerstner, H. Sprekeler, and G. Deco, Science **338**, 60 (2012).
[12] *Lectures in Supercomputational Neuroscience: Dynamics in Complex Brain Networks*, edited by P. beim Graben, C. Zhou, M. Thiel, and J. Kurths (Springer-Verlag, Berlin, 2008).
[13] M. Breakspear, Nat. Neurosci. **20**, 340 (2017).
[14] W. J. Freeman, *Mass Action in the Nervous System: Examination of the Neurophysiological Basis of Adaptive Behavior through the EEG* (Academic Press, London, 1975).
[15] N. Fourcaud and N. Brunel, Neural Comput. **14**, 2057 (2002).
[16] S. El Boustani, and A. Destexhe, Neural Comput. **21**, 46 (2009).
[17] S. E. Folias and P. C. Bressloff, Phys. Rev. Lett. **95**, 208107 (2005).
[18] S. E. Folias and P. C. Bressloff, SIAM J. Appl. Math. **65**, 2067 (2005).
[19] C. R. Laing, W. C. Troy, B. Gutkin, and G. B. Ermentrout, SIAM J. Appl. Math. **63**, 62 (2002).
[20] P. C. Bressloff, Phys. Rev. E **82**, 051903 (2010).

[21] M. A. Buice and J. D. Cowan, Phys. Rev. E **75**, 051919 (2007).
[22] N. Brunel and V. Hakim, Neural Comput. **11**, 1621 (1999).
[23] H. Hasegawa, Phys. Rev. E **67**, 041903 (2003).
[24] N. F. Rulkov, Phys. Rev. E **65**, 041922 (2002).
[25] N. F. Rulkov, I. Timofeev, and M. Bazhenov, J. Comput. Neurosci. **17**, 203 (2004).
[26] D. Q. Wei and X. S. Luo, Europhys. Lett. **78**, 68004 (2007).
[27] Q. Y. Wang, Z. Duan, M. Perc, and G. Chen, Europhys. Lett. **83**, 50008 (2008).
[28] C. A. S. Batista, A. M. Batista, J. A. C. de Pontes, R. L. Viana, and S. R. Lopes, Phys. Rev. E **76**, 016218 (2007).
[29] B. Ibarz, J. M. Casado, and M. A. F. Sanjuán, Phys. Rep. **501**, 1 (2011).
[30] I. Franović and V. Miljković, Europhys. Lett. **92**, 68007 (2010).
[31] I. Franović and V. Miljković, Commun. Nonlinear Sci. Numer. Simul. **16**, 623 (2011).
[32] E. M. Izhikevich, Neural Comput. **18**, 245 (2006).
[33] E. M. Izhikevich and G. M. Edelman, Proc. Natl. Acad. Sci. U.S.A. **105**, 3593 (2008).
[34] B. Lindner, J. Garcia-Ojalvo, A. Neiman, and L. Schimansky-Geier, Phys. Rep. **392**, 321 (2004).
[35] I. Franović, K. Todorović, N. Vasović, and N. Burić, Phys. Rev. E **89**, 022926 (2014).
[36] I. Franović, K. Todorović, N. Vasović, and N. Burić, Phys. Rev. E **87**, 012922 (2013).
[37] I. Franović, K. Todorović, N. Vasović, and N. Burić, Chaos **22**, 033147 (2012).
[38] V. Klinshov and I. Franović, Phys. Rev. E **92**, 062813 (2015).
[39] M. A. Zaks, X. Sailer, L. Schimansky-Geier, and A. B. Neiman, Chaos **15**, 026117 (2005).
[40] B. Sonnenschein, M. A. Zaks, A. B. Neiman, and L. Schimansky-Geier, Eur. Phys. J. Special Topics **222**, 2517 (2013).
[41] O. V. Maslennikov and V. I. Nekorkin, Phys. Rev. E **90**, 012901 (2014).

[42] O. V. Maslennikov, D. V. Kasatkin, N. F. Rulkov, and V. I. Nekorkin, Phys. Rev. E **88**, 042907 (2013).

[43] O. V. Maslennikov, V. I. Nekorkin, and J. Kurths, Phys. Rev. E **92**, 042803 (2015).

[44] O. V. Maslennikov and V. I. Nekorkin, Commun. Nonlinear Sci. Numer. Simul. **23**, 10 (2015).

[45] V. I. Nekorkin and L. V. Vdovin, Izv. Vyssh. Uchebn. Zaved. Prikladn. Nelinejn. Din. **15**, 36 (2007).

[46] M. Courbage, V. I. Nekorkin, and L. V. Vdovin, Chaos **17**, 043109 (2007).

[47] O. V. Maslennikov and V. I. Nekorkin, Chaos **23**, 023129 (2013).

[48] O. V. Maslennikov and V. I. Nekorkin, Map-based approach to problems of spiking neural network dynamics, in *Nonlinear Dynamics and Complexity*, edited by V. Afraimovich, A. C. J. Luo, and X. Fu (Springer International, Switzerland, 2014), pp. 143–161.

[49] A. Destexhe and M. Rudolph-Lilith, *Neuronal Noise* (Springer, New York, 2012).

[50] I. A. Khovanov, A. V. Polovinkin, D. G. Luchinsky, and P. V. E. McClintock, Phys. Rev. E **87**, 032116 (2013).

[51] I. Franović, K. Todorović, M. Perc, N. Vasović, and N. Burić, Phys. Rev. E **92**, 062911 (2015).

[52] L. Arnold, *Random Dynamical Systems* (Springer Verlag, Berlin, 1999).

[53] J. A. Acebrón, A. R. Bulsara, and W.-J. Rappel, Phys. Rev. E **69**, 026202 (2004).

[54] M. Gaudreault, J. M. Berbert, and J. Viñals, Phys. Rev. E **83**, 011903 (2011).

[55] P. Kaluza, C. Strege, and H. Meyer-Ortmanns, Phys. Rev. E **82**, 036104 (2010).

[56] S. Tanabe and K. Pakdaman, Phys. Rev. E **63**, 031911 (2001).

[57] V. I. Nekorkin and O. V. Maslennikov, Radiophys. Quantum Electron. (Engl. Transl.) **54**, 56 (2011).

[58] M. Courbage, O. V. Maslennikov, and V. I. Nekorkin, Chaos Soliton. Fract. **45**, 645 (2012).

[59] O. V. Maslennikov and V. I. Nekorkin, Radiophys. Quantum Electron. (Engl. Transl.) **55**, 198 (2012).

[60] C. W. Gardiner, *Handbook of Stochastic Methods for Physics, Chemistry and the Natural Sciences*, 3rd ed. (Springer-Verlag, Berlin, 2004).

[61] *Phase Response Curves in Neuroscience: Theory, Experiment, and Analysis*, edited by N. W. Schultheiss, A. A. Prinz, and R. J. Butera (Springer, New York, 2012).

[62] P. A. Tass, *Phase Resetting in Medicine and Biology: Stochastic Modeling and Data Analysis* (Springer, Berlin, 2007).

[63] E. M. Izhikevich, *Dynamical Systems in Neuroscience: The Geometry of Excitability and Bursting* (MIT Press, Cambridge, 2007), Chap. 10.

[64] C. C. Canavier, Scholarpedia **1**, 1332 (2006).

Disordered configurations of the Glauber model in two-dimensional networks

IVA BAČIĆ[1], IGOR FRANOVIĆ[1] and MATJAŽ PERC[2,3,4]

[1] *Scientific Computing Laboratory, Center for the Study of Complex Systems, Institute of Physics Belgrade, University of Belgrade - Pregrevica 118, 11080 Belgrade, Serbia*
[2] *Faculty of Natural Sciences and Mathematics, University of Maribor - Koroška cesta 160, SI-2000 Maribor, Slovenia*
[3] *CAMTP – Center for Applied Mathematics and Theoretical Physics, University of Maribor - Mladinska 3, SI-2000 Maribor, Slovenia*
[4] *Complexity Science Hub - Josefstädterstraße 39, A-1080 Vienna, Austria*

Abstract – We analyze the ordering efficiency and the structure of disordered configurations for the zero-temperature Glauber model on Watts-Strogatz networks obtained by rewiring 2D regular square lattices. In the small-world regime, the dynamics fails to reach the ordered state in the thermodynamic limit. Due to the interplay of the perturbed regular topology and the energy neutral stochastic state transitions, the stationary state consists of two intertwined domains, manifested as multiclustered states on the original lattice. Moreover, for intermediate rewiring probabilities, one finds an additional source of disorder due to the low connectivity degree, which gives rise to small isolated droplets of spins. We also examine the ordering process in paradigmatic two-layer networks with heterogeneous rewiring probabilities. Comparing the cases of a multiplex network and the corresponding network with random inter-layer connectivity, we demonstrate that the character of the final state qualitatively depends on the type of inter-layer connections.

The interplay of local dynamics and the underlying network topology has been in the focus of research in physics and various interdisciplinary fields [1–3], having recently attracted considerable interest in the context of phase ordering processes [4–6]. The Ising-Glauber model [7] constitutes one of the paradigmatic models for analyzing such processes [8]. While it has been introduced to describe the nonequilibrium dynamical behavior of magnetic systems consisting of a large number of interacting particles, it has since been applied to a variety of other problems, including those in social sciences [9], geology [10], and electrochemistry [11].

Within the Glauber model, the spin variables can assume two discrete values, having the states of nodes evolve according to the local majority rule. The Glauber model was initially defined on a regular lattice [7]. Nevertheless, given that non-lattice topologies including random, scale-free [12] and small-world [13] networks are often better suited to describe real-world systems, the issue of Glauber dynamics on complex networks has been gaining

increasing attention [8,14–16]. Apart from such models, complexity of interactions in many real-world systems may also involve "networks of networks" featuring modular or multilayer architecture [17], the scenarios which have been much less explored in the framework of Glauber dynamics.

Our work addresses two problems of ordering in complex networks: i) the disordered states of the zero-temperature Glauber model on monolayer rewired networks, where we identify two types of disordered configurations, and ii) the ordering process on two-layer rewired networks, where we find that the ordering process is strongly affected by the type of inter-layer connections.

In case of the two-dimensional square lattice, when only interactions between four nearest neighbors are taken into account, see fig. 1(a), the zero-temperature Glauber dynamics is multistable [18]. In particular, the system either reaches the ground state for $\approx 2/3$ of all the process realizations, or ends up in the frozen striped state with probability $p_f \approx 1/3$. Concerning rewired square lattices with coordination number $\langle k \rangle = 4$, it has been shown that
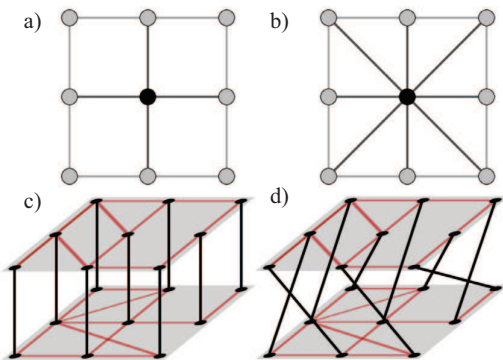
Fig. 1: (Color online) Considered network topologies. Panel (a) shows the scenario of a monolayer network with nearest-neighbor interactions ($k = 4$), whereas panel (b) shows the case where the next-nearest neighbor interactions are also included ($k = 8$). Panel (c) shows results for the multiplex two-layer network, whereas panel (d) shows results when there is random connectivity between the two layers.

the dynamics fails to reach the ground state [15,19], but little is known about the nature of the associated disordered configurations.

Our immediate goals are to understand why the Glauber model on small-world networks fails to reach ground state and to gain insight into the character of the disordered states on rewired networks with $\langle k \rangle = 4$ and $\langle k \rangle = 8$. We also study the ordering process on two-layer rewired networks with $\langle k \rangle = 4$, comparing the effects of different types of inter-layer connectivity, including multiplexing, see fig. 1(c), and the scenario with connections distributed between randomly selected pairs of nodes, cf. fig. 1(d).

Model. – In the Glauber model, the interactions are usually confined (but not necessarily restricted) to nearest-neighboring units. Incorporating higher-order competing (frustrated) interactions is one of the classical scenarios for the onset of new phases and potentially new types of phase transitions lying outside of Ising universality class. While the ferromagnetic interactions imposed by the model favor parallel alignment of spins, thermal noise prevents the system from reaching the ground state at any nonzero value of temperature. To avoid such stochastic effects which prevent full ordering, we consider systems quenched from an infinitely high temperature to absolute zero, in which spin states are initially uncorrelated and the net magnetization is vanishing. The Hamiltonian of the system is given by $H = -\sum_{\langle ij \rangle} J_{ij} S_i S_j$ where $S_i = \pm 1$ are Ising spin variables, the sum $\langle ij \rangle$ is over pairs of neighbors, and $J_{ij} > 0$ are ferromagnetic coupling constants, assumed to be uniform in our paper ($J_{ij} = J$). Each pair of parallel neighboring spins contributes $-J$ to the energy, while the contribution of antiparallel pairs is $+J$. Without loss of generality, we set $J = 1$ in the present study.

The state of the system evolves according to the majority rule applied to spins sequentially selected at random in each time step. This dynamical rule allows only energy lowering or the energy neutral state transitions. The former correspond to events where the spin variable is updated to the state prevalent in its local neighborhood, while the latter conform to scenario without a local majority, such that the given spin evolves stochastically with both orientations being equally likely.

Watts and Strogatz [13] have introduced an algorithm for generating small-world and random graphs by gradually rewiring a regular lattice. In their model, links from the regular lattice are chosen at random and replaced with new ones until a desired fraction of links p is rewired. Rewiring effectively introduces shortcuts between distant nodes, thereby drastically reducing the mean shortest path even in the limit $p \to 0$. By increasing the amount of disorder ($p \to 1$) one obtains a random network with the mean connectivity conserved. Small-world networks are generated by introducing an intermediate level of disorder ($0 < p \ll 1$), and are characterized by the high clustering coefficient and the short average path length. The former implies that neighboring nodes tend to group in well connected clusters, whereas the latter means that an arbitrary distant node can be reached by a small number of intermediate links.

We simulate Glauber dynamics of Ising spins on Watts-Strogatz rewired networks generated from two-dimensional regular $L \times L$ lattices with periodic boundary conditions. To understand the interplay between topological effects and the local majority dynamical rule, we vary several parameters in addition to L and the rewiring probability p, including the mean connectivity degree $\langle k \rangle$ and the initial magnetization m_0. As an additional ingredient, we also examine how the ordering process is affected by whether the Glauber dynamical rule allows for stochastic flipping or not. We refer to the rule without stochastic flipping as the modified Glauber rule.

To distinguish the influence of rewiring itself from the effect of connectivity of the network, we compare the results of simulations on networks with $\langle k \rangle = 4$ and $\langle k \rangle = 8$ in the small-world regime. We regard the next nearest neighbors as first neighbors in the topological sense by setting all interactions to be of equal strength. Assigning a finite value to the initial magnetization $m_0 \neq 0$ can be understood as introducing an initial bias toward local state clustering in the network. Modifying the Glauber dynamical rule by allowing state transitions only in the case of a strong local majority allows us to understand the effect of energy neutral processes on ordering in disordered topologies. In this scenario, nodes with an equal number of neighbors in both states are ignored when encountered during a trial rather than having their state determined stochastically. It turns out that the ground state is always reached on regular square lattices when a strong majority is necessary for state transition, *i.e.*, the striped state turns out to be the consequence of energy neutral stochastic flips.

To gain a more comprehensive insight into structure of the disordered configurations, we make a distinction between the domains comprised of topologically connected

nodes in the same state, and the clusters with respect to positions of the nodes on the original regular lattice. The lattice and the graph neighborhoods are always identical for spins placed on regular lattices. However, as the lattice structure is modified such that the links between neighbors are replaced by links to distant nodes, the lattice and the topological neighbors may not necessarily coincide, which results in rich patterns on the lattice. In order to investigate the crossover from frozen striped configurations occurring in regular lattices to disordered states occurring in the rewired lattices, we compare the correlation length ξ to characteristic graph length measures, namely the radius R, diameter D and the mean shortest path $\langle s \rangle$. The correlation length is defined as the decay rate of the two-point correlation function $G(l) = \langle S_i S_j \rangle - \langle S_i \rangle \langle S_j \rangle$ which measures the correlation of states as a function of the Manhattan distance l between the nodes. Note that ξ characterizes the competition between topology and dynamics on the state of distant nodes, while R, D and $\langle s \rangle$ are purely topological measures.

We also address the issue of how connecting two networks of the same size with different rewiring probabilities affects the ordering process. To do so, we compare the results obtained for the two-layer multiplex network (N bonds connecting nodes of two layers in one-to-one fashion) with the results for the case where the same number of inter-layer connections is distributed between randomly chosen pairs of nodes.

The main quantity of interest is the fraction of configurations that have not reached the ground state ("active configurations") f_a after a given simulation time T as a function of p. The absolute value of net magnetization $|m|$ is an order parameter for individual systems: $|m| = 1$ corresponds to the ground case, whereas $|m| = 0$ corresponds to the case in which there is an equal number of spins in both states. Thus, we measure the dependence of the final value of the magnetization $|m_f|$ in disordered configurations on p. However, $|m_f|$ contains no information about clustering in the network.

We simulate the dynamics on networks consisting of 50×50, 80×80 and 150×150 nodes for fixed values of N, $\langle k \rangle$, p and m_0. The total number of trials in each particular case is set to 1000. In summary, our numerical algorithm consists of the following steps:

I) *Regular network initialization.* Construct lattices with $k = 4$ or $k = 8$ as in fig. 1.

II) *Rewiring.* Following the method described in [15], our rewiring process ensures that there are no self-loops or multiple links between pairs of nodes, and that the minimal connectivity degree is 2. Bonds are sequentially selected at random and rewired with probability p until a desired fraction p of the total number of bonds is rewired.

III) *Spin state initialization.* The initial state is set by randomly putting each of the N spins into one of the possible states. If the initial magnetization is m_0, the state of each spin is set to $+1$ with the probability $p_{spin} = \frac{1+m_0}{2}$ and to -1 with probability $1 - p_{spin}$.

IV) *Glauber dynamics.* The evolution of the system is governed by the original or the modified (non-stochastic) Glauber dynamical rule, proceeding either until it reaches the ground state or until it fails to do so after a predetermined number of steps. We choose this value to be $T = 5000N$ (5000 attempted spin flips per node).

In what follows, we first analyze the case of a monolayer Watts-Strogatz network, and then consider the ordering process in paradigmatic two-layer networks with two types of inter-layer connections.

Monolayer networks. – Figure 2(a) shows how the fraction of active configurations f_a depends on p for Watts-Strogatz networks with local Glauber dynamics following a zero-temperature quench ($m_0 = 0$). The nonlinear dependence of f_a on p is observed regardless of $\langle k \rangle$, but turns out to be qualitatively different for the cases $\langle k \rangle = 4$ and $\langle k \rangle = 8$. When $\langle k \rangle = 8$, with increasing randomness ($p \gtrsim 0.5$), the dynamics leads to almost complete ordering. Nevertheless, when $\langle k \rangle = 4$, a finite fraction of configurations fails to reach the ground state in the thermodynamic limit over the whole range of p values. In the small-world regime, however, the ground state is not reached in the thermodynamic limit in either case. The result that ordering cannot be attained in small worlds when state transitions are governed by Glauber dynamics has been previously demonstrated for rewired rings ($d = 1$) and rewired square lattices ($d = 2$) with $\langle k \rangle = 4$ [15,19].

One infers that the local neighborhood majority rule with stochastic spin flips cannot lead to an ordered state on graphs with a perturbed regular topology. While the neighborhood from the regular lattice is mostly conserved in the small-world limit, R, D and $\langle s \rangle$ on the other hand monotonically decrease with p due to the presence of short-cuts (see fig. 3). Thus, it follows that perturbing the local neighborhood essentially leads to dynamical frustration of the local majority rule. A very small amount of topological disorder is sufficient to induce the critical slowing-down of dynamics, causing the disordered states to appear as deformed stripes on the lattice. Further deformation of the stripes leads to multiclustering on the lattice, which is reflected in the crossover effect [20]. We have established that this effect corresponds to the drop of ξ below the topological distances. At the same time, the low value of ξ indicates the absence of long-range ferromagnetic order. The two-point correlation function is found to satisfy an exponential scaling law $G(l) \propto e^{-\frac{l}{\xi}}$ over the whole range of p. Furthermore, depending on the p value, both ξ and R, D and $\langle s \rangle$ exhibit different scaling regimes.

In particular, in the small-world regime, $R, D, \langle s \rangle$ and ξ exhibit a power law dependence on p, $r \propto p^{-a}$ with $r \in \{R, D, \langle s \rangle, \xi\}$ and $a \in \{a_R, a_D, a_{\langle s \rangle}, a_\xi\}$. For 80×80
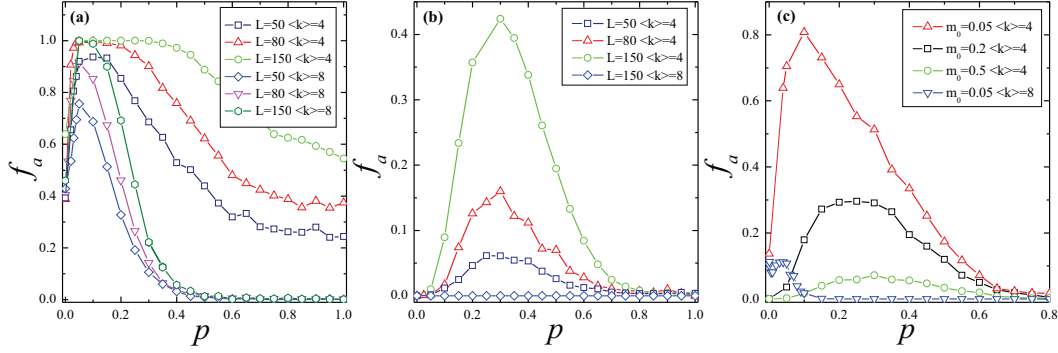
Fig. 2: (Color online) (a) Final fraction of active runs f_a in terms of rewiring probability p for the standard Glauber rule with $m_0 = 0$. The results are provided for networks with $\langle k \rangle = 4$ and $\langle k \rangle = 8$ neighbors and $L \in \{50, 80, 150\}$. Note that complete ordering is not observed in the small-world regime $0 < p \ll 1$ independent of $\langle k \rangle$. (b) Impact of modified Glauber rule: for $\langle k \rangle = 8$, the system reaches complete ordering (hence only the curve corresponding to $L = 150$ is shown), whereas for $\langle k \rangle = 4$, the frustration effect emerges at intermediate p, becoming more pronounced with the network size. Panel (c) displays f_a for systems governed by the standard Glauber rule starting from initial conditions $m_0 \neq 0$. The influence of small worldliness is such that it suppresses disorder regardless of $\langle k \rangle$ with increasing m_0, while it still promotes disorder at intermediate p range for $\langle k \rangle = 4$.
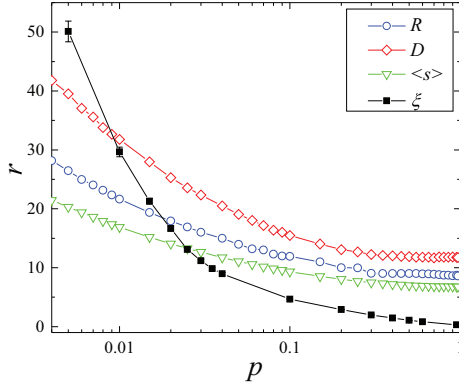
Fig. 3: (Color online) Correlation length ξ compared to graph distance measures (radius R, diameter D, and average path length $\langle s \rangle$) as functions of p. While ξ reflects the interplay between the dynamics and the network structure, the remaining quantities characterize purely topological features of the network. Crossing of $\xi(p)$ with other curves indicates the transition between the dynamics typical for the regular lattices and that for the rewired networks. Note that all four quantities exhibit a power law dependence $r \propto p^{-a}$ in the p region approximately coinciding with the small-world regime. The results refer to networks with 80×80 nodes and $\langle k \rangle = 4$.

networks, the following values for the exponent a are found: $a_R = -0.259 \pm 0.004$, $a_D = -0.296 \pm 0.005$, $a_{\langle s \rangle} = -0.25 \pm 0.003$ and $a_\xi = -0.77 \pm 0.01$. For larger values of p, the topological measures do not change significantly with increasing p indicating that topological effects remain the same after ≈ 0.5. Nevertheless, ξ decays to zero as $p \to 1$, which implies that the dynamics is sensitive to rewiring over the whole range of p, as corroborated by the growing number of "clusters" of decreased sizes in disordered configurations for large p, see fig. 4.

Interestingly, a deeper understanding of the difference in ordering efficiency in terms of p may be gained by

considering f_a for configurations governed by the modified Glauber rule. Evidently, the difficulty in attaining order subsides when stochasticity is eliminated from the dynamics in the small-world limit regardless of $\langle k \rangle$, see fig. 2(b). In other words, the ground state is reached with probability one if energy-neutral state transitions are not allowed. This always holds for $\langle k \rangle = 8$, and also for networks with $\langle k \rangle = 4$ in the limits $p \to 0$ and $p \to 1$. For intermediate p, ordering remains suppressed to a certain degree.

The next objective is to demonstrate that varying initial magnetization m_0 allows one to interpolate between the influences of dynamics and topology. Figure 2(c) shows f_a as a function of p for $m_0 \neq 0$ under the standard Glauber rule. While initial bias towards local clustering promotes complete ordering for regular networks, the dynamical outcome is different for rewired networks. In case $\langle k \rangle = 8$, small values of $m_0 \neq 0$ significantly increase ordering, whereby the position of the peak of $f_a(p)$ coincides with the peak value of $f_a(p)$ at $m_0 = 0$. Perturbing the quenched initial state on graphs in the small-world regime increases the prevalence of the ground state. Nevertheless, the peaks of $f_a(p)$ curves for $\langle k \rangle = 4$ networks in fig. 2(c) shift toward the peak value from fig. 2(b) as m_0 is increased. A fraction of configurations still fails to reach the ground state for some values of p, even for high values of m_0. The shift demonstrates that as the number of stochastic state transitions decreases due to the initial bias in clustering, the dynamical frustration is reduced. Nonetheless, the topological obstructions in networks with low $\langle k \rangle$ can suppress ordering even for high values of m_0.

Further insight on this issue can be gained by observing how $|m_f|$ averaged over active configurations depends on p, see fig. 5. The initial increase in magnetization corresponds to the divergence of relaxation time in the limit $p \to 0$, *i.e.*, the crossover from large-world to small-world behavior. Expectedly, there is a qualitative difference in
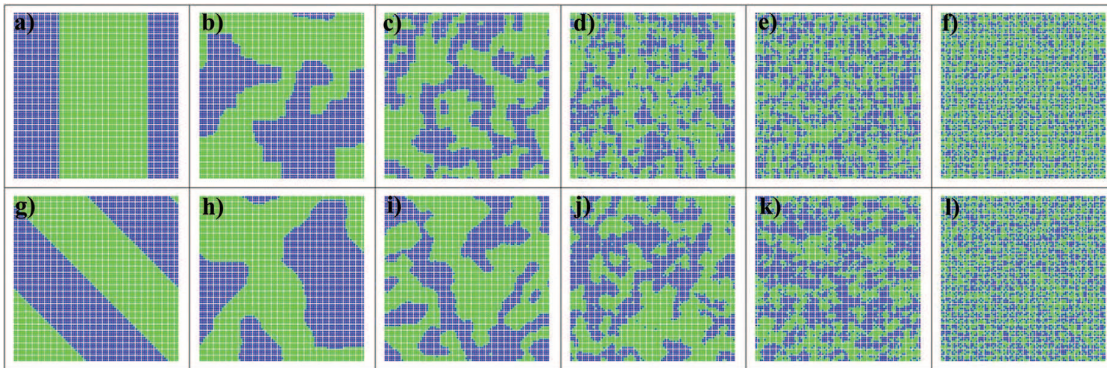
Fig. 4: (Color online) Snapshots of disordered configurations at $T = T_f$ on the lattice. The top (bottom) row refers to networks with $\langle k \rangle = 4$ ($\langle k \rangle = 8$). The rewiring probabilities are $p = 0$ in (a) and (g), $p = 0.02$ in (b) and (h), $p = 0.1$ in (c) and (i), $p = 0.3$ in (d) and (j), $p = 0.5$ in (e) and (k), as well as $p = 1$ in (f) and (l). The stripe structure is gradually lost with increasing p, giving way to the multiclustered states with respect to the original lattice. The number of domains increases with p as the network topology substantially departs from the lattice one. In terms of the network structure, each of the disordered configurations consists of two connected components. All the results are obtained for networks with 80×80 nodes.
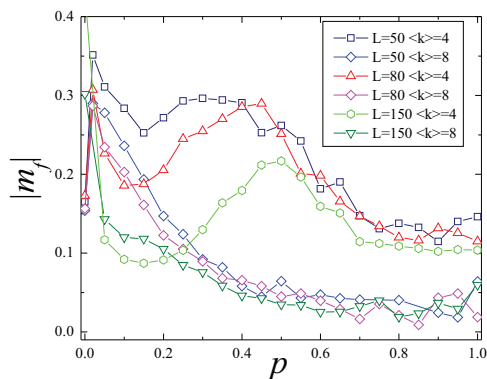
Fig. 5: (Color online) Final magnetization averaged over the ensemble of disordered configurations $|m_f|$ in dependence of p. For $\langle k \rangle = 8$, one finds approximately equal numbers of nodes in both states as $p \to 0$. For $\langle k \rangle = 4$, within the small-world regime, $|m_f|$ is reduced compared to the regular lattice, while for intermediate p, the droplet configurations lead to an increase of $|m_f|$. The peak of $|m_f|(p)$ gets shifted because the fraction of active runs is higher at a wider range of p values for larger networks, cf. fig. 2(a).

the $|m_f|(p)$ profile for different $\langle k \rangle$ under increasing p. The curves for $\langle k \rangle = 8$ monotonically decrease, indicating that the small number of configurations that does survive converges to a state consisting of a similar number of opposite spins in the limit $p \to 1$. In contrast, the initial decrease in $|m_f|$ for networks with $\langle k \rangle = 4$ is followed by the peak at intermediate values of p, associated to the presence of droplet configurations with $|m_f| \to 1$.

Moreover, we have verified that the disordered configurations in the small-world regime consist of two intertwined topological spin domains of almost similar size with stochastically fluctuating interfaces. An example of such a two-component state for $p = 0.1$ is provided in fig. 6, whereby the corresponding lattice domain configuration is shown in fig. 4(c). Blinkers that arise as a result of the
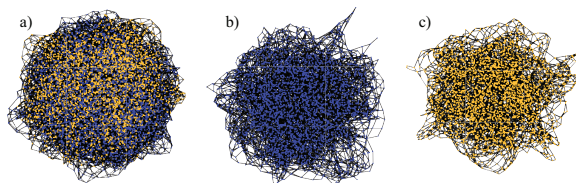

Fig. 6: (Color online) Example of a disordered configuration obtained for the network of size 80×80, with $\langle k \rangle = 4$ neighbors on average and $p = 0.1$ rewired links. (a) refers to the full configuration, whereas (b) and (c) show the larger component (3637 nodes) and the smaller component (2763 nodes), respectively. The final magnetization is $|m_f| \approx 0.14$. The nodes are separated into two domains of similar size, forming a multi-domain state on the lattice, cf. fig. 5(c).

long-range connections can be present along with stochastic flipping of interfaces on the lattice. Increasing p corresponds to the formation of domains with decreasing size with respect to the lattice. Several examples of configurations with two topological components for different p are shown in fig. 4. The number of these domains counted on the lattice grows exponentially with p (not shown). In the random network limit, as the fraction of links belonging to the original lattice $1 - p$ decreases, clusters become indistinguishable when observed on the lattice. Topologically, the two-domain configuration is reminiscent of the disordered configurations of the voter model on small-world networks [8,21]. Once the dynamics cannot cause further decrease in energy, the interface length reaches a constant value, as interface diffusion is no longer possible. In this scenario, while a fraction of nodes with even connectivity degrees continues to flip indefinitely with no energy cost, the states of the odd-degree nodes become stationary.

Nevertheless, the disordered configurations associated to the increase of f_a in fig. 2(b) for $\langle k \rangle = 4$ are frozen at very high values of $|m_f|$, viz. $|m_f| \to 1$ in
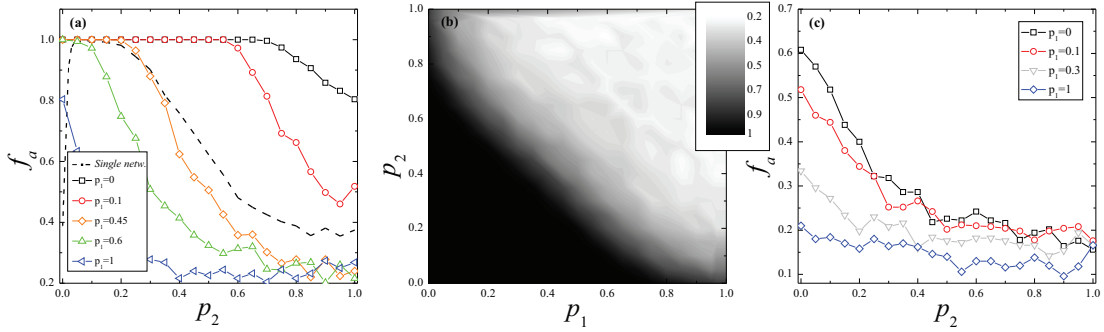
Fig. 7: (Color online) (a) Ordering in two-layer multiplex networks: f_a for the layer with rewiring probability p_1 (see the legend) in terms of the rewiring probability p_2 of the other layer. For comparison, the results for the single (monolayer) network are indicated by the dashed line. (b) f_a of a single layer of a multiplex network as a function of p_1 and p_2. The states of two layers are strongly correlated, but the ordering is completely inhibited in the small-world regime. (c) f_a of a layer of the network with random inter-layer connectivity. Ordering is significantly improved for all values of p. All the results are obtained for networks with 80×80 nodes and $\langle k \rangle = 4$.

the thermodynamic limit, and correspond to *absorbing* states of the network. These configurations result from low connectivity and consist of a tiny fraction of spins isolated in small domains surrounded by the "sea" of nodes of the opposite orientation. In this scenario, nodes with small k form stable droplets of opposing magnetization which cannot be dynamically influenced by the nodes from the rest of the network, preventing the system from reaching the full order. These droplets may appear on the remnants of the regular lattice, such that their interior consists of nodes connected by links from the regular lattice ($k = 4$), whereas their boundary is mainly comprised of nodes with one removed link ($k = 3$), thereby trapping the "interior" in the same state. Even-degree nodes that appear on the boundaries have more links with nodes within the droplet than with other neighbors, such that their state cannot be changed either. With further rewiring of the lattice, stable droplets may still form as even smaller groups of interconnected nodes with small degrees ($k = 2$ or $k = 3$), likewise disconnected from the rest of the network. The larger the network, the more likely becomes such a scenario. Also, for larger network sizes, a larger number of droplets may be present, which is the reason why a larger fraction of configurations fails to reach order. This peculiar frustration on the remnants of a regular lattice also accounts for the incomplete ordering of systems governed by the standard Glauber dynamics in rewired networks with $\langle k \rangle = 4$, and explains for the difference in the behavior in the limit $p \to 1$. Final configurations in networks with $\langle k \rangle = 4$ can consist of two large components and a few isolated droplets for p above the small-world regime, similar to final configurations obtained for $m_0 \neq 0$.

Two-layer networks. – We now address the ordering process in multilayer networks, focussing on the paradigmatic example of two coupled $\langle k \rangle = 4$ networks with different rewiring probabilities p_1 and p_2. By our

algorithm, the individual layers are rewired consecutively, after which N links are introduced between them, either at random or with the one-to-one correspondence between the layers' nodes. The simulation is terminated after $2T$ steps if order is not reached. Note that introducing new links effectively generates a large network with $\langle k \rangle = 5$ and $5N$ bonds.

Our findings indicate that both cases lead to highly correlated states of layers, which are simultaneously ordered/disordered and have $m_{f1} \approx m_{f2}$. For this reason, f_a of a single layer presents an appropriate quantity to characterize the ordering process. We find that the dependence of f_a on rewiring probability changes qualitatively depending on the nature of the inter-layer bonds, cf. fig. 7(a) and fig. 7(c). The multiplex configuration turns out to suppress ordering of both networks in the small-world regime, as indicated in fig. 7(a) and fig. 7(b). However, fig. 7(a) shows that ordering efficiency can be increased if at least one of the networks is "sufficiently random", with a smooth transition taking place at $0.35 \lesssim p \lesssim 0.45$. Interestingly, the other scenario, which involves placing the same number of bonds between randomly chosen pairs of nodes from both networks, promotes both ordering and correlation between the layer states. This is corroborated by fig. 7, suggesting that regardless of p_1 and p_2, ordering in this case is significantly improved compared to that on a single network and the multiplex network.

The curves obtained for multiplex networks resemble the ones obtained for the single network even for p as large as 0.6, while those obtained for random inter-layer connections are monotonically decreasing as p_2 is increased over the whole range of p. Even though in both cases networks become correlated in terms of m_f and ordering, multiplexing seems to preserve the type of dynamics obtained on small-world structures of one network, while introducing random bonds between the layers destroys the small-worldliness effect.

Conclusions. – We have analyzed ordering efficiency of the Glauber model of Ising spin kinetics on the Watts-Strogatz networks obtained by rewiring from the two-dimensional square lattices with coordination numbers $\langle k \rangle = 4$ and $\langle k \rangle = 8$. We have extended the previous results concerning the failure of such systems to reach the ground state in the small-world regime $0 < p \ll 1$, gaining insight into the associated disordered configurations. The fraction of active configurations exhibits a nonlinear dependence on the rewiring probability. It is interesting that a similar type of dependence has been observed in relation to the synchronization process on small-world networks [22]. It is found that the Glauber dynamics on small-world networks becomes stuck in metastable stationary active configurations, which consist of two intertwined domains of opposite spins, whereby the fraction of nodes on the interfaces flips indefinitely. This effect is manifested as clustering patterns in the lattice representation. The size of domains on the lattice becomes smaller as p is increased. We have demonstrated that the limiting value of p at which the number of lattice and topological domains is equal (to two) corresponds to the value where the correlation length ξ becomes smaller than the average path length in the network.

Our analysis shows that the active configurations in the small-world regime emerge when the perturbed regular topology constrains the number of possible energy lowering processes, while the stochastic energy-neutral spin-flipping processes contribute to dynamical frustration and trap the system in a set of metastable states with the same energy. While the ground state is not accessible because energy lowering processes are not possible, the energy-neutral processes allow for the transitions between states of the same energy. This is similar to what has been reported for Glauber dynamics on 3D regular lattices [23], Glauber dynamics on random graphs [8], and the voter model on small-world networks [21].

We have further demonstrated that there exists a finite probability of finding another type of disordered configuration in networks with low connectivity for intermediate values of p. These are frozen, almost completely ordered states with a few isolated droplets of opposing magnetization. For $\langle k \rangle = 8$, such configurations become unlikely due to the high average connectivity degree in the network, giving way to fully ordered states if p is sufficiently increased ($p > 0.5$). In networks with $\langle k \rangle = 4$, a certain fraction of configurations exists as a combination of these states, especially if an initial bias towards clustering ($m_0 \neq 0$) is introduced.

We have also examined the features of the ordering process in paradigmatic two-layer networks. It has been found that the structure of inter-layer connections strongly affects the ordering process. In particular, multiplexing decreases ordering efficiency in the small-world regime $0 < p \ll 1$, but improves it if the rewiring probability in both layers is sufficiently high. Nevertheless, random connectivity between the layers always promotes ordering, regardless of layer topology. In all the considered scenarios, the layers typically end up in highly correlated states.

We believe that the future research may be directed towards extending our findings on the dynamics of interacting rewired networks. In particular, it could be interesting to modify inter-layer coupling strengths, vary the number of connections between the layers or consider hierarchical networks and networks with a large number of layers.

$* * *$

REFERENCES

[1] STROGATZ S., *Nature*, **410** (2001) 268.
[2] ALBERT R. and BARABÁSI A.-L., *Rev. Mod. Phys.*, **74** (2002) 47.
[3] BOCCALETTI S., LATORA V., MORENO Y., CHAVEZ M. and HWANG D.-U., *Phys. Rep.*, **424** (2006) 175.
[4] BRAY A. J., *Adv. Phys.*, **51** (2002) 481.
[5] CASTELLANO C., *Rev. Mod. Phys.*, **81** (2009) 591.
[6] PASTOR-SATORRAS R., CASTELLANO C., VAN MIEGHEM P. and VESPIGNANI A., *Rev. Mod. Phys.*, **87** (2015) 925.
[7] KRAPIVSKY P. L., REDNER S. and BEN-NAIM E., *A Kinetic View of Statistical Physics* (Cambridge University Press, Cambridge) 2010.
[8] CASTELLANO C., LORETO V., BARRAT A., CECCONI F. and PARISI D., *Phys. Rev. E*, **71** (2005) 066107.
[9] STAUFFER D., *Am. J. Phys.*, **76** (2008) 470.
[10] GANGULY J., *Advances in Physical Geochemistry: Diffusion, Atomic Ordering, and Mass Transport* (Springer, New York) 2012.
[11] BOSCO E., *J. Electroanal. Chem.*, **346** (1993) 433.
[12] BARABÁSI A.-L. and ALBERT R., *Science*, **286** (1999) 509.
[13] WATTS D. J. and STROGATZ S. H., *Nature*, **393** (1998) 440.
[14] CASTELLANO C. and PASTOR-SATORRAS R., *J. Stat. Mech.* (2006) P05001.
[15] HERRERO C. P., *J. Phys. A: Math. Theor.*, **42** (2009) 415102.
[16] BAEK Y., HA M. and JEONG H., *Phys. Rev. E*, **85** (2012) 031123.
[17] BOCCALETTI S. *et al.*, *Phys. Rep.*, **544** (2014) 1.
[18] SPIRIN V., KRAPIVSKY P. L. and REDNER S., *Phys. Rev. E*, **65** (2001) 016119.
[19] BOYER D. and MIRAMONTES O., *Phys. Rev. E*, **67** (2003) 035102.
[20] BARTHÉLÉMY M. and AMARAL L. A. N., *Phys. Rev. Lett.*, **82** (1999) 3180.
[21] CASTELLANO C., VILONE D. and VESPIGNANI A., *Europhys. Lett.*, **63** (2003) 153.
[22] GRABOW C., HILL S. M., GROSSKINSKY S. and TIMME M., *Europhys. Lett.*, **90** (2010) 48002.
[23] SPIRIN V., KRAPIVSKY P. L. and REDNER S., *Phys. Rev. E*, **63** (2001) 036118.

Regular Article

Noise-induced switching in two adaptively coupled excitable systems

Iva Bačić[1], Serhiy Yanchuk[2], Matthias Wolfrum[3], and Igor Franović[1,a]

[1] Scientific Computing Laboratory, Center for the Study of Complex Systems, Institute of Physics Belgrade, University of Belgrade, Pregrevica 118, 11080 Belgrade, Serbia
[2] Institute of Mathematics, Technische Universität Berlin, Straße des 17. Juni 136, 10623 Berlin, Germany
[3] Weierstrass Institute, Mohrenstrasse 39, 10117 Berlin, Germany

Abstract. We demonstrate that the interplay of noise and plasticity gives rise to slow stochastic fluctuations in a system of two adaptively coupled active rotators with excitable local dynamics. Depending on the adaptation rate, two qualitatively different types of switching behavior are observed. For slower adaptation, one finds alternation between two modes of noise-induced oscillations, whereby the modes are distinguished by the different order of spiking between the units. In case of faster adaptation, the system switches between the metastable states derived from coexisting attractors of the corresponding deterministic system, whereby the phases exhibit a bursting-like behavior. The qualitative features of the switching dynamics are analyzed within the framework of fast-slow analysis.

1 Introduction

In many complex systems, ranging from biology, physics and chemistry to social sciences and engineering, the interaction patterns are not static, but are rather affected by the states of constituent units [1–4]. This gives rise to complex feedback mechanisms, where the coupling weights adapt to dynamical processes at the units, which in turn influences the evolution of units itself. Modeling of such systems is based on the paradigm of adaptive networks, where self-organization unfolds both at the level of coupling weights and the collective states of the units, typically involving a separation of characteristic timescales. The faster and the slower timescales are naturally associated to the dynamics of units and couplings, respectively, such that the short-term evolution of the units occurs on a quasi-static network, whereas the slow changes in coupling weights depend on the time-averaged dynamics of the units. An important example of adaptive connectivity is provided by neuronal systems, where the strength of synaptic couplings is adjusted to the underlying spiking activity via spike-time-dependent plasticity (STDP), a temporally asymmetric form of Hebbian learning [5],

---

a e-mail: franovic@ipb.ac.rs

promoting causal relationship between the spikes of pre- and postsynaptic neurons [6–8].

Motivated by the research on neuronal systems, in the present paper we study a simplified model which incorporates the basic ingredients of neurodynamics, such as excitability, plasticity and noise. The considered system consists of two adaptively coupled active rotators, whose intrinsic dynamics is set to excitable regime and subjected to noise. The plasticity rule is introduced in such a way that one may continuously interpolate between the coupling dynamics characteristic to Hebbian learning and STDP. We demonstrate that the interplay of plasticity and noise may facilitate two qualitatively different forms of slow stochastic fluctuations, depending on the adaptation rate. While for slower adaptation the self-organized dynamics consists of switching between the two modes of noise-induced oscillations, in case of faster adaptation, the switching dynamics comprises metastable states associated to attractors of the deterministic system.

In the context of neuroscience, one may compare the considered system to a binary neuron motif. It is well known that the same structural motif, defined at the level of anatomy, can support multiple functional motifs [9–12], characterized by different weight configurations and potentially distinct directions of information flow. In these terms, our study will show that the co-effect of plasticity and noise may (i) contribute to the emergence of different functional motifs on top of the given structural one and (ii) trigger slow alternation between the functional motifs.

So far, the co-effects of noise and the STDP plasticity rule have been analyzed in systems of two coupled neural oscillators, as well as in networks of oscillators. In case of two units, multistability between different weight configurations has been found, surprisingly indicating that noise may stabilize configurations of strong bidirectional coupling absent in the deterministic system [13]. At variance with this, our study concerns excitable local dynamics and explicitly addresses the slow stochastic fluctuations between metastable states. For networks of adaptively coupled neural or phase oscillators, the previous research has mainly focused on the impact of plasticity on the synchronization behavior. In the absence of noise, several generic forms of macroscopic dynamics have been identified, including desynchronized or partially synchronized states with weak couplings, as well as cluster states [14–18]. In presence of noise, an interesting effect of self-organized noise resistance to desynchronization has been reported in the case of a network of neural oscillators [19]. In networks of excitable units, the STDP rule has been shown to give rise to oscillating coupling configurations that facilitate switching between strongly and weakly synchronized states [20–22].

The paper is organized as follows. The details of the model are introduced in Section 2. An overview of the underlying deterministic dynamics, characterizing the impact of plasticity on the stationary states and the onset of emergent oscillations, is provided in Section 3. Section 4 is dedicated to a fast–slow analysis of the deterministic dynamics, whereas in Section 5 are explained the features of the two generic types of switching behavior. In Section 6 we provide a summary of our main results.

2 Model

We consider a system of two stochastic active rotators interacting by adaptive couplings, where the dynamics of the phases $\{\varphi_1(t), \varphi_2(t)\}$ and the coupling weights $\{\kappa_1(t), \kappa_2(t)\}$ is given by

$$
\begin{aligned}
\dot{\varphi_1} &= I_0 - \sin \varphi_1 + \kappa_1 \sin (\varphi_2 - \varphi_1) + \sqrt{D}\xi_1 \\
\dot{\varphi_2} &= I_0 - \sin \varphi_2 + \kappa_2 \sin (\varphi_1 - \varphi_2) + \sqrt{D}\xi_2 \\
\dot{\kappa_1} &= \epsilon(-\kappa_1 + \sin(\varphi_2 - \varphi_1 + \beta)) \\
\dot{\kappa_2} &= \epsilon(-\kappa_2 + \sin(\varphi_1 - \varphi_2 + \beta)),
\end{aligned}
\tag{1}
$$

where $\varphi_1, \varphi_2 \in S^1$, while κ_1 and κ_2 are real variables. The rotators are assumed to be identical, having their local dynamics governed by the excitability parameter I_0, which gives rise to a SNIPER bifurcation at $I_0 = 1$. We focus on the excitable regime, such that $I_0 = 0.95$ is kept fixed throughout the paper. In this case, the uncoupled system always converges to a steady state, whereas the collective dynamics emerges due to interaction and noise. The parameter $\epsilon \ll 1$ defines the scale separation between the fast dynamics of the phases and the slow dynamics of adaptation. White noise of variance D acts only within the subspace of fast variables, whereby the terms $\xi_1(t)$ and $\xi_2(t)$ are independent $(\xi_i(t)\xi_j(t') = \delta_{ij}\delta(t - t')$ for $i, j \in \{1, 2\})$. In the context of neuroscience, I_0 can be interpreted as external bias current, whereas the impact of stochastic terms is analogous to that of synaptic noise. Note that the deterministic version of (1) is symmetric with respect to the exchange of indices $1 \leftrightarrow 2$.

The plasticity rule is controlled by the parameter β, which allows one to interpolate between the different adaptation modalities. The analogy between the adaptivity dynamics in classical neuronal systems and the systems of coupled phase oscillators has been addressed in [14,23,24], whereas a deeper analysis of the correspondence between the phase-dependent plasticity rules and the STDP has been provided in [13]. From these studies, it follows that the scenario found for $\beta = 3\pi/2$, where the stationary weights increase for smaller phase differences and decrease for larger ones ("like-and-like" form of behavior), qualitatively resembles the Hebbian learning rule [23,24]. Nevertheless, in the case $\beta = \pi$, the two coupling weights always change in opposite directions, which may be interpreted as promoting an STDP-like plasticity rule. In the present paper, we are interested in the β interval between these two limit cases, since it admits two coexisting excitable fixed points.

3 Deterministic dynamics of the full system

In this section, we analyze the details of the *deterministic* dynamics of the full system (1), considering first the stationary states and the associated excitability feature, and then focusing on the scenario that gives rise to emergent oscillations.

3.1 Stationary states and excitable dynamics

Fixed points $(\varphi_1^*, \varphi_2^*, \kappa_1^*, \kappa_2^*)$ of the complete system (1) for $D = 0$ are given by the solutions of the following set of equations:

$$\sin\varphi_1^* - \sin(\varphi_2^* - \varphi_1^* + \beta)\sin(\varphi_2^* - \varphi_1^*) = I_0,$$
$$\sin\varphi_2^* - \sin(\varphi_1^* - \varphi_2^* + \beta)\sin(\varphi_1^* - \varphi_2^*) = I_0, \tag{2}$$

with

$$\kappa_1^* = \sin(\varphi_2^* - \varphi_1^* + \beta),$$
$$\kappa_2^* = \sin(\varphi_1^* - \varphi_2^* + \beta). \tag{3}$$

Equation (2) can be solved numerically for any fixed parameter set, or numerical path-following can be applied in order to study the dependence of the fixed points on the parameters.

The bifurcation diagram in Figure 1 shows how the number and stability of fixed points of the full system change with β. In particular, depending on β, there may be two, four or six fixed points. Due to symmetry, the solutions always appear in pairs of points sharing the same stability features. Since our study concerns plasticity rules which support excitable fixed points, we have confined the analysis to the interval $\beta \in (3.298, 4.495)$, where the system has *two stable* fixed points, which lie off the synchronization manifold $\varphi_1 = \varphi_2$. Apart from that, there are also four unstable
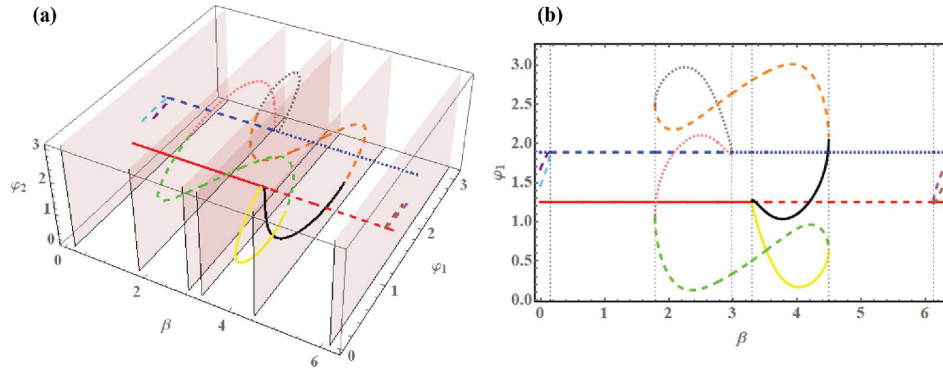
Fig. 1. (a) Bifurcation diagram for the fixed points of system (1) with $D = 0$ in the $(\beta, \varphi_1, \varphi_2)$ space. (b) Projection of the bifurcation diagram to (β, φ_1) plane. The two fixed points independent on β belong to the synchronization manifold: the red (blue) one is always longitudinally stable (unstable). The solid lines denote stable fixed points, whereas the dashed and dotted lines denote saddles of unstable dimension 1 and 2, respectively.

fixed points. The bifurcations associated to the boundaries of the given β interval are as follows: at $\beta = 3.298$ the system undergoes a supercritical symmetry-breaking pitchfork bifurcation where a symmetry related pair of two stable fixed points off the synchronization manifold is created, whereas at $\beta = 4.495$, this pair meets another pair of unstable fixed points off the synchronization manifold such that both are annihilated in symmetry related inverse saddle-node bifurcations. For instance, at $\beta = 4.1$, one finds the symmetry related pair of stable foci given by $(\varphi_1, \varphi_2, \kappa_1, \kappa_2) = (1.177, 0.175, 0.032, -0.92)$ and $(\varphi_1, \varphi_2, \kappa_1, \kappa_2) = (0.175, 1.177, -0.92, 0.032)$. Note that these weight levels support effective master-slave configurations, where one unit exerts a much stronger influence on the other unit than vice versa.

The two stable asymmetric fixed points in the interval $\beta \in (3.298, 4.495)$ are excitable, and may exhibit several different types of response to external perturbations, see the classification in Figure 2. Introducing the perturbations by setting different initial conditions, we plot in Figure 2 the phase dynamics in the fast subspace while keeping the weights (κ_1, κ_2) fixed. Note that in the case where both units respond with a single spike, the order of firing is such that the unit with larger initial phase $\varphi_i(0), i \in \{1, 2\}$ fires first.

3.2 Onset of oscillations

The onset of emergent oscillations in system (1) with $D = 0$ depends on the interplay between the plasticity rule, specified by β, and the speed of adaptation, characterized by ϵ. A parameter scan indicating the variation of κ_1, $A_{\kappa_1} = \max(\kappa_1(t)) - \min(\kappa_1(t))$ in terms of (β, ϵ) is shown in Figure 3a. The results are obtained by numerical continuation beginning from a stable periodic solution, such that the final state reached for a certain set of (β, ϵ) values provides the initial conditions for the simulation of the system at incremented parameter values. By this method, we have determined the maximal stability region of the periodic solution.

One finds that for a fixed β, there actually exists an interval of timescales separation $\epsilon \in (\epsilon_{min}, \epsilon_{max})$ admitting oscillations, cf. Figure 3b. The periodic solutions in this interval coexist with the two symmetry-related stable stationary states. One observes that the threshold ϵ_{min} reduces with β, whereas the upper boundary value ϵ_{max} grows with increasing β. The detailed bifurcation mechanisms behind the onset
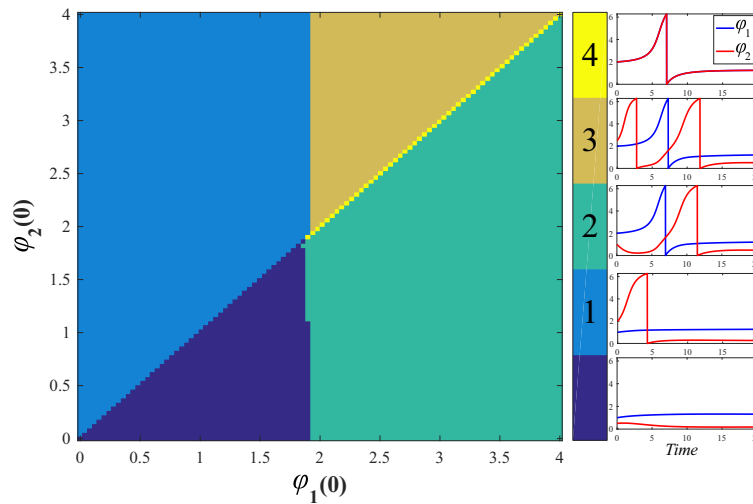
Fig. 2. Modalities of the response to external perturbation for system (1) with $D = 0$. The system parameters are $I_0 = 0.95$, $\epsilon = 0.01$ and $\beta = 4.212$, whereas the initial conditions for the coupling weights are set to $\kappa_1(0) = -0.0077$, $\kappa_2(0) = -0.846$. Depending on the initial phases $(\varphi_1(0), \varphi_2(0))$, one may observe the following regimes: (0) no spikes; (1) the unit with larger $\varphi(0)$ emits one spike and the other does not; (2) both units emit a single spike, with the unit with larger $\varphi(0)$ firing first; (3) the unit with larger $\varphi(0)$ emits two spikes and the other unit emits one; (4) both units spike synchronously.

of oscillations and multistability are beyond the scope of this paper, and essentially involve an interplay between the fast and slow variables.

Enhancing ϵ under fixed β gives rise to a supercritical symmetry-breaking pitchfork bifurcation of limit cycles, indicated by PFL in Figure 3b. Below the bifurcation, the phases $\varphi_1(t)$ and $\varphi_2(t)$ maintain a small phase-shift, while the oscillation profiles $\kappa_i(t), i \in \{1, 2\}$ are rather different, see Figures 3d and 3e, respectively. Above the bifurcation, the system gains the anti-phase space-time symmetry $\varphi_1(t) = \varphi_2(t + T/2), \kappa_1(t) = \kappa_2(t + T/2)$ where T denotes the oscillation period, cf. the associated waveforms in Figures 3g and 3f.

4 Slow-fast analysis of the deterministic dynamics

The deterministic dynamics in case of slow adaptation, corresponding to a strong timescale separation between the fast and slow variables, may be analyzed within the framework of standard fast-slow analysis. In general, one may either consider the layer problem, defined on the fast timescale, or the reduced problem, which concerns the slow timescale. Within the layer problem, the aim is to determine the fast flow dynamics $\varphi_1(t; \kappa_1, \kappa_2), \varphi_2(t; \kappa_1, \kappa_2)$ by treating the slow variables κ_1 and κ_2 as parameters, whereas the reduced problem consists in determining the dynamics of the slow flow $(\kappa_1(t), \kappa_2(t))$ (reduced flow) assuming that the fast flow of the layer problem is either at a stable equilibrium or at the averaged value of a stable regime.

In this section, we first investigate the fast layer problems. Depending on the values of the slow variables (κ_1, κ_2), the fast flow can exhibit several attractors, such that multiple sheets of the slow flow emerge from the averaged dynamics on the different attractors of the fast flow.
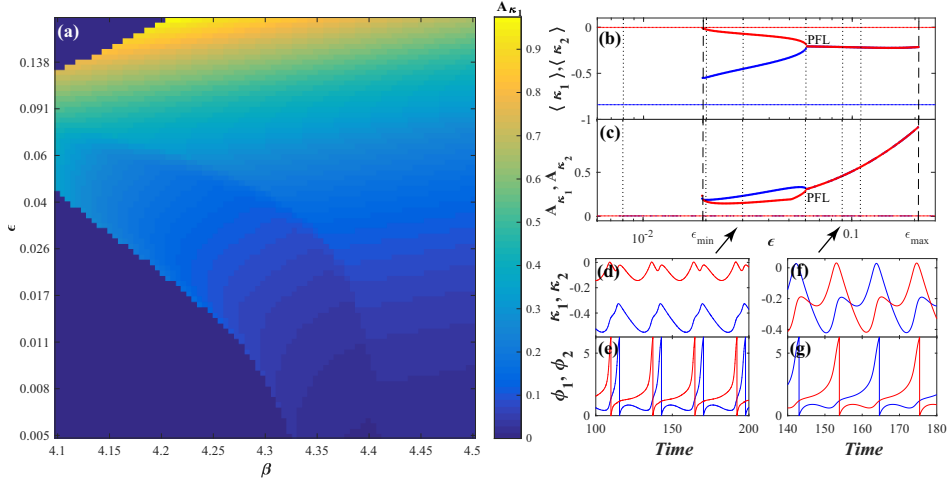
Fig. 3. Onset of oscillations in the full system (1) for $D = 0$. In panel (a) is shown how the variation A_{κ_1} of coupling weight κ_1 changes in the (β, ϵ) plane. Panel (b) shows how the mean coupling weights $\langle \kappa_1 \rangle$ and $\langle \kappa_2 \rangle$ of oscillatory states (thick lines) change with ϵ under fixed $\beta = 4.212$. The thin solid lines indicate the stationary state. In panel (c) are plotted the analogous dependencies for variation of the oscillation. The dotted lines in (b) and (c) indicate the ϵ values corresponding to the time traces in Figure 7, whereas the dashed lines indicate the boundaries of the ϵ region supporting the stable periodic solutions. The symmetry-breaking pitchfork bifurcation of limit cycles is denoted by PFL. In panels (d)–(g) are shown the waveforms of periodic solutions without and with the anti-phase space-time symmetry, obtained for $\epsilon = 0.03$ and $\epsilon = 0.09$, respectively (see the arrows). The excitability parameter is fixed to $I_0 = 0.95$.

4.1 Dynamics of the fast flow

Within the layer problem, one studies the dynamics of the fast variables

$$
\begin{aligned}
\dot{\varphi}_1 &= I_0 - \sin \varphi_1 + \kappa_1 \sin (\varphi_2 - \varphi_1) \\
\dot{\varphi}_2 &= I_0 - \sin \varphi_2 + \kappa_2 \sin (\varphi_1 - \varphi_2),
\end{aligned}
\tag{4}
$$

where $\kappa_1, \kappa_2 \in [-1, 1]$ are considered as additional system parameters. Formally, system (4) is obtained by setting $\varepsilon = 0$ in (1) for $D = 0$.

The numerically obtained bifurcation diagram in Figure 4a shows that the fast flow is monostable for most of the (κ_1, κ_2) values, possessing either an equilibrium or a limit cycle attractor. The stability boundary of the periodic solution (red curves) has been obtained by the method of numerical continuation where, beginning from a stable periodic solution, the initial conditions for incremented parameter values are given by the final state reached for the previous set of (β, ϵ) values. The coexistence between a stable fixed point, lying on the synchronization manifold, and a limit cycle is found within a small region near the diagonal, see Figure 4a. Let us first classify the fixed points of the fast flow and then examine the scenarios that give rise to oscillations.

It can be shown that the fast flow admits either two or four fixed points, with the associated regions indicated in Figure 4b. In particular, two fixed points FP1 and FP2 on the synchronization manifold are *independent* on κ_1 and κ_2. They are given by $(\varphi_1^*, \varphi_2^*) = (\arcsin I_0, \arcsin I_0)$ and $(\varphi_1^*, \varphi_2^*) = (\pi - \arcsin I_0, \pi - \arcsin I_0)$. One may also find two additional fixed points off the synchronization manifold, referred
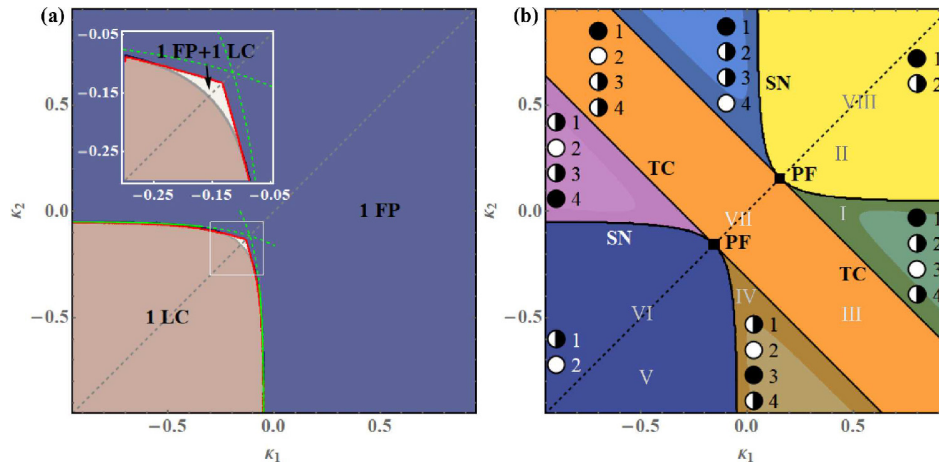
Fig. 4. (a) Attractors of the fast flow (4) in terms of κ_1 and κ_2, now considered as parameters. The fast flow is typically monostable, supporting either a stable fixed point (FP) or a stable limit cycle (LC), apart from a small region around the main diagonal, where it exhibits bistable behavior. The green dashed curves indicate approximations of two branches of SNIPER bifurcations, obtained by the method described in the text. The red lines correspond to the numerically determined stability boundaries of the oscillatory solution. (b) Classification of the fixed points of the fast flow (4). The fixed points are labeled the same way as in the main text, with their stability indicated as follows: full circles denote stable fixed points, semi-full circles represent saddle points and white circles correspond to doubly unstable fixed points. Within the four light-shaded triangular-shaped regions, the doubly unstable fixed point is a focus, rather than a node. The notation I–VIII refers to parameter values corresponding to the phase portraits in Figure 5.

to as FP3 and FP4 in Figure 4b. The bifurcations affecting the number and stability of the fixed points, beginning from the lower left region of the (κ_1, κ_2) plane, can be summarized as follows. Along the main diagonal $\kappa_1 = \kappa_2$, we find two points of supercritical pitchfork bifurcations (PF), where from the symmetric fixed points the saddles FP3 and FP4 appear and disappear. Off the main diagonal, the pitchforks are unfolded into curves of saddle-node (SN) and transcritical bifurcations (TC), see Figure 4b.

The (κ_1, κ_2) region featuring stable oscillations almost completely matches the lower left domain admitting two unstable fixed points. Within this region, each periodic solution obtained for (κ_1, κ_2) above the main diagonal $\kappa_1 = \kappa_2$ has a counterpart in the domain below the main diagonal, related to it by the exchange symmetry of units indices. Typically, the periodic solutions emerge via SNIPER bifurcations, comprising two branches where either κ_1 or κ_2 remain almost constant and close to zero. In both cases, the two fixed points that collide and disappear are FP3 and FP4. Nevertheless, such scenarios cannot be maintained in the small (κ_1, κ_2) region admitting coexistence between a fixed point and a limit cycle, because the SNIPER bifurcation is accompanied by a change in the number of fixed points. Our findings suggest that near the main diagonal, the limit cycle emerges via a heteroclinic bifurcation, where an orbit connects two saddles lying off the synchronization manifold (not shown). Note that the orbit of the limit cycle follows the unstable manifold of the saddle point FP2 on the synchronization manifold. To the left or the right of the main diagonal, instead of a heteroclinic bifurcation, one finds homoclinic bifurcations, whereby a saddle point, either FP3 or FP4, touches the limit cycle orbit. The schematic phase portraits indicating the stable and unstable manifolds of the fixed points and the limit
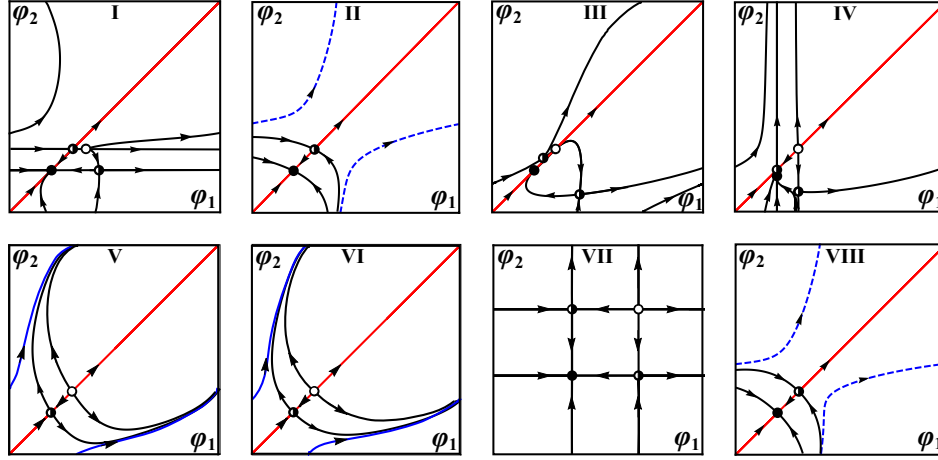
Fig. 5. Schematic phase portraits corresponding to the characteristic regimes of the fast flow. The panels I–VIII refer to representative parameter values indicated in Figure 4b. Also, the stability of fixed points is presented the same way as in Figure 4b. The invariant synchronization manifold is denoted by the red color, whereas the orbit of a stable/unstable limit cycle is indicated by the solid/dashed blue lines.

cycle for the characteristic regimes of the fast flow, denoted by I–VIII in Figure 4b, are illustrated in Figure 5.

The two branches of SNIPER bifurcations may readily be approximated for small values of κ_1 and κ_2 by a simple scheme, which amounts to reducing the fast flow to a normal form of saddle-node bifurcation. Suppose first that $\kappa_1 \ll 1$ and $I_0 - 1 \ll 1$. More specifically, let $\xi \ll 1$ be a small parameter such that $I_0 - 1 = \xi$ (close to the threshold) and $\kappa_1 = \gamma\xi$, i.e. γ is a rescaling parameter of κ_1, allowing for a zoom in the neighborhood of zero. Then, the steady states are given by the system

$$1 + \xi - \sin\varphi_1 + \xi\gamma\sin(\varphi_2 - \varphi_1) = 0,$$
$$1 + \xi - \sin\varphi_2 + \kappa_2\sin(\varphi_1 - \varphi_2) = 0. \tag{5}$$

The first equation in the zeroth order approximation leads to $\varphi_1 = \pi/2$. Hence, using the perturbation approach, we have

$$\varphi_1^* = \frac{\pi}{2} + \sqrt{\xi}\Psi_1 + \cdots; \quad \varphi_2^* = \Psi_2 + \cdots, \tag{6}$$

where the $\sqrt{\xi}$ scaling follows from the Taylor expansion of the function $\sin\varphi_1$ at $\pi/2$. Inserting (6) into (5), one obtains the system of equations for Ψ_1 and Ψ_2

$$1 + \frac{1}{2}\Psi_1^2 - \gamma\cos\Psi_2 = 0,$$
$$1 - \sin\Psi_2 + \kappa_2\cos\Psi_2 = 0. \tag{7}$$

From system (7), it is not difficult to see that the saddle-node bifurcation takes place if the condition $1 - \gamma\cos\Psi_2 = 0$ is satisfied. This leads to the parametric representation $\kappa_1 = \xi\gamma = \frac{I_0 - 1}{\cos\Psi_2}, \kappa_2 = \frac{\sin\Psi_2 - 1}{\cos\Psi_2}$, of the saddle-node curve for small κ_1 values, where Ψ_2 plays the role of the parameter along the curve. An analogous approach may be used to capture the second branch of saddle-node bifurcations, cf. the green dashed lines in Figure 4a.

4.2 Dynamics of the slow flow

We have numerically obtained the dynamics of the slow flow by applying a two-step approach. First, for fixed values (κ_1, κ_2), we determine the time-averaged dynamics of the fast flow (4), $\langle \varphi_2 - \varphi_1 \rangle_t = f(\kappa_1, \kappa_2)$. Here, the averaging $\langle \cdot \rangle_t$ is performed over a sufficiently large time interval, having eliminated a transient. Hence, this average depends on the attractor of the fast flow for the given (κ_1, κ_2). In particular, if the fast flow possesses a stable fixed point, then $\langle \varphi_2 - \varphi_1 \rangle_t = \varphi_2^* - \varphi_1^*$, where $(\varphi_1^*, \varphi_2^*)$ is a solution of

$$I_0 - \sin \varphi_1^* + \kappa_1 \sin (\varphi_2^* - \varphi_1^*) = 0$$
$$I_0 - \sin \varphi_2^* + \kappa_2 \sin (\varphi_1^* - \varphi_2^*) = 0. \tag{8}$$

This procedure just results in determining the slow critical manifold of the system. In case when the attractor of the fast flow is periodic, $\langle \varphi_2 - \varphi_1 \rangle_t$ presents the time average over the period. Averaging approximation in case of a periodic attractor of the fast flow constitutes a standard approach [13,25], rather natural for describing the influence of oscillations in the fast flow on the dynamics of the slow flow. At the second stage, the obtained time-averages are substituted into the dynamics of the weights

$$\dot{\kappa}_1 = \epsilon[-\kappa_1 + \sin(f(\kappa_1, \kappa_2) + \beta)]$$
$$\dot{\kappa}_2 = \epsilon[-\kappa_2 + \sin(-f(\kappa_1, \kappa_2) + \beta)]. \tag{9}$$

The system (9) is used to determine the vector field of the slow flow by taking into account only the attractors of the fast flow, such that the vector field associated to each attractor is plotted within its respective stability region, cf. Figure 6.

In regions of the (κ_1, κ_2) plane where there are coexisting stable solutions of the fast flow, the corresponding vector field of the slow flow is given on multiple overlapping sheets, since the value of the average $f(\kappa_1, \kappa_2)$ depends on the initial conditions. In our case, this occurs only in a small region of coexistence between an equilibrium and a stable limit cycle.

One should single out two important features of the slow flow: (i) it exhibits two symmetry-related fixed points in the green and blue regions in Figure 6, and (ii) the slow vector field is pointed in opposite directions close to the boundary between the fast oscillatory regime (orange region) and the steady states of the fast flow (blue, green and white regions). The latter in particular implies that interesting effects occur close to the border of the oscillatory and the steady state regime of the fast flow. Moreover, adding noise gives rise to fluctuations around this boundary, which leads to switching between the quasi-stationary and the fast spiking dynamics. Such effects are studied in more detail within the next section.

5 Switching dynamics

Our main observation in this section is that the interplay of plasticity and noise induces slow stochastic fluctuations (switching dynamics), mediating two qualitatively different scenarios depending on the speed of adaptation. The latter include (i) switching between two modes of *noise-induced* oscillations for slower adaptation (small $\epsilon \simeq 0.01$) and (ii) switching between multiple coexisting attractors of the deterministic dynamics for faster adaptation (intermediate $\epsilon \simeq 0.05$).

In case (i), the impact of noise is twofold: on a short timescale, it gives rise to spiking dynamics, whereas on a long time scale, it induces random transitions between
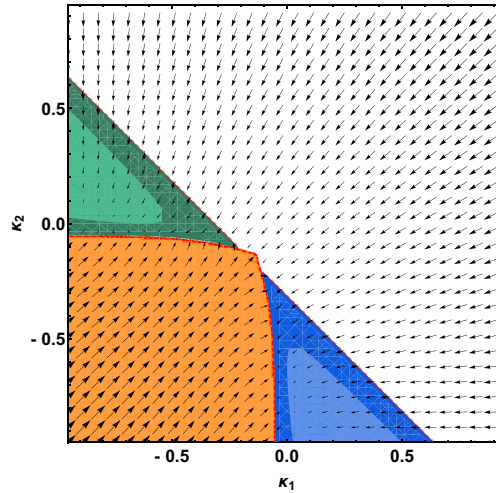
Fig. 6. Vector field of the slow flow obtained by taking into account only stable attractors of the fast flow for $\beta = 4.212, I_0 = 0.95$. The color coding is as follows: orange color denotes the region associated to the stable limit cycle of the fast flow, white stands for the stable fixed point of the fast flow FP1, whereas blue and green color correspond to the two stable fixed points FP3 and FP4. Within the light-shaded regions, FP3 and FP4 are foci rather than nodes, cf. Figure 4b.

the two oscillatory modes. In case (ii), the switching dynamics comprises metastable states derived from two fixed points, as well as two limit cycles associated to emergent oscillations of the corresponding deterministic system. The key difference between the effects (i) and (ii) is that for slower adaptation, the system switches between the oscillatory modes that do not exist as deterministic attractors. Moreover, the two generic types of switching are characterized by distinct phase dynamics: for slower adaptation, one finds alternation of patterns with different order of spiking between the units, whereas for faster adaptation, the phases effectively exhibit bursting behavior, involving a succession between episodes of spiking and relative quiescence. An overview on how the typical dynamics of couplings changes with ϵ at fixed β is provided in Figure 7. Note that the difference between the average coupling weights of the stable periodic solutions of the deterministic system are much smaller than a typical distance between the coupling levels for the stationary states. The prevalence of metastable states is affected by ϵ so that intermediate adaptation favors oscillatory modes, whereas the fast adaptation apparently promotes the two quasi-stationary states. In the next two subsections, we provide further insight into the mechanisms behind the switching dynamics using the results of the fast-slow analysis.

5.1 Switching dynamics under slow adaptation

As already indicated, ϵ is here taken sufficiently small, such that it cannot facilitate emergent oscillations in the full system (1). For $\epsilon \simeq 0.01$ and under appropriate noise levels, one observes noise-induced oscillations [26]. The latter arise via a scenario involving a multiple-timescale stochastic bifurcation, whereby noise acts only within the fast subsystem of (1). The onset of oscillations under increasing D occurs in two stages. In the first stage, the phase dynamics gradually exhibits more induced spikes,
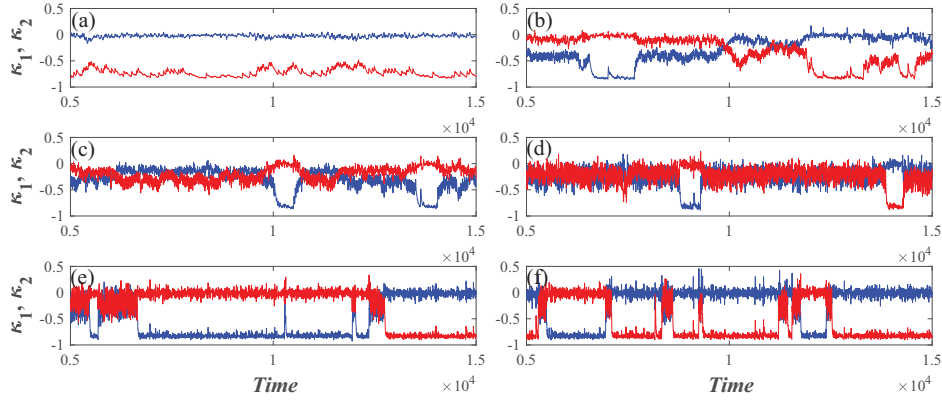
Fig. 7. Switching dynamics under variation of ϵ. The time traces $(\kappa_1(t), \kappa_2(t))$ are obtained for fixed $I_0 = 0.95$, $D = 0.006$, $\beta = 4.212$, whereas ϵ assumes the following values: (a) $\epsilon = 0.008$, (b) $\epsilon = 0.02$, (c) $\epsilon = 0.03$, (d) $\epsilon = 0.06$, (e) $\epsilon = 0.09$, (f) $\epsilon = 0.11$.
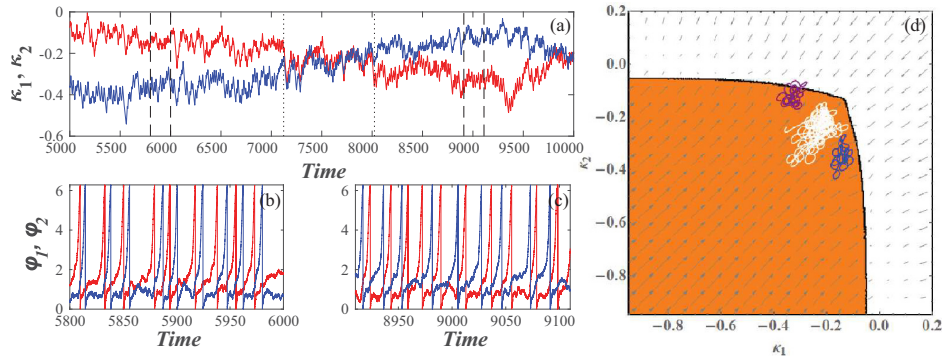

Fig. 8. Switching dynamics between the two modes of noise-induced oscillations. Time traces of the weights are shown in panel (a), whereas panel (b) and (c) display the corresponding time traces of the phases during the intervals between the dashed lines in panel (a). In panel (d), the $(\kappa_1(t), \kappa_2(t))$ projections of the orbits associated to each of the two modes (blue color), as well as the switching episode, shown in white, are superimposed to the vector field of the slow flow from Figure 6. The shaded area corresponds to the stable limit cycle. The system parameters are $I_0 = 0.95, \beta = 4.212, \epsilon = 0.01, D = 0.009$.

such that the stationary distributions of phases eventually acquire a longer tail reflecting the occurrence of spikes (not shown). Nevertheless, the stationary distributions $P(\kappa_i)$ change appreciably only at the second stage, which takes place for sufficiently large D. Such a change accompanies the emergence of coupling oscillations. Note that the system (1) actually exhibits *two modes* of noise-induced oscillations, characterized by the different order of firing between the two units, cf. the time traces of phase dynamics and the associated evolution of couplings in Figure 8a.

It is interesting to examine whether the vector field of the slow flow from Section 4.2 can be used to explain the slow stochastic fluctuations of the coupling weights. To this end, we have superimposed the $(\kappa_1(t), \kappa_2(t))$ orbits of the two noise-induced modes, as well as a switching episode, to a vector field of the slow flow from Figure 6. Note that the orbits typically lie close to the boundary outlining the transition between the two attractors of the fast flow, featuring non-negligible coupling weights. Moreover, the two modes are confined to small areas of the (κ_1, κ_2) plane
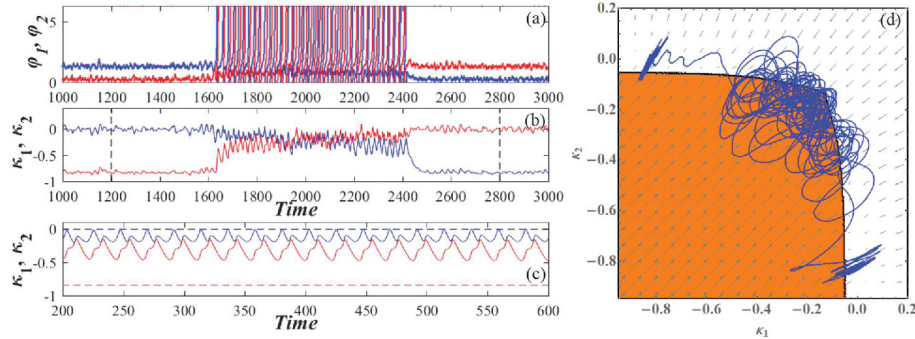
Fig. 9. Time traces of the phases (a) and weights (b) associated to noise-induced switching between the coexisting attractors of the deterministic system. The results are obtained for $I_0 = 0.95, \beta = 4.212, \epsilon = 0.05, D = 0.004$. In panel (c) is provided the deterministic dynamics of weights obtained for the same parameter values. In panel (d), the $(\kappa_1(t), \kappa_2(t))$ orbit corresponding to the interval between the dashed lines in (b) is super-imposed on the vector field of the slow flow cf. Figure 6.

symmetrical with respect to the main diagonal $\kappa_1 = \kappa_2$, whereas the switching episode virtually takes place on the diagonal. Apparently, the noise-induced modes occupy regions where the oscillations in the fast flow emerge via homoclinic bifurcations, rather than the SNIPER scenario. Nonetheless, the switching episode seems to involve the domain featuring coexistence of the two stable sheets of the slow vector field. Within these sheets, which correspond to two attractors of the fast flow (a stable node and a stable limit cycle), the vector fields are oriented in opposite directions, thereby contributing to switching.

5.2 Switching dynamics for faster adaptation

In case of faster adaptation associated to intermediate ϵ, the switching dynamics involves four metastable states, derived from the attractors of the deterministic system. The deterministic multistable behavior includes two symmetry-related stationary states, as well as two symmetry-related limit cycles. Note that while the two stable steady states exist for arbitrary small ϵ and are therefore visible in the slow flow in Figure 6, the oscillatory solutions disappear for small ϵ and hence cannot be observed in the slow flow. The two oscillatory regimes are characterized by the same phase shift, but the reverse order of firing between the two units. Influenced by noise, the phases effectively engage in bursting behavior, manifesting slow stochastic fluctuations between episodes of intensive spiking activity and periods of relative quiescence, see Figure 9a. For a fixed noise level, the prevalence of metastable states, defined by transition probabilities between them, changes with adaptation speed. One observes that for $\epsilon \simeq 0.05$, the oscillatory dynamics is preferred, whereas for $\epsilon \simeq 0.1$, the quasi-stationary states are more ubiquitous.

A comparison of the (κ_1, κ_2) orbits displaying switching dynamics and the vector field of the slow flow from Figure 6 again shows that the former is confined to the criticality region at the boundary between the stationary and oscillatory regimes in the fast flow, cf. Figure 9. One should remark on how the transitions between the different metastable states take place. In particular, from Figure 9b, it is clear that there can be no direct transitions between the two quasi-stationary states, but they rather have to be mediated by the system passing through the oscillatory states. Also, the transition from oscillatory to quasi-stationary states typically occurs

once the couplings approach a master-slave-like configuration, where the coupling in one direction is much stronger than the other one. This scenario coincides with the SNIPER bifurcation of the fast flow described in Section 4.1. The scenario of transition between the two metastable oscillatory states resembles closely the one from Section 5.2.

6 Summary

In the present study, we have analyzed a system of two adaptively coupled active rotators with excitable intrinsic dynamics, demonstrating that the interplay of plasticity and noise may give rise to slow stochastic fluctuations. Two qualitatively different types of self-organized behavior have been identified, depending on the adaptation speed. For slower adaptation, the switching dynamics consists of an alternation between two modes of noise-induced oscillations, associated to a preferred order of spiking between the two units. In this case, noise plays a twofold role: on one hand, it perturbs the excitable local dynamics giving rise to oscillations on a short timescale, whereas on the other hand, it elicits the alternation between the two oscillatory states on a long timescale. The underlying phase dynamics shows slow switching between two patterns distinguished by the different order in which the units are spiking. In case of faster adaptation, the coupling becomes capable of eliciting emergent oscillations in the deterministic system [27]. The latter then exhibits complex multistable behavior, involving two stationary and two oscillatory regimes. Under the influence of noise, the system undergoes switching between these four different metastable states, whose prevalence at fixed noise level depends on the speed of adaptation. The deterministic attractors associated to metastable states are related by the Z_2 symmetry. Thus, a mismatch in excitability parameters would lead to symmetry-breaking, whereby a small mismatch would induce a bias in switching dynamics, whereas a larger mismatch, corresponding to a scenario with one excitable and one oscillatory unit, would completely alter the observed dynamics.

Though the underlying phenomena are not found in the singular limit of infinite scale separation, the fast-slow analysis we have applied still allows one to explain the qualitative features of both considered types of switching behavior. Studying the layer problem, and in particular the vector field of the slow flow, has enabled us to gain insight into the metastable states and the transitions between them. It has been demonstrated that the coupling dynamics is always in a state of "criticality", being confined to the boundary between the stationary and oscillatory regimes of the fast flow.

Given that excitability, plasticity and noise are inherent ingredients of neuronal systems, the obtained results can be interpreted in the context of neuroscience. It is well known that the backbone of neural networks is made up of binary and ternary neuron motifs, whereby the structural motifs typically support multiple functional motifs, essentially characterized by the weight configuration and the underlying direction of the information flow. With this in mind, the scenario of switching under slow adaptation may be important, because it implies that a binary motif can display slow alternation between two effectively unidirectional weight configurations, promoting opposite direction of information flow. For faster adaptation, one finds multistability between unidirectional coupling and bidirectional coupling of moderate strength. Nonetheless, the underlying phase dynamics, if extended to networks, may be considered as a paradigm for UP-DOWN states, typical for cortical dynamics [28,29]. Thus, it would be of interest to examine the impact of plasticity in networks of noisy excitable units, where one may expect different types of emergent behavior, such as cluster, non-synchronized and partially synchronized states, depending on the frustration of local dynamics and the impact of noise.

Author contribution statement

I.F. and S.Y. conceived the model and defined the analysis of noise-induced switching as the main goal of the research. S.Y. and M.W. developed the general framework to investigating the deterministic fast-slow problem and the bifurcation analysis of the associated reduced systems. I.B. obtained all the numerical results, whereas I.B. and I.F. carried out the bifurcation analysis, identified the two types of noise-induced switching behavior and made the main contribution to writing the manuscript. All the authors discussed the findings and participated in interpretation of the results.

References

1. F. Sorrentino, E. Ott, Phys. Rev. Lett. **100**, 114101 (2008)
2. F. Vazquez, V.M. Eguiluz, M.S. Miguel, Phys. Rev. Lett. **100**, 108702 (2008)
3. N. Caporale, Y. Dan, Ann. Rev. Neurosci. **31**, 25 (2008)
4. C. Furusawa, K. Kaneko, Phys. Rev. Lett. **90**, 088102 (2003)
5. D.O. Hebb, *The Organization of Behavior: a Neuropsychological Approach* (John Wiley & Sons, New York, 1949)
6. S. Song, K.D. Miller, L.F. Abbott, Nat. Neurosci. **3**, 919 (2000)
7. R.C. Froemke, Y. Dan, Nature (London) **416**, 433 (2002)
8. H.-X. Wang, R.C. Gerkin, D.W. Nauen, G.-Q. Bi, Nat. Neurosci. **8**, 187 (2005)
9. O. Sporns, R. Kotter, PLoS Biol. **2**, e369 (2004)
10. I. Franović, V. Miljković, Chaos Soliton. Fract. **44**, 122 (2011)
11. I. Franović, V. Miljković, Chaos Soliton. Fract. **45**, 527 (2012)
12. I. Franović, V. Miljković, EPL **92**, 68007 (2011)
13. L. Lücken, O.V. Popovych, P.A. Tass, S. Yanchuk, Phys. Rev. E **93**, 032210 (2016)
14. Y.L. Maistrenko, B. Lysyansky, C. Hauptmann, O. Burylko, P.A. Tass, Phys. Rev. E **75**, 066207 (2007)
15. P. Seliger, S.C. Young, L.S. Tsimring, Phys. Rev. E **65**, 041906 (2002)
16. M. Li, S. Guan, C.-H. Lai, New J. Phys. **12**, 103032 (2010)
17. P.S. Skardal, D. Taylor, J.G. Restrepo, Physica D **267**, 27 (2014)
18. D. Kasatkin, S. Yanchuk, E. Schöll, V. Nekorkin, Phys. Rev. E **96**, 062211 (2017)
19. O.V. Popovych, S. Yanchuk, P.A. Tass, Sci. Rep. **3**, 2926 (2013)
20. K. Mikkelsen, A. Imparato, A. Torcini, Phys. Rev. Lett. **110**, 208101 (2013)
21. D. Millman, S. Mihalas, A. Kirkwood, E. Niebur, Nat. Phys. **6**, 801 (2010)
22. A. Levina, J.M. Hermann, T. Geisel, Phys. Rev. Lett. **102**, 118110 (2009)
23. T. Aoki, T. Aoyagi, Phys. Rev. Lett. **102**, 034101 (2009)
24. T. Aoki, T. Aoyagi, Phys. Rev. E **84**, 066109 (2011)
25. A. Shilnikov, Int. J. Bifurc. Chaos **18**, 2141 (2008)
26. S.-J. Wang, G. Ouyang, J. Guang, M. Zhang, Phys. Rev. Lett. **116**, 018101 (2016)
27. Q. Ren, K.M. Kolwankar, A. Samal, J. Jost, Phys. Rev. E **86**, 056103 (2012)
28. T.T.G. Hahn, J.M. McFarland, S. Berberich, B. Sakmann, M.R. Mehta, Nat. Neurosci. **15**, 1531 (2012)
29. V.V. Vyazovskiy, K.D. Harris, Nat. Rev. Neurosci. **14**, 443 (2013)

Inverse stochastic resonance in a system of excitable active rotators with adaptive coupling

Iva Bačić[1], Vladimir Klinshov[2], Vladimir Nekorkin[2], Matjaž Perc[3] and Igor Franović[1(a)]

[1] *Scientific Computing Laboratory, Center for the Study of Complex Systems, Institute of Physics Belgrade,*
University of Belgrade - Pregrevica 118, 11080 Belgrade, Serbia
[2] *Institute of Applied Physics of the Russian Academy of Sciences - 46 Ulyanov Street,*
603950 Nizhny Novgorod, Russia
[3] *Faculty of Natural Sciences and Mathematics, University of Maribor - Koroška cesta 160,*
SI-2000 Maribor, Slovenia

Abstract – Inverse stochastic resonance is a phenomenon where an oscillating system influenced by noise exhibits a minimal oscillation frequency at an intermediate noise level. We demonstrate a novel generic scenario for such an effect in a multi-timescale system, considering an example of emergent oscillations in two adaptively coupled active rotators with excitable local dynamics. The impact of plasticity turns out to be twofold. First, at the level of multiscale dynamics, one finds a range of intermediate adaptivity rates that give rise to multistability between the limit cycle attractors and the stable equilibria, a condition necessary for the onset of the effect. Second, applying the fast-slow analysis, we show that the plasticity also plays a facilitatory role on a more subtle level, guiding the fast flow dynamics to parameter domains where the stable equilibria become focuses rather than nodes, which effectively enhances the influence of noise. The described scenario persists for different plasticity rules, underlying its robustness in the light of potential applications to neuroscience and other types of cell dynamics.

Introduction. – Noise in coupled excitable or bistable systems may induce two types of generic effects [1]. On the one hand, it can modify the deterministic behavior by acting non-uniformly on different states of the system, thus amplifying or suppressing some of its features. On the other hand, noise may give rise to completely novel forms of behavior, typically based on crossing the thresholds or separatrices, or involving enhanced stability of deterministically unstable structures. In neuronal systems, the constructive role of noise at different stages of information processing, referred to as "stochastic facilitation" [2,3], mainly comprises resonant phenomena. A classical example is the stochastic resonance [4], which allows for the detection of weak subthreshold periodic signals. A more recent development concerns the effect of inverse stochastic resonance (ISR) [3,5–12], where noise selectively reduces the spiking frequency of neuronal oscillators, converting the tonic firing into intermittent bursting-like activity or a short-lived transient followed

by a long period of quiescence. The name of the effect should be taken *cum grano salis*, because in contrast to stochastic resonance, it involves no additional external signal: one rather observes a non-monotonous dependence of the spiking rate on noise variance, whereby the oscillation frequency becomes minimal at a preferred noise level. Such an inhibitory effect of noise has recently been shown for cerebellar Purkinje cells [11], having explicitly demonstrated how the lifetimes of the spiking ("up") and the silent ("down") states [13–15] are affected by the noise variance. ISR has been indicated to play important functional roles in neuronal systems, including the reduction of spiking frequency in the absence of neuromodulators, suppression of pathologically long short-term memories, triggering of on-off tonic spiking activity and even optimization of information transfer along the signal propagation pathways [3,7,9,11].

So far, theoretical studies on ISR have mostly concerned the scenario where a single neuron exhibits bistable deterministic dynamics, featuring coexistence between a limit cycle and a stable equilibrium. Such bistability is

---

typical for Type-II neurons below the subcritical Hopf bifurcation, *e.g.*, classical Hodgkin-Huxley and Morris-Lecar models [3,6–8]. There, applying noise induces switching between the metastable states, but at an intermediate noise level, one surprisingly finds a strong asymmetry of the associated switching rates, which makes the periods spent in the vicinity of equilibrium much longer than the periods of spiking activity.

An important open problem concerns conditions giving rise to ISR in coupled excitable systems, where noise influences the emergent oscillations. Here we address in detail this issue, as it may be crucial to understanding the prevalence of the effect in neural networks, whose activity depends on the interplay of excitability, coupling properties and noise. Synaptic dynamics typically involves the plasticity feature, which makes self-organization in neuronal systems a multi-timescale process: the short-term spiking activity unfolds on a quasi-static coupling configuration, while the slow adjustment of coupling weights depends on the time-averaged evolution of units.

Motivated by the findings in neuroscience, we focus on the onset of ISR in a simplified, yet paradigmatic system of two adaptively coupled stochastic active rotators with excitable local dynamics. Active rotators are canonical for Type-I excitability and may be seen as equivalent to the theta-neuron model. Adaptivity is introduced in a way that allows continuous interpolation between a spectrum of plasticity rules, including Hebbian learning and spike-time-dependent plasticity (STDP) [16–18].

We demonstrate a generic scenario for the plasticity-induced ISR, where the system's multiscale structure, defined by the adaptivity rate, plays a crucial role. On a basic level, plasticity gives rise to multistable behavior involving coexisting stationary and oscillatory regimes. An additional subtlety, which we show by the fast-slow analysis, is that the plasticity promotes the resonant effect by guiding the fast flow toward the parameter region where the stable fixed points are focuses rather than nodes.

The paper is organized as follows. In the next section the details of the model and the numerical bifurcation analysis of the deterministic dynamics are presented. The third section contains the results on the ISR effect and the supporting conditions. In the fourth section the fast-slow analysis is applied to explain the mechanism by which plasticity enhances the system's non-linear response to noise. Apart from providing a brief summary, in the last section we also discuss the prevalence of the observed effect.

Model and bifurcation analysis of deterministic dynamics. – Our model involves two stochastic active rotators interacting by adaptive couplings [19–22],

$$
\begin{aligned}
\dot{\varphi}_1 &= I_0 - \sin\varphi_1 + \kappa_1 \sin(\varphi_2 - \varphi_1) + \sqrt{D}\xi_1(t), \\
\dot{\varphi}_2 &= I_0 - \sin\varphi_2 + \kappa_2 \sin(\varphi_1 - \varphi_2) + \sqrt{D}\xi_2(t), \\
\dot{\kappa}_1 &= \epsilon(-\kappa_1 + \sin(\varphi_2 - \varphi_1 + \beta)), \\
\dot{\kappa}_2 &= \epsilon(-\kappa_2 + \sin(\varphi_1 - \varphi_2 + \beta)),
\end{aligned} \tag{1}
$$

where the phases $\{\varphi_1, \varphi_2\} \in S^1$, while the coupling weights $\{\kappa_1, \kappa_2\}$ are real variables.

The excitability parameters I_0, which one may interpret as external bias currents in the context of neuroscience, are assumed to be identical for both units. For such a setup, the deterministic version of (1) possesses a Z_2 symmetry, being invariant to the exchange of units' indices. The uncoupled units undergo a SNIPER bifurcation at $I_0 = 1$, with the values $I_0 < 1$ ($I_0 > 1$) corresponding to the excitable (oscillatory) regime. We consider the case of excitable local dynamics, keeping $I_0 = 0.95$ fixed throughout the paper, such that the oscillations may emerge only due to the coupling terms and/or noise. The scale separation between the fast dynamics of the phases and the slow dynamics of adaptation is adjusted by the parameter $\epsilon \ll 1$. The fast variables are influenced by independent white noise of variance D such that $\xi_i(t)\xi_j(t') = \delta_{ij}\delta(t-t')$ for $i,j \in \{1,2\}$. Conceptually, adding stochastic input to the fast variables embodies the action of synaptic noise in neuronal systems [23].

The modality of the plasticity rule is specified by the parameter β, whose role may be understood by invoking the qualitative analogy between the adaptation dynamics in classical neuronal systems and the systems of coupled phase oscillators. This issue has first been addressed in [24–26], and a deeper analysis of the correspondence between the phase-dependent plasticity rules and the STDP has been carried out in [19]. In particular, it has been shown that the plasticity dynamics for $\beta = 3\pi/2$, where the stationary weights between the oscillators with smaller/larger phase differences increase/decrease, qualitatively resembles the Hebbian learning rule [25,26]. Nevertheless, when $\beta = \pi$, the coupling weights encode a causal relationship between the spiking of oscillators by changing in the opposite directions, in analogy to an STDP-like plasticity rule. Our interest lies with the β interval interpolating between these two limiting cases.

Using bifurcation analysis of the deterministic dynamics of (1), we first show how the modality of the plasticity rule influences the number of stationary states, and then explain how the onset of oscillations depends on adaptivity rate. The bifurcation diagram in fig. 1 indicates that the number and the stability of fixed points of (1) change with β in such a way that the system may possess two, four or six fixed points. Due to invariance to Z_2 symmetry, one always finds pairs of solutions sharing the same stability features. We consider the plasticity rules described by $\beta \in (3.298, 4.495)$, cf. the shaded region in fig. 1, where the system has two stable fixed points lying off the synchronization manifold $\varphi_1 = \varphi_2$, as well as four unstable fixed points. The bifurcations occurring at the boundaries of the relevant β interval are as follows. At $\beta = 3.298$, the system undergoes a supercritical symmetry-breaking pitchfork bifurcation giving rise to a pair of stable fixed points off the synchronization manifold. For $\beta = 4.495$, this pair of stable fixed points collides with a pair of unstable fixed points off
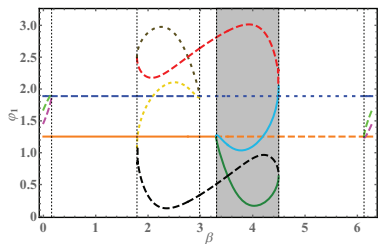
Fig. 1: (Color online) Bifurcation diagram for the fixed points of (1) with $D = 0$ under variation of β. Solid lines refer to stable fixed points, while dashed and dotted lines correspond to saddles of unstable dimension 1 and 2, respectively. Shading indicates the considered range of plasticity rules. The two fixed points independent on β belong to the synchronization manifold. The remaining parameters are $I_0 = 0.95, \epsilon = 0.05$.

Fig. 2: (Color online) Onset of oscillations in (1) for $D = 0$. (a) Variation σ_{κ_1} of the coupling weight κ_1 in the (β, ϵ)-plane. (b) Mean coupling weights $\langle \kappa_1 \rangle(\epsilon)$ and $\langle \kappa_2 \rangle(\epsilon)$ for oscillatory (thick lines) and stationary states (thin lines) at $\beta = 4.2$. (c) Variation $\sigma_{\kappa_1}(\epsilon)$ and $\sigma_{\kappa_2}(\epsilon)$, presented as in (b). Shading in (b) and (c) indicates the ϵ interval admitting the stable periodic solutions.

the synchronization manifold, getting annihilated in two symmetry-related inverse fold bifurcations. Note that the weight levels typical for the two stable stationary states support effective unidirectional interaction, in a sense that one unit exerts a much stronger impact on the dynamics of the other unit than vice versa. When illustrating the effect of ISR, we shall mainly refer to the case $\beta = 4.2$. For this β, the two stable focuses of (1) at $D = 0$ are given by $(\varphi_1, \varphi_2, \kappa_1, \kappa_2) = (1.177, 0.175, 0.032, -0.92)$ and $(\varphi_1, \varphi_2, \kappa_1, \kappa_2) = (0.175, 1.177, -0.92, 0.032)$. Within the considered β interval, the two stable fixed points of the coupled system exhibit excitable behavior, responding to external perturbation by generating either the successive spikes or synchronized spikes [21].

The onset of oscillations for the deterministic version of (1) relies on the interplay between the plasticity rule, controlled by β, and the adaptation rate, characterized by ϵ. In fig. 2(a) are shown the results of parameter sweep indicating the variation of κ_1 variable, $\sigma_{\kappa_1} = \max(\kappa_1(t)) - \min(\kappa_1(t))$, within the (β, ϵ) parameter plane. The sweep indicates the maximal stability region of the two emerging periodic solutions, related by the exchange symmetry of units indices. The data are obtained by numerical continuation starting from a stable periodic solution, such that the final state reached for the given parameter set is used as initial conditions of the system dynamics for incremented parameter values. One observes that for fixed β, there exists an interval of timescale separation ratios $\epsilon \in (\epsilon_{min}, \epsilon_{max})$ admitting oscillations, see fig. 2(b). Within the given ϵ range, the system exhibits multistability where periodic solutions coexist with the two symmetry-related stable stationary states. The lower threshold for oscillations, ϵ_{min}, reduces with β, whereas the upper boundary value, ϵ_{max}, is found to grow as β is enhanced. Note that the waveform of oscillations also changes as ϵ is increased under fixed β. In particular, for smaller ϵ, the waveforms corresponding to the two units are rather different. Nevertheless, around $\epsilon \approx 0.06$ the system undergoes a pitchfork bifurcation of limit cycles, such that
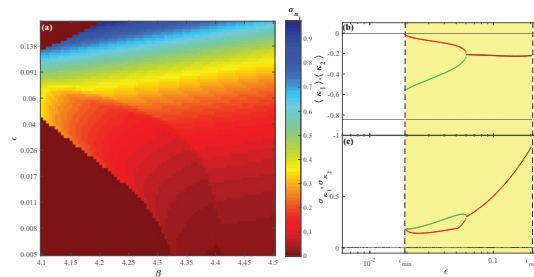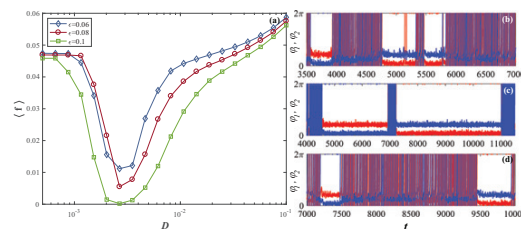

Fig. 3: (Color online) (a) Mean spiking rate $\langle f \rangle$ in terms of D for $\epsilon \in \{0.06, 0.08, 0.1\}$. The curves exhibit a characteristic minimum at an intermediate noise level. (b)–(d) Time traces $\varphi_1(t)$ and $\varphi_2(t)$ for noise levels below, at and above the resonant value. The remaining parameters are $I_0 = 0.95$, $\beta = 4.2, \epsilon = 0.06$.

the oscillatory solution gains the anti-phase space-time symmetry $\varphi_1(t) = \varphi_2(t + T/2), \kappa_1(t) = \kappa_2(t + T/2)$, where T denotes the oscillation period [21].

Numerical results on ISR. – Inverse stochastic resonance manifests itself as noise-mediated suppression of oscillations, whereby the frequency of noise-perturbed oscillations becomes minimal at a preferred noise level. For system (1), we find such an effect to occur generically for intermediate adaptivity rates, supporting multistability between the stationary and the oscillatory solutions, as described in the previous section. A family of curves describing the dependence of the oscillation frequency on noise variance $\langle f \rangle(D)$ for different ϵ values is shown in fig. 3. All the curves corresponding to $\epsilon \geq \epsilon_{min}(\beta)$ show a characteristic non-monotonous behavior, displaying a minimum at the optimal noise intensity. For weaker noise, the oscillation frequency remains close to the deterministic one, whereas for much stronger noise, the frequency increases above that of unperturbed oscillations. The displayed results are obtained by averaging over an ensemble of 1000 different stochastic realizations, having excluded the transient behavior, and having fixed a single set of initial conditions within the basin of attraction of the limit cycle attractor. Nevertheless, we have verified that the
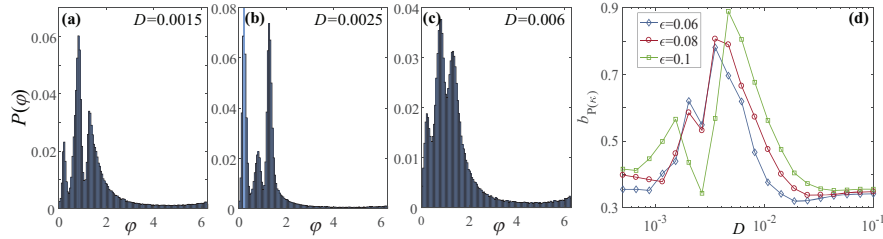
Fig. 4: (Color online) (a)–(c) Stationary distribution $P(\varphi_1)$ for the noise levels below, at and above the resonant value. System parameters are $I_0 = 0.95$, $\beta = 4.2$ and $\epsilon = 0.06$. From the three observable peaks, the middle one, prevalent in (a) and (c), refers to the metastable state associated to the oscillatory mode of (1) for $D = 0$. The two lateral peaks, dominant in (b), correspond to quasi-stationary states derived from the stable equilibria of the deterministic version of (1). (d) Bimodality coefficient for the stationary distribution of κ_1, $b_{P(\kappa_1)}$, as a function of D. The three curves refer to $\epsilon = 0.06$ (diamonds), $\epsilon = 0.08$ (circles) and $\epsilon = 0.1$ (squares).
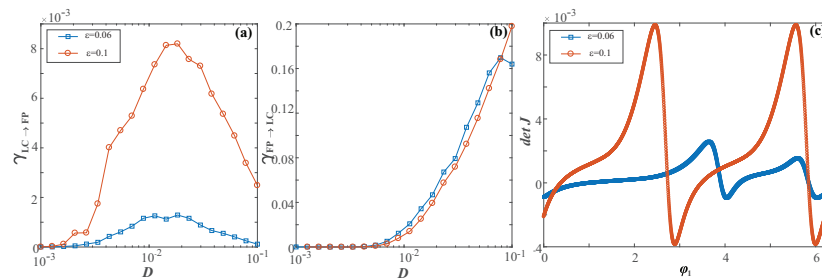
Fig. 5: (Color online) (a) and (b): transition rates from the stability basin of the limit cycle to the fixed point, $\gamma_{LC \to FP}(D)$ and vice versa, $\gamma_{FP \to LC}(D)$, numerically obtained for $\epsilon = 0.06$ (squares) and $\epsilon = 0.1$ (circles). The remaining parameters are $I_0 = 0.95, \beta = 4.2$. (c) Determinant of the Jacobian calculated along the limit cycle orbit as a function of the phase variable. The quantity provides an indication of the sensitivity of certain sections of the orbit to external perturbation. Blue and red colors correspond to $\epsilon = 0.06$ and $\epsilon = 0.1$, respectively.

qualitatively analogous results are obtained if for each realization of stochastic process one selects a set of random initial conditions lying within the stability basin of the periodic solution. The suppression effect of noise depends on the adaptivity rate, and is found to be more pronounced for faster adaptivity. Indeed, for smaller ϵ, $\varphi(t)$ series corresponding to the noise levels around the minimum of $\langle f \rangle(D)$ exhibit bursting-like behavior, whereas for larger ϵ, noise is capable of effectively quenching the oscillations, such that the minimal observed frequency approaches zero.

The core of the described effect concerns switching dynamics between the metastable states associated to coexisting attractors of the deterministic version of system (1). To illustrate this, in fig. 4 we have considered the stationary distributions of one of the phase variables, $P(\varphi)$, for the noise levels below, at and above the minimum of the $\langle f \rangle(D)$, having fixed the remaining parameters to $(\beta, \epsilon) = (4.2, 0.06)$. The distribution $P(\varphi)$ is characterized by two lateral peaks, reflecting the two symmetry-related quasi-stationary states, and the area around the central peak, corresponding to the oscillatory mode. For small noise $D = 0.0015$, see fig. 4(a), and very large noise $D = 0.006$, cf. fig. 4(c), the central peak of $P(\varphi)$ is expectedly prevalent compared to the two lateral peaks. Nevertheless, the switching dynamics for

$D = 0.0025$, the noise level about the minimum of $\langle f \rangle(D)$, is fundamentally different, and the corresponding distribution $P(\varphi)$ in fig. 4(b) shows that the system spends much more time in the quasi-stationary states than performing the oscillations. The onset of ISR in the dynamics of fast variables is accompanied by the increased bimodality of the stationary distribution of the couplings, see fig. 4(d).

In order to observe the non-monotonous response of the system's frequency to noise, the geometry of the phase space has to be asymmetrical with respect to the separatrix between the coexisting attractors in such a way that the limit cycle attractor lies much closer to the separatrix than the stationary states. Such structure of phase space gives rise to asymmetry in switching dynamics, whereby at the preferred noise level around the minimum of $\langle f \rangle(D)$, the transition rate from the stability basin of the limit cycle attractor to that of stationary states $\gamma_{LC \to FP}$ becomes much larger than the transition rate in the inverse direction, $\gamma_{FP \to LC}$. Figures 5(a) and (b) corroborate that the dependences $\gamma_{LC \to FP}(D)$ and $\gamma_{FP \to LC}(D)$ are qualitatively distinct: the former displays a maximum at the resonant noise level, whereas the latter just increases monotonously with noise. The fact that ISR is more pronounced for higher adaptivity rates is reflected in that the curve $\gamma_{LC \to FP}(D)$ for $\epsilon = 0.1$ lies substantially above that for $\epsilon = 0.06$, see fig. 5(a).

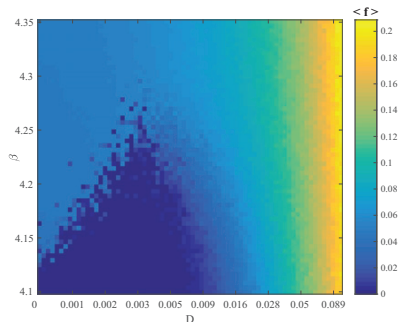Fig. 6: (Color online) Mean spiking rate $\langle f \rangle$ as a function of β and D for fixed $\epsilon = 0.05$. The results evince the robustness of the ISR effect with respect to different plasticity rules.

To understand why the interplay of adaptivity rate and noise yields a stronger resonant effect for larger ϵ, we have investigated the susceptibility of the limit cycle attractor to external perturbation. In particular, fig. 5(c) shows how the determinant of the Jacobian calculated along the limit cycle orbit change for $\epsilon = 0.06$ (blue line) and $\epsilon = 0.1$ (red line), respectively. For smaller ϵ, one may identify two particular points where the determinant of the Jacobian is the largest, *i.e.*, where the impact of external perturbation is felt the strongest. This implies that noise is most likely to drive the systems trajectory away from the limit cycle attractor around these two sections of the orbit, which should lie closest to the boundary to the stability basins of the stationary states. Such a physical picture is maintained for larger ϵ, but one should stress that the sensitivity of limit cycle attractor to external perturbation substantially increases along the entire orbit, cf. fig. 5(c). In other words, faster adaptivity enhances the impact of noise, contributing to a more pronounced ISR effect. This point is addressed from another perspective in the next section.

We also examine the robustness of ISR to different modalities of the plasticity rule specified by β. Figure 6 shows how the average oscillation frequency changes with β and D for fixed $\epsilon = 0.05$. The non-linear response to noise, conforming to a resonant effect with a minimum of oscillation frequency at an intermediate noise level, persists in a wide range of β, essentially interpolating between the Hebbian-like and the STDP-like adaptive dynamics.

Fast-slow analysis: role of plasticity in the resonant effect. – Though ISR is observed for intermediate ϵ, here we show that the fast-slow analysis may still be applied to demonstrate a peculiar feature of the mechanism behind the resonant effect. In particular, we find that the plasticity enhances the resonant effect by driving the fast flow dynamics toward the parameter domain where the stationary state is a focus rather than a node. It is well known that the response to noise in multi-timescale systems qualitatively depends on the character of stationary states. Indeed, by using the sample-paths approach and other advanced techniques, it has already been shown

that such systems may exhibit fundamentally different scaling regimes with respect to noise variance and the scale-separation ratio [27,28]. Moreover, the resonant effects may typically be expected in the case in which quasi-stationary states are focuses [27], essentially because the local dynamics around the stationary state then involves an eigenfrequency.

Within the standard fast-slow analysis, one may either consider the layer problem, defined on the fast timescale, or the reduced problem, concerning the slow timescale [29]. For the layer problem, the fast flow dynamics $\varphi_1(t; \kappa_1, \kappa_2), \varphi_2(t; \kappa_1, \kappa_2)$ is obtained by treating the slow variables κ_1 and κ_2 as system parameters, whereas in the case of the reduced problem, determining the dynamics of the slow flow $(\kappa_1(t), \kappa_2(t))$ involves time-averaging over the stable regimes of the fast flow of the layer problem. The fast flow can in principle exhibit several attractors, which means that multiple stable sheets of the slow flow may emerge from the averaged dynamics on the different attractors of the fast flow. Our key point concerns the dynamics of the slow flow, which requires us to first classify the attractors of the fast flow.

The fast flow dynamics is given by

$$
\begin{aligned}
\dot{\varphi}_1 &= I_0 - \sin \varphi_1 + \kappa_1 \sin (\varphi_2 - \varphi_1), \\
\dot{\varphi}_2 &= I_0 - \sin \varphi_2 + \kappa_2 \sin (\varphi_1 - \varphi_2),
\end{aligned}
\tag{2}
$$

where $\kappa_1, \kappa_2 \in [-1, 1]$ are considered as additional system parameters. One may formally obtain (2) by setting $\epsilon = 0$ in (1) with $D = 0$. We find that the fast flow is monostable for most of the (κ_1, κ_2) values, exhibiting either a stable equilibrium or a limit cycle attractor, see fig. 7(a). In general, the fast flow admits either two or four fixed points, and a more detailed physical picture, including the associated bifurcations, is presented in [21]. The stability region of the oscillatory regime, outlined by the red color, has been calculated by numerical continuation starting from a stable periodic solution. Bistability between a stable fixed point and a limit cycle is observed only in a small area near the main diagonal $\kappa_1 = \kappa_2$. Within the region featuring oscillatory regime, each periodic solution obtained for (κ_1, κ_2) above the main diagonal has a Z_2 symmetry-related counterpart below the diagonal. Typically, the periodic solutions emanate from SNIPER bifurcations, which make up two branches where either κ_1 or κ_2 are almost constant and close to zero.

Using the results from the analysis of the layer problem, our goal is to determine the vector fields corresponding to the stable sheets of the slow flow. We have numerically obtained the dynamics of the slow flow by a standard two-step approach [19,30]. First, for fixed values (κ_1, κ_2), we have determined the time-averaged dynamics of the fast flow (2), $\langle \varphi_2 - \varphi_1 \rangle_t = h(\kappa_1, \kappa_2)$, whereby the averaging $\langle \cdot \rangle_t$ is carried out over a sufficiently long time interval, having excluded the transient behavior. As already indicated, such an average depends on the attractor of the fast flow for the given (κ_1, κ_2). If the fast flow possesses
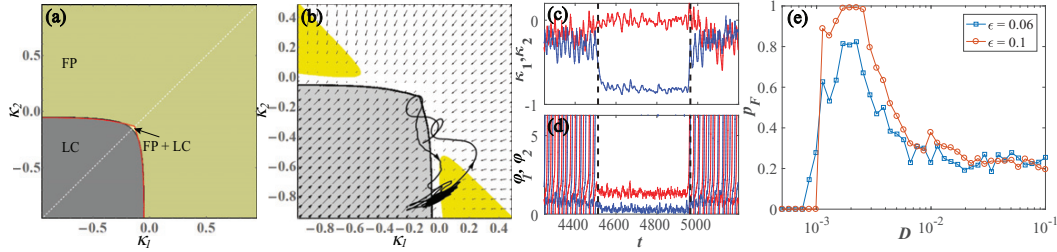
Fig. 7: (Color online) (a) Attractors of the fast flow (2) in terms of κ_1 and κ_2, now treated as free parameters. The fast flow is typically monostable, admitting either a stable fixed point (FP) or a stable limit cycle (LC), apart from a small region of bistability (FP+LC) around the main diagonal. (b) Vector field of the slow flow (3) determined by considering only the stable regimes of the fast flow for $\beta = 4.2, I_0 = 0.95$. Within the yellow-highlighted regions, the stable fixed point of the fast flow is a focus rather than the node. The displayed orbit $(\kappa_1(t), \kappa_2(t))$ corresponds to a switching episode from the oscillatory state to the quasi-stationary state and back (evolution direction indicated by arrows). Panels (c) and (d) show the time traces of phases and couplings during the switching episode. (e) Conditional probability $p_F(D)$ for $\epsilon = 0.06$ (blue squares) and $\epsilon = 0.1$ (red circles).

a stable fixed point, then $\langle \varphi_2 - \varphi_1 \rangle_t = \varphi_2^* - \varphi_1^*$, which corresponds to the slow critical manifold of the system. For (κ_1, κ_2) where the attractor of the fast flow is a periodic solution, $\langle \varphi_2 - \varphi_1 \rangle_t$ amounts to the time average over the period. Averaging over a periodic attractor of the fast flow is a standard approximation [30], quite natural when describing the influence of oscillations in the fast flow to the dynamics of the slow flow.

As the second step, the obtained time averages are substituted into the coupling dynamics

$$\begin{aligned}\dot{\kappa}_1 &= \epsilon[-\kappa_1 + \sin(h(\kappa_1, \kappa_2) + \beta)], \\ \dot{\kappa}_2 &= \epsilon[-\kappa_2 + \sin(-h(\kappa_1, \kappa_2) + \beta)].\end{aligned} \quad (3)$$

The system (3) allows one to determine the vector fields on the stable sheets of the slow flow, which correspond to the attractors of the fast flow. In fig. 7(b), the vector fields associated to each of the attractors (fixed point or limit cycle) are presented within its respective (κ_1, κ_2) stability region. In the small region of the (κ_1, κ_2)-plane supporting coexisting stable solutions of the fast flow, the corresponding vector field of the slow flow is given on multiple overlapping sheets, since the value of the average $f(\kappa_1, \kappa_2)$ depends on the initial conditions.

Within the above framework, one is able to explain a subtle influence of adaptivity on the mechanism behind the ISR. To this end, in fig. 7(b) we have projected a typical example of the $(\kappa_1(t), \kappa_2(t))$ trajectory of the full system (1) corresponding to a switching episode between the metastable states associated to a limit cycle attractor and a stable equilibrium of the deterministic system, see the time traces in figs. 7(c), (d). One observes that for the oscillating regime, the coupling dynamics always remains close to the SNIPER bifurcation of the fast flow, cf. fig. 7(a), which makes the oscillations quite susceptible to noise. Recall that the fast flow is typically monostable. Thus, switching events in the full system are naturally associated to the fast flow undergoing the SNIPER bifurcation: either a direct one, leading from the oscillatory to the stationary regime, or the inverse one, unfolding in the

opposite direction. For (κ_1, κ_2) values immediately after the SNIPER bifurcation toward the quiescent state, the stable equilibrium of the fast flow is a node. Nevertheless, for the noise levels where the effect of ISR is most pronounced, we find that the coupling dynamics guides the system into the region where the equilibrium is a stable focus rather than a node, see the yellow highlighted region in fig. 7(b). We have verified that this feature is a hallmark of the resonant effect by numerically calculating the conditional probability p_F that the events of crossing the SNIPER bifurcation are followed by the system's orbit visiting the (κ_1, κ_2) region where the stable equilibrium is a focus. The $p_F(D)$ dependences for two characteristic ϵ values at fixed $\beta = 4.2$ are plotted in fig. 7(e). One learns that $p_F(D)$ has a maximum for the resonant noise levels, where the corresponding curve $f(D)$ displays a minimum. In other words, the fact that the coupling dynamics drives the fast flow to the focus-associated regions of the (κ_1, κ_2)-plane results in trapping the phase variables for a longer time in the quasi-stationary (quiescent) state. Small noise below the resonant values is insufficient to drive the system to this region, whereas for too large a noise, the stochastic fluctuations completely take over, washing out the quasi-stationary regime. Note that for the faster adaptivity rate, the facilitatory role of coupling becomes more pronounced, as evinced by the fact that the curve $p_F(D)$ for $\epsilon = 0.1$ lies above the one for $\epsilon = 0.06$.

Discussion. – In the present paper, we have demonstrated a novel generic scenario for the onset of ISR, which involves an interplay between the local excitability feature and the adaptive dynamics of the couplings. For the example of two active rotators with coupling plasticity, we have shown that the spiking frequency corresponding to emergent oscillations varies non-monotonously with noise, displaying a minimum at a preferred noise level. Though the model *per se* is simplified, the underlying paradigm is relevant for combining the two core features of typical neuronal systems. The effect derives from the multi-timescale structure of the system, whereby the scale

separation between the local and the weight dynamics is tuned via adaptivity rate. Within a range of intermediate adaptivity rates, the deterministic dynamics of the full system exhibits multistability between the limit cycle attractors and the stable equilibria, each appearing in pairs due to the systems invariance to Z_2 symmetry. Applying the standard fast-slow analysis, we have shown that the resonant effect with noise is in fact plasticity-enhanced: plasticity promotes the impact of noise by guiding the fast flow toward the parameter domain where the stable equilibria become focuses instead of nodes. This mechanism increases the trapping efficiency by which the noise is able to deviate the systems trajectory from the metastable oscillatory states to the non-spiking regime. For faster adaptivity, the resonant effect is found to be more pronounced in a sense that the frequency dependence on noise shows deeper minima. Our scenario has proven to persist in a wide range of plasticity rules, interpolating between the cases analogous to Hebbian learning and STDP.

In earlier studies, observation of ISR has mostly been confined to Type-II neurons with intrinsic bistable dynamics, as in case of Hodgkin-Huxley or Morris-Lecar neurons near the subcritical Hopf bifurcation [3,6–9]. Even in case of networks, the macroscopic ISR effect has been linked to dynamical features of single units, only being modulated by the details of synaptic dynamics and the network topology [10]. In contrast to that, our results show that ISR may not rely on bistability of local dynamics, but may rather emerge due to the facilitatory role of coupling, here reflected in the interplay of multiscale dynamics and plasticity. Another distinction from most of the previous studies is that our scenario concerns Type-I units. For this class of systems, it is known that the dependence of the oscillating frequency of a single unit with noise is just monotonous [3,12], so that the resonant effect can only be observed in case of coupled units. So far, the latter case has been analyzed only once [5], but the underlying scenario is different from ours insofar as it involves static, rather than the adaptive couplings, and the effect *per se* is confined to a narrow region of the parameter space.

Quite recently, the onset of ISR has been reported for a single Fitzhugh-Nagumo oscillator [12], which is the first observation of the effect for Type-II neuron model in the vicinity of the supercritical Hopf bifurcation. Similar to the scenario we elaborated, ISR there also derives from the multiscale structure of the system. However, the actual mechanism behind the effect is associated to phase-sensitive (non-uniform) excitability of a limit cycle orbit conforming to relaxation oscillations [12]. These findings and the results here suggest that ISR may indeed provide a generic means of controlling and optimizing the firing rate in multi-timescale systems, which can be applied to neuronal activity, calcium signaling and other types of cell dynamics.

$$* * *$$

REFERENCES

[1] LINDNER B., GARCIA-OJALVO J., NEIMAN A. and SCHIMANSKY-GEIER L., *Phys. Rep.*, **392** (2004) 321.
[2] MCDONNELL M. D. and WARD L. M., *Nat. Rev. Neurosci.*, **12** (2011) 415.
[3] SCHMERL B. A. and MCDONNELL M. D., *Phys. Rev. E*, **88** (2013) 052722.
[4] GAMMAITONI L., HÄNGGI P., JUNG P. and MARCHESONI F., *Rev. Mod. Phys.*, **70** (1998) 223.
[5] GUTKIN B. S., JOST J. and TUCKWELL H. C., *EPL*, **81** (2008) 20005.
[6] TUCKWELL H. C., JOST J. and GUTKIN B. S., *Phys. Rev. E*, **80** (2009) 031907.
[7] UZUNTARLA M., CRESSMAN J. R., OZER M. and BARRETO E., *Phys. Rev. E*, **88** (2013) 042712.
[8] UZUNTARLA M., *Phys. Lett. A*, **377** (2013) 2585.
[9] UZUNTARLA M., TORRES J. J., SO P., OZER M. and BARRETO E., *Phys. Rev. E*, **95** (2017) 012404.
[10] UZUNTARLA M., BARRETO E. and TORRES J. J., *PLoS Comput. Biol.*, **13** (2017) e1005646.
[11] BUCHIN A., RIEUBLAND S., HÄUSSER M., GUTKIN B. S. and ROTH A., *PLoS Comput. Biol.*, **12** (2016) e1005000.
[12] FRANOVIĆ I., OMEL'CHENKO O. E. and WOLFRUM M., *Chaos*, **28** (2018) 071105.
[13] HAHN T. T. G., MCFARLAND J. M., BERBERICH S., SAKMANN B. and MEHTA M. R., *Nat. Neurosci.*, **15** (2012) 1531.
[14] FRANOVIĆ I. and KLINSHOV V., *Chaos*, **28** (2018) 023111.
[15] FRANOVIĆ I. and KLINSHOV V., *EPL*, **116** (2016) 48002.
[16] SONG S., MILLER K. D. and ABBOTT L. F., *Nat. Neurosci.*, **3** (2000) 919.
[17] FROEMKE R. C. and DAN Y., *Nature*, **416** (2002) 433.
[18] WANG H.-X., GERKIN R. C., NAUEN D. W. and BI G.-Q., *Nat. Neurosci.*, **8** (2005) 187.
[19] LÜCKEN L., POPOVYCH O. V., TASS P. A. and YANCHUK S., *Phys. Rev. E*, **93** (2016) 032210.
[20] KASATKIN D. V. and NEKORKIN V. I., *Radiophys. Quantum Electron.*, **58** (2016) 877.
[21] BAČIĆ I., YANCHUK S., WOLFRUM M. and FRANOVIĆ I., *Eur. Phys. J. ST*, **227** (2018) 1077.
[22] KASATKIN D., YANCHUK S., SCHÖLL E. and NEKORKIN V., *Phys. Rev. E*, **96** (2017) 062211.
[23] DESTEXHE A. and RUDOLPH-LILITH M., *Neuronal Noise* (Springer, New York) 2012.
[24] MAISTRENKO Y. L., LYSYANSKY B., HAUPTMANN C., BURYLKO O. and TASS P., *Phys. Rev. E*, **75** (2007) 066207.
[25] AOKI T. and AOYAGI T., *Phys. Rev. Lett.*, **102** (2009) 034101.
[26] AOKI T. and AOYAGI T., *Phys. Rev. E*, **84** (2011) 066109.
[27] BERGLUND N. and GENTZ B., *Noise-Induced Phenomena in Slow-Fast Dynamical Systems* (Springer, Berlin) 2006.
[28] LAING C. and LORD G. J. (Editors), *Stochastic Methods in Neuroscience* (Oxford University Press, London) 2009.
[29] KUEHN C., *Multiple Time Scale Dynamics* (Springer International Publishing, Switzerland) 2015.
[30] SHILNIKOV A., *Int. J. Bifurcat. Chaos*, **18** (2008) 2141.

Two paradigmatic scenarios for inverse stochastic resonance

View Online　　　Export Citation　　　CrossMark

Iva Bačić and Igor Franović[a]) iD

AFFILIATIONS

Scientific Computing Laboratory, Center for the Study of Complex Systems, Institute of Physics Belgrade, University of Belgrade, Pregrevica 118, 11080 Belgrade, Serbia

[a])**Author to whom correspondence should be addressed:** franovic@ipb.ac.rs

ABSTRACT

Inverse stochastic resonance comprises a nonlinear response of an oscillatory system to noise where the frequency of noise-perturbed oscillations becomes minimal at an intermediate noise level. We demonstrate two generic scenarios for inverse stochastic resonance by considering a paradigmatic model of two adaptively coupled stochastic active rotators whose local dynamics is close to a bifurcation threshold. In the first scenario, shown for the two rotators in the excitable regime, inverse stochastic resonance emerges due to a biased switching between the oscillatory and the quasi-stationary metastable states derived from the attractors of the noiseless system. In the second scenario, illustrated for the rotators in the oscillatory regime, inverse stochastic resonance arises due to a trapping effect associated with a noise-enhanced stability of an unstable fixed point. The details of the mechanisms behind the resonant effect are explained in terms of slow–fast analysis of the corresponding noiseless systems.

The effects of noise may generically be classified into two groups: on the one hand, the noise may enhance or suppress certain features of deterministic dynamics by acting on the system states in an inhomogeneous fashion, while on the other hand, it may give rise to novel forms of behavior, associated with crossing of thresholds and separatrices or to a stability of deterministically unstable states. The constructive role of noise has been evinced in a wide range of real-world applications, from neural networks and chemical reactions to lasers and electronic circuits. The classical examples of stochastic facilitation concern the resonant phenomena, including stochastic resonance, where noise of appropriate intensity may induce oscillations in bistable systems that are preferentially locked to a weak periodic forcing, and coherence resonance, where an intermediate level of noise may trigger coherent oscillations in excitable systems. Recently, a novel form of nonlinear response to noise, called inverse stochastic resonance (ISR), has been discovered while studying individual neural oscillators and models of neuronal populations. It has come to light that noise may reduce the intrinsic spiking frequency of neuronal oscillators, transforming the tonic firing into a bursting-like activity or even quenching the oscillations. Within the present study, we demonstrate two paradigmatic mechanisms of inverse stochastic resonance, one based on biased switching between the metastable states, and the other associated with a noise-enhanced stability of an unstable fixed point. We show that the effect is robust, in a sense that it may emerge in coupled excitable and coupled oscillatory systems, and both in cases of Type I and Type II oscillators.

I. INTRODUCTION

Noise in excitable or multistable systems may fundamentally change their deterministic dynamics, giving rise to qualitatively novel forms of behavior, associated with crossing of thresholds and separatrices, or stabilization of certain unstable structures.[1,2] The emergent dynamics may involve noise-induced oscillations and stochastic bursting,[3–5] switching between metastable states,[6,7] or noise-enhanced stability of metastable and unstable states,[8–12] to name but a few. In neuronal systems, the phenomena reflecting the constructive role of noise are collected under the notion of stochastic facilitation,[13–15] which mainly comprises the resonant effects. The most prominent examples concern coherence resonance,[16–20] where the regularity of noise-induced oscillations becomes maximal at a preferred noise level, and stochastic resonance,[13,21] where the sensitivity of a system to a subthreshold periodic stimulation becomes

maximal at an intermediate noise level. Recent studies on the impact of noise in neuronal oscillators have revealed that the noise may also give rise to an inhibitory effect, which consists in reducing the intrinsic spiking frequency such that it becomes minimal at an intermediate noise intensity.[14,22–30] This effect has been called inverse stochastic resonance (ISR), but in contrast to stochastic resonance, it concerns autonomous rather than periodically driven systems. Apart from reports in models of neurons and neuronal populations, ISR has recently been evinced for cerebellar Purkinje cells *in vitro*,[28] having shown how the lifetimes of the so-called UP states with elevated spiking activity and the DOWN states of relative quiescence[7,31–33] depend on the noise intensity.

The studies of the mechanism behind ISR have so far mostly been focused on Type II neural oscillators with bistable dynamics poised close to a subcritical Hopf bifurcation,[14,23–25] considering Hodgkin–Huxley and Morris–Lecar models. Under the influence of noise, such systems exhibit switching between the two metastable states, derived from the periodic and the stationary attractor of the deterministic dynamics. At an intermediate noise level, one observes that the switching rates become strongly asymmetric, with the system spending substantially more time in a quasi-stationary state. This is reflected in a characteristic non-monotone dependence of the spiking frequency on noise, which is a hallmark of ISR.

Nevertheless, a number of important issues on the mechanism giving rise to ISR have remained unresolved. In particular, is the effect dependent on the type of neuronal excitability? Also, can there be more than a single mechanism of ISR? And finally, how does the effect depend on the form of couplings and whether it can be robust for adaptively changing couplings, typical for neuronal systems?

To address these issues, we invoke a simple, yet paradigmatic model that combines the three typical ingredients of neuronal dynamics, including excitability, noise, and coupling plasticity. In particular, we consider a system of two identical, adaptively coupled active rotators[6,29,34] influenced by independent Gaussian white noise sources

$$\dot{\varphi}_i = I_0 - \sin\varphi_i + \kappa_i \sin(\varphi_j - \varphi_i) + \sqrt{D}\xi_i(t),$$
$$\dot{\kappa}_i = \varepsilon(-\kappa_i + \sin(\varphi_j - \varphi_i + \beta)). \tag{1}$$

The indices $i, j \in \{1, 2\}, i \neq j$ denote the particular units, described by the respective phases $\{\varphi_1, \varphi_2\} \in S^1$, which constitute the fast variables and the slowly varying coupling weights $\{\kappa_1, \kappa_2\} \in \mathcal{R}$. The scale separation between the characteristic timescales is set by the small parameter $\varepsilon \ll 1$ that defines the adaptivity rate. The local dynamics is controlled by the excitability parameter I_0 such that the saddle-node of infinite period (SNIPER) bifurcation at $I_0 = 1$ mediates the transition between the excitable ($I_0 \lesssim 1$) and the oscillatory regimes ($I_0 > 1$). The excitable units may still exhibit oscillations, induced either by the action of the coupling (*emergent oscillations*) and/or evoked by the stochastic terms (*noise-induced oscillations*). The noiseless coupled system (1) is invariant with respect to exchange of the units' indices such that all the stationary or the periodic solutions always appear in pairs connected by the Z_2 symmetry. Given the similarity between the active rotators and the theta neurons, which also conform to Type I excitability, system (1) may be considered qualitatively analogous to a motif of two adaptively coupled neurons,[37] influenced by an external bias current

I_0 and the synaptic noise. Adaptivity is modeled in terms of phase-dependent plasticity[36,38–40] of coupling weights, having the modality of the plasticity rule adjusted by parameter β. This form of plasticity has already been shown to be capable of qualitatively reproducing the features of some well-known neuronal plasticity rules.[39,40] In particular, for $\beta = 3\pi/2$, one recovers Hebbian-like learning,[41] where the synaptic potentiation promotes phase synchronization, while for $\beta = \pi$, adaptation acts similarly to spike-timing-dependent plasticity (STDP),[42–46] whose typical form[35,45] favors a causal relationship between the pre- and post-synaptic neuron firing times.[39,40]

II. INVERSE STOCHASTIC RESONANCE DUE TO A BIASED SWITCHING

The first generic scenario for ISR we demonstrate is based on *biased switching* between the metastable states associated with coexisting stationary and periodic attractors of the corresponding deterministic system. As an example, we consider the noise-induced reduction of frequency of emergent oscillations on a motif of two adaptively coupled stochastic active rotators with excitable local dynamics ($I_0 = 0.95$). To elucidate the mechanism behind the effect, we first summarize the details of the noise-free dynamics and then address the switching behavior. A complete bifurcation analysis of the noiseless version of (1) with excitable local dynamics has been carried out in Refs. 6 and 29, having shown (i) how the number and stability of the fixed points depends on the plasticity rule, characterized by β, as well as (ii) how the interplay between β and the adaptivity rate, controlled by the small parameter ε, gives rise to limit cycle attractors. Our focus is on the interval $\beta \in (3.298, 4.495)$, which approximately interpolates between the limiting cases of Hebbian-like and STDP-like plasticity rules. There, the system exhibits two stable equilibria born from the symmetry-breaking pitchfork bifurcation and has four additional unstable fixed points. For the particular case $\beta = 4.2$ analyzed below, the two stable equilibria, given by EQ1 $:= (\varphi_1^*, \varphi_2^*, \kappa_1^*, \kappa_2^*)$ $= (1.2757, 0.2127, -0.0078, -0.8456)$ and EQ2 $:= (\varphi_1^*, \varphi_2^*, \kappa_1^*, \kappa_2^*)$ $= (0.2127, 1.2757, -0.8456, -0.0078)$, have been shown to manifest excitable behavior.[6]

The onset of emergent oscillations, as well as the coexistence between the stable stationary and periodic solutions in the noiseless version of (1), is illustrated in Fig. 1. The maximal stability region of the two Z_2 symmetry-related periodic solutions is indicated in Fig. 1(a), which shows the variation of κ_1 variable, $\sigma_{\kappa_1} = \max(\kappa_1(t)) - \min(\kappa_1(t))$, in the (β, ε) parameter plane. The scan was performed by the method of numerical continuation starting from a stable periodic solution such that the initial conditions for an incremented parameter value are given by the final state obtained for the previous iteration step. One finds that for a given β, there exists an interval $\varepsilon \in (\varepsilon_{\min}, \varepsilon_{\max})$ of intermediate scale-separation ratios supporting the oscillations, cf. the highlighted region in Fig. 1(b). In particular, the two Z_2-symmetry related branches of stable periodic solutions emanate from the fold of cycles bifurcations, denoted by FC in Fig. 1(b) such that the associated threshold scale-separation $\varepsilon_{\min}(\beta)$ decreases with β. The two branches of oscillatory solutions merge around $\varepsilon \approx 0.06$, where the system undergoes an inverse pitchfork bifurcation (PFC) of limit cycles. The incipient stable limit cycle acquires the anti-phase space–time symmetry

$\varphi_1(t) = \varphi_2(t + T_{osc}/2), \kappa_1(t) = \kappa_2(t + T_{osc}/2)$, with T_{osc} denoting the oscillation period.[6] An example illustrating the basins of stability of stationary and oscillatory solutions for $\varepsilon = 0.1$, obtained by fixing the initial values of phases and varying the initial coupling weights within the range $\kappa_{i,ini} \in (-1, 1)$, is shown in Fig. 1(c). In the presence of noise, the coexisting attractors of the deterministic system turn to metastable states, which are connected by the noise-induced switching.

Inverse stochastic resonance manifests itself as the noise-mediated suppression of oscillations, whereby the frequency of noise-perturbed oscillations becomes minimal at an intermediate noise level. For the motif of two adaptively coupled excitable active rotators, such characteristic non-monotone dependence on noise is generically found for intermediate adaptivity rates supporting multistability between the stationary and the oscillatory solutions. A family of curves illustrating the dependence of the oscillation frequency on noise variance $\langle f \rangle(D)$ for a set of different ε values is shown in Fig. 2(a). The angular brackets $\langle \cdot \rangle$ refer to averaging over an ensemble of a 100 different stochastic realizations, having fixed a set of initial conditions within the basin of attraction of the limit cycle attractor. Nonetheless, qualitatively analogous results are recovered if for each realization of the stochastic process, one selects a set of random initial conditions lying within the stability basin of a periodic solution. In Ref. 29, we have shown that the noise-induced switching gives rise to a bursting-like behavior, where the spiking is interspersed by the quiescent episodes which correspond to the system residing in the vicinity of the quasi-stationary metastable states. Such episodes become prevalent at the noise levels around the minimum of $\langle f \rangle(D)$. For weaker noise $D \lesssim 10^{-3}$, the frequency of emergent oscillations remains close to the deterministic one, whereas for a much stronger noise, it increases above that of unperturbed oscillations. One observes that the suppression effect of noise depends on the adaptivity rate such that it is enhanced for faster adaptivity, see Ref. 29 for a more detailed analysis. In order to illustrate how the ISR effect is reflected at the level of the dynamics

of coupling weights, in Figs. 2(b)–2(d) are shown the stationary distributions $P(\kappa_1)$ for the noise levels below, at, and above the resonant level. To provide a reference to the deterministic case, we have denoted by the dashed-dotted lines the weight levels associated with the two equilibria EQ1 and EQ2, while the blue shading indicates the variation σ_κ of the stable limit cycle. Note that the stable periodic solution is unique because for the considered ε value, the deterministic system lies above the pitchfork of cycles bifurcation, cf. PFC in Fig. 1(b). The stationary distribution $P(\kappa_1)$ at the resonant noise expectedly shows a pronounced peak at one of the quasi-stationary states, while the distributions below or above the resonant noise level indicate a high occupancy of the oscillatory metastable state.

In order to elucidate the mechanism behind ISR, we have calculated how the fraction of the total time spent at the oscillatory metastable states, T_{osc}/T_{tot}, changes with noise. In terms of numerical experiments, the quasi-stationary and the oscillatory metastable states can readily be distinguished by considering the corresponding $\kappa_i(t)$ series, using the fact that the typical distance $|\kappa_1(t) - \kappa_2(t)|$ is much larger for the quasi-stationary than the oscillatory solutions. This has allowed us to employ a simple threshold method to identify the particular system's states and trace the associated transitions. Figure 3(a) indicates a non-monotone dependence of $T_{osc}/T_{tot}(D)$, implying that the switching process around the resonant noise level becomes strongly biased toward the quasi-stationary state, even more so for a faster adaptivity. The biased switching is facilitated by the geometry of the phase space, featuring an asymmetrical structure with respect to the separatrix between the coexisting attractors such that the limit cycle lies much closer to the separatrix than the stationary states.

The nonlinear response to noise may be understood in terms of the competition between the transition processes from and to the limit cycle attractor. These processes are characterized by the transition rates from the stability basin of the limit cycle attractor to that of the stationary states $\gamma_{LC \to FP}$ and vice versa, $\gamma_{FP \to LC}$, which are numerically estimated as the reciprocal values of the corresponding

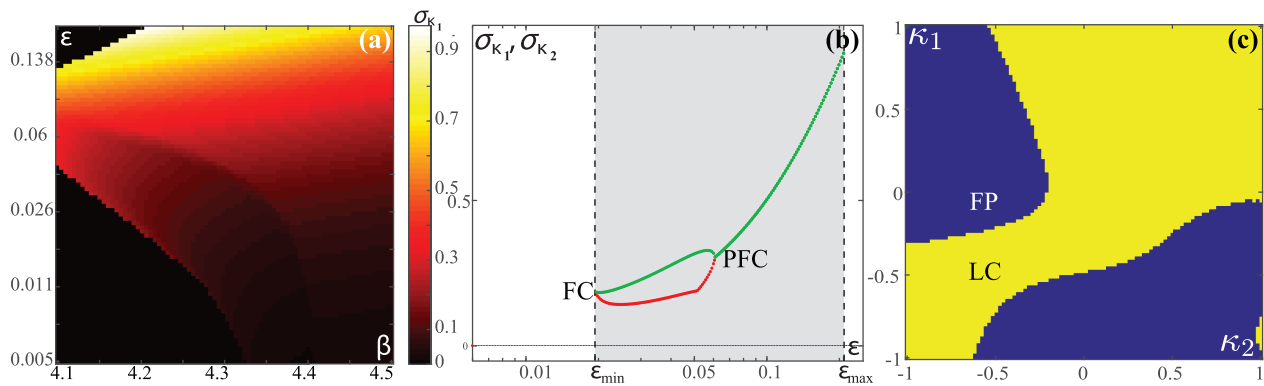**FIG. 1.** Emergent oscillations in (1) for $I_0 = 0.95, D = 0$. (a) Variation σ_{κ_1} of the coupling weight κ_1 in the (β, ε) plane. (b) Dependencies $\sigma_{\kappa_i}(\varepsilon), i \in \{1, 2\}$ for the representative stationary (blue) and oscillatory solution (red and green refer to the two units) at fixed $\beta = 4.2$. Shading indicates the ε interval that supports multistability between the two symmetry-related stable equilibria and the limit cycle attractor(s). FC and PFC denote the ε values where the fold of cycles and pitchfork of cycles occur. (c) Basins of stability of the stationary (FP, blue) and oscillatory solutions (LC, yellow) in the (κ_1, κ_2) plane, obtained by fixing the initial phases to $(\varphi_1, \varphi_2) = (1.32, 0.58)$. The remaining parameters are $\beta = 4.2, \varepsilon = 0.1$.
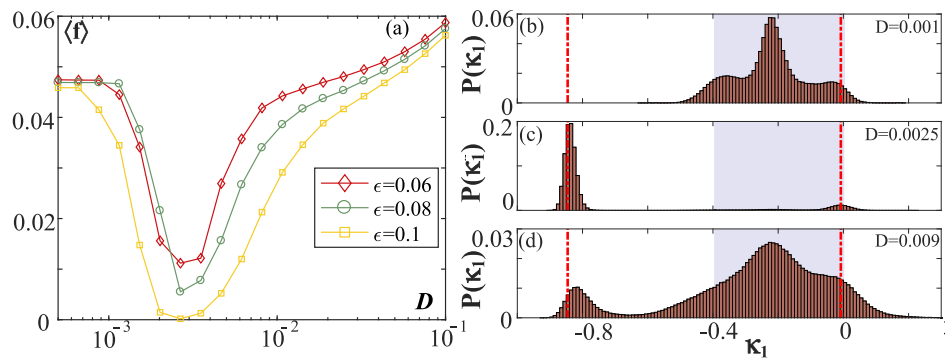
FIG. 2. (a) Dependencies of the mean oscillation frequency on noise for scale separation $\varepsilon = 0.06$ (diamonds), $\varepsilon = 0.08$ (circles) and $\varepsilon = 0.1$ (squares), obtained for fixed $I_0 = 0.95$, $\beta = 4.2$. Averaging has been performed over an ensemble of 100 different stochastic realizations. (b)–(d) show the stationary distributions $P(\kappa_1)$ below ($D = 0.001$), at ($D = 0.0025$), and above ($D = 0.009$) the resonant noise intensity for $\varepsilon = 0.1$. The dashed-dotted lines denote the κ_1 levels associated with the two stable equilibria, $\kappa_1^*(EQ1)$ and $\kappa_1^*(EQ2)$, while the blue shaded interval indicates the variation σ_{κ_1} of the unique stable periodic solution.

mean first-passage times.[47] In Figs. 3(b) and 3(c) is illustrated the qualitative distinction between the noise-dependencies of the transition rates: while $\gamma_{LC \rightarrow FP}$ displays a maximum at the resonant noise level, $\gamma_{FP \rightarrow LC}$ just increases monotonously with noise. For small noise $D \lesssim 10^{-3}$, one observes virtually no switches to the quasi-stationary state, as evinced by the fact that the corresponding oscillation frequency is identical to the deterministic one. For increasing noise, the competition between the two processes is resolved in such a way that at an intermediate/large noise, the impact of $\gamma_{LC \rightarrow FP}/\gamma_{FP \rightarrow LC}$ becomes prevalent. The large values of $\gamma_{FP \rightarrow LC}$ found for quite strong noise $D \gtrsim 0.04$ reflect the point that the system there spends most of the time in the oscillatory metastable state, making only quite short excursions to the quasi-stationary state.

Though ISR is most pronounced for intermediate ε, it turns out that an additional subtlety in the mechanism of biased switching may be explained by employing the singular perturbation theory to

the noiseless version of (1). In particular, by combining the critical manifold theory[48] and the *averaging* approach,[49] one may demonstrate the *facilitatory role of plasticity* in enhancing the resonant effect, showing that the adaptation drives the fast flow toward the parameter region where the stationary state is a focus rather than a node.[29] The response to noise in multiple timescale systems has already been indicated to qualitatively depend on the character of the stationary states, yielding fundamentally different scaling regimes with respect to noise variance and the scale-separation ratio.[50–52] Intuitively, one expects that the resonant effects should be associated with the quasi-stationary states derived from the focuses rather than the nodes[50] because the local dynamics then involves an eigenfrequency.

The fast–slow analysis of (1) for $I_0 = 0.95$ has been carried out in detail in Refs. 6 and 29 such that here we only summarize the main results concerning the associated layer and reduced
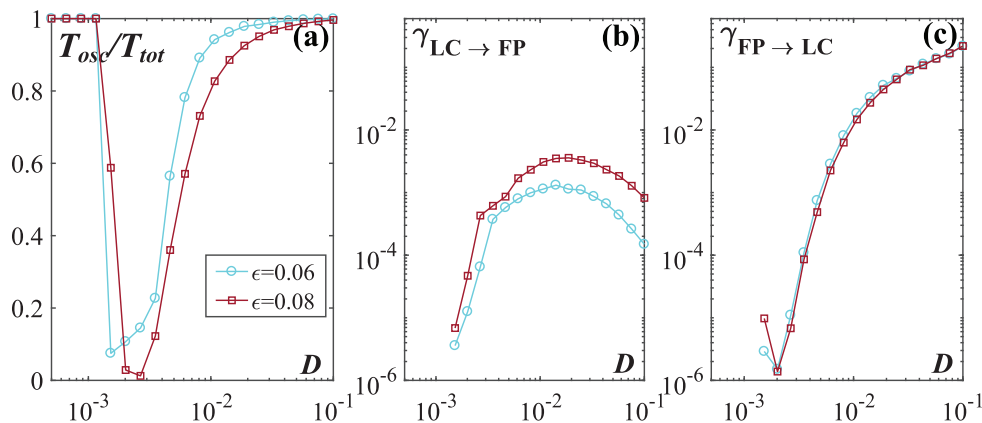

FIG. 3. (a) Fraction of the time spent at the oscillatory metastable state T_{osc}/T_{tot} as a function of noise for $\varepsilon = 0.06$ (circles) and $\varepsilon = 0.08$ (squares). (b) and (c) Numerically estimated transition rates from the oscillatory to the quasi-stationary metastable states, $\gamma_{LC \rightarrow FP}(D)$ and vice versa, $\gamma_{FP \rightarrow LC}(D)$. The remaining parameters are $I_0 = 0.95$, $\beta = 4.2$.
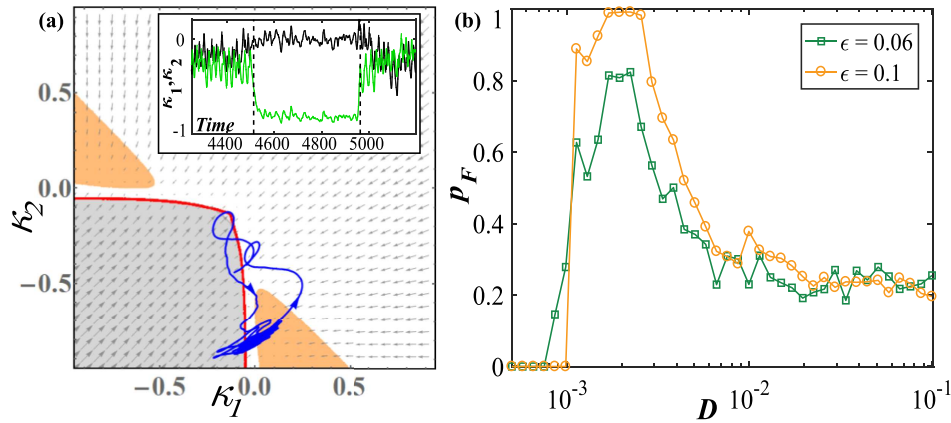
FIG. 4. (a) Fast–slow analysis of (1) for $I_0 = 0.95$, $D = 0$. The fast flow exhibits a periodic attractor (grey shaded region) and a stable equilibrium (white region), with two branches of SNIPER bifurcations (red lines) outlining the boundary between them. The arrows indicate the vector fields corresponding to the stable sheets of the slow flow. The inset shows $\kappa_i(t)$ series corresponding to a switching episode from the oscillatory to the stationary state and back, obtained for $\varepsilon = 0.06$, $\beta = 4.2$. The corresponding $(\kappa_1(t), \kappa_2(t))$ orbit is indicated by the blue line. Within the two orange regions, the two stable equilibria are focuses rather than the nodes. (b) Conditional probability $p_F(D)$ of having the crossing of SNIPER bifurcation followed by a visit to the orange-shaded region from (a), obtained for $\varepsilon = 0.06$ (squares) and $\varepsilon = 0.1$ (circles).

problems.[48] Within the layer problem, the fast flow dynamics

$$\dot{\varphi}_1 = I_0 - \sin\varphi_1 + \kappa_1 \sin(\varphi_2 - \varphi_1),$$
$$\dot{\varphi}_2 = I_0 - \sin\varphi_2 + \kappa_2 \sin(\varphi_1 - \varphi_2) \tag{2}$$

is considered by treating the slow variables $\kappa_1, \kappa_2 \in [-1, 1]$ as additional system parameters. Depending on κ_1 and κ_2, the fast flow dynamics is found to be almost always *monostable*, exhibiting either a stable equilibrium or a limit cycle attractor, apart from a small region of bistability between the two.[6,29] The maximal stability region of the oscillatory regime, encompassing both the domain where the oscillatory solution is monostable and where it coexists with a stable equilibrium, is indicated by the gray shading in Fig. 4(a). The latter has been determined by the method of numerical continuation, starting from a periodic solution. The thick red lines outlining the region's boundaries correspond to the two branches of SNIPER bifurcations.[6] Note that for each periodic solution above the main diagonal $\kappa_1 = \kappa_2$, there exists a Z_2 symmetry-related counterpart below the diagonal.

By averaging over the different attractors of the fast flow dynamics, we have obtained multiple stable sheets of the slow flow.[49] The explicit procedure consists in determining the time average $\langle \varphi_2 - \varphi_1 \rangle_t = h(\kappa_1, \kappa_2)$ by iterating (2) for each fixed set (κ_1, κ_2)[6,49] and then substituting these averages into the equations of the slow flow

$$\kappa_1' = [-\kappa_1 + \sin(h(\kappa_1, \kappa_2) + \beta)],$$
$$\kappa_2' = [-\kappa_2 + \sin(-h(\kappa_1, \kappa_2) + \beta)], \tag{3}$$

where the prime refers to a derivative over the rescaled time variable $T := t/\varepsilon$. The arrows in Fig. 4(a) show the vector fields on the two stable sheets of the slow flow (3) associated with the stationary and the periodic attractors of the fast flow.

The performed fast–slow analysis has allowed us to gain a deeper insight into the facilitatory role of adaptivity within the

ISR. In particular, in the inset of Fig. 4(a) are extracted the time series $(\kappa_1(t), \kappa_2(t))$, which (from left to right) illustrate the switching episode from an oscillatory to the quasi-stationary metastable state. The triggering/termination of this switching event is associated with an inverse/direct SNIPER bifurcation of the fast flow. Note that for (κ_1, κ_2) values immediately after the inverse SNIPER bifurcation, the stable equilibrium of the fast flow is a node. Nevertheless, for the noise levels corresponding to the most pronounced ISR effect, the coupling dynamics guides the system into the triangular orange-shaded regions in Fig. 4(a), where the equilibrium is a stable focus rather than a node. We have verified that this feature is a hallmark of ISR by numerically calculating the conditional probability p_F that the events of crossing the SNIPER bifurcation are followed by the system's orbit visiting the (κ_1, κ_2) regions with a focus equilibrium. The $p_F(D)$ dependencies for two characteristic ε values in Fig. 4(b) indeed show a maximum for the resonant noise levels, corresponding to the minima of the frequency dependencies in Fig. 2(a). The local dynamics around the focus gives rise to a *trapping* effect such that the phase variables remain for a longer time in the associated quasi-stationary states than in case where the metastable states derive from the nodes of the fast flow. Small noise below the resonant values is insufficient to drive the system to the regions featuring focal equilibria, whereas for too strong noise, the stochastic fluctuations completely take over, washing out the quasi-stationary regime. The trapping effect is enhanced for the faster adaptivity rate, as evinced by the fact that the curve $p_F(D)$ for $\varepsilon = 0.1$ lies above the one for $\varepsilon = 0.06$.

III. INVERSE STOCHASTIC RESONANCE DUE TO A TRAPPING EFFECT

As the second paradigmatic scenario for ISR, we consider the case where the oscillation frequency is reduced due to a noise-induced trapping in the vicinity of an *unstable* fixed point of the
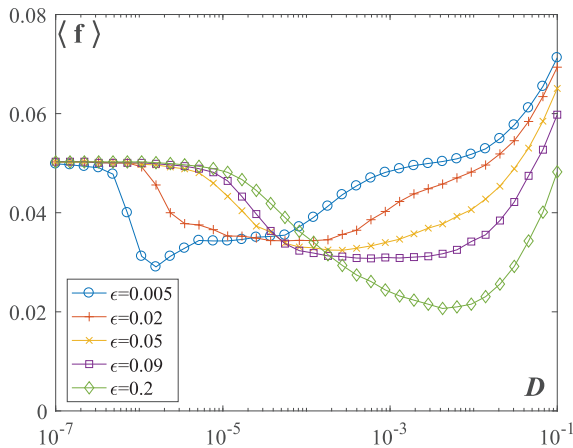
FIG. 5. Family of dependencies $\langle f \rangle(D)$ for scale separations $\varepsilon \in \{0.005, 0.02, 0.05, 0.09, 0.2\}$ at fixed $I_0 = 1.05$, $\beta = \pi$. Stochastic averaging has involved an ensemble of 100 different process realizations.

noiseless system. Such a trapping effect may be interpreted as an example of the phenomenon of *noise-enhanced stability* of an unstable fixed point.[8–12] This mechanism is distinct from the one based on biased switching because there the quasi-stationary states derive from the *stable* equilibria of the noise-free system such that the noise gives rise to crossing over the separatrix between the oscillatory and the quiescent regime. Nevertheless, in the scenario below, noise induces "tunneling" through the bifurcation threshold, temporarily stabilizing an unstable fixed point of the deterministic system.

In particular, we study an example of a system (1) comprised of two adaptively coupled active rotators in the *oscillatory*, rather than the excitable regime, setting the parameter $I_0 = 1.05$ close to a bifurcation threshold. The plasticity parameter is fixed to $\beta = \pi$ such that the modality of the phase-dependent adaptivity resembles the STDP rule in neuronal systems. One finds that this system exhibits a characteristic non-monotone response to noise, with the oscillation frequency of the phases $\langle f \rangle$ displaying a minimum at an intermediate noise level (see Fig. 5). In contrast to the mechanism described in Sec. II, the onset of ISR here does not qualitatively depend on the adaptivity rate. One only finds a quantitative dependence of the system's nonlinear response to noise on ε, in a sense that the resonant noise level shifts to larger values with increasing ε. Our exhaustive numerical simulations indicate that the ISR effect persists for slow adaptivity rates, cf. the example of the $\langle f(D) \rangle$ for $\varepsilon = 0.005$ in Fig. 5, and the results of the fast–slow analysis below will further show that all the ingredients required for the ISR effect remain in the singular perturbation limit $\varepsilon \to 0$. The persistence of the ISR effect has also been numerically confirmed for faster adaptivity rates $\varepsilon \sim 0.1$. In this case, we have observed that the minima of the $\langle f(D) \rangle$ curves become deeper with ε, suggesting that the ISR becomes more pronounced for higher adaptivity rates.

To elucidate the mechanism behind ISR, we again perform the fast–slow analysis of the corresponding noise-free system. Prior to this, we briefly summarize the results of the numerical bifurcation analysis for the noiseless system in the case of finite scale

separation. First note that selecting a particular plasticity rule $\beta = \pi$ confines the dynamics of the couplings to a symmetry invariant subspace $\kappa_1(t) = -\kappa_2(t) \equiv \kappa(t)$. Due to this, the noiseless version of the original system (1) can be reduced to a three-dimensional form

$$\dot{\varphi}_1 = I_0 - \sin \varphi_1 + \kappa \sin (\varphi_2 - \varphi_1),$$
$$\dot{\varphi}_2 = I_0 - \sin \varphi_2 + \kappa \sin (\varphi_2 - \varphi_1), \qquad (4)$$
$$\dot{\kappa} = \varepsilon(-\kappa - \sin(\varphi_2 - \varphi_1)).$$

By numerically solving the eigenvalue problem, we have verified that (4) possesses no stable fixed points, but rather a pair of saddle nodes and a pair of saddle focuses. Also, we have determined that the maximal real part of the eigenvalues of the focuses displays a power-law dependence on the scale separation, tending to zero in the singular limit $\varepsilon \to 0$. Concerning the oscillatory states, our numerical experiments show that (4) exhibits multistability between three periodic solutions, whereby two of them are characterized by the non-zero couplings and a constant phase-shift between the fast variables, whereas the third solution corresponds to a case of effectively uncoupled units [$\kappa(t) = 0$] and the fast variables synchronized in-phase.

A deeper understanding of the ingredients relevant for the trapping mechanism can be gained within the framework of the fast–slow analysis, considering the layer problem

$$\dot{\varphi}_1 = I_0 - \sin \varphi_1 + \kappa \sin (\varphi_2 - \varphi_1),$$
$$\dot{\varphi}_2 = I_0 - \sin \varphi_2 + \kappa \sin (\varphi_2 - \varphi_1). \qquad (5)$$

Treating $\kappa \in [-1, 1]$ as an additional system parameter, we first look for the stationary and periodic attractors of the fast flow. It is convenient to apply the coordinate transformation $(\varphi_1, \varphi_2) \mapsto (\Phi, \delta\varphi) = (\frac{\varphi_1 + \varphi_2}{2}, \frac{\varphi_1 - \varphi_2}{2})$, rewriting (5) as

$$\delta\dot{\varphi} = -\sin \delta\varphi \cos \Phi,$$
$$\dot{\Phi} = I_0 - \cos \delta\varphi (\sin \Phi + 2\kappa \sin \delta\varphi). \qquad (6)$$

From the second equation, one readily finds that the fast flow cannot possess any fixed points on the synchronization manifold $\delta\varphi = 0$ because $I_0 > 1$ such that the stationary solutions derive only from the condition $\cos \Phi = 0$. A numerical analysis shows that, depending on κ, the fast flow for $I_0 \gtrsim 1$ can exhibit two or no fixed points. For the particular value $I_0 = 1.05$, one finds that two fixed points, namely, a saddle and a *center*, exist within the interval $\kappa \in [-0.1674, 0.1674]$. The appearance of a center point is associated with the time-reversal symmetry of the fast flow (5). Indeed, one may show that the fast flow is invariant to a symmetry-preserving map R of the form

$$R = \begin{cases} \varphi_1 \to \pi - \varphi_2, \\ \varphi_2 \to \pi - \varphi_1, \\ t \to -t. \end{cases} \qquad (7)$$

Note that in case of the finite scale separation, the counterpart of the center point of the fast flow is a weakly unstable focus of the complete system (4).

The structure of the fast flow is organized around the saddle-center bifurcation, which occurs at $\kappa = \kappa_{SC} = -0.1674$. There, the
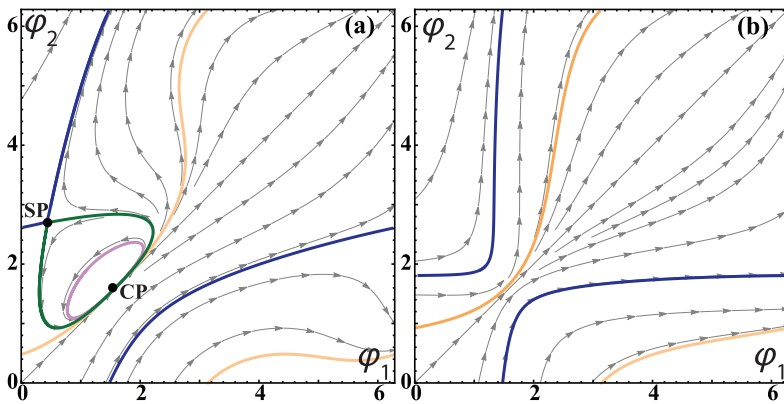
FIG. 6. Typical dynamics of the fast flow (5) for $I_0 = 1.05$ below ($\kappa = -0.8$) and above the saddle-center bifurcation ($\kappa = -0.08$) are illustrated in (a) and (b), respectively. In (a), the system possesses two unstable fixed points, a saddle (SP) and a center (CP), and exhibits three types of closed orbits: a limit cycle attractor (orange), homoclinic connections to SP (blue and green), and subthreshold oscillations around the center (purple). In (b), the system exhibits bistability between two oscillatory states, shown in orange and blue.

two fixed points get annihilated as a homoclinic orbit associated with the saddle collapses onto the center. To gain a complete picture of the dynamics of the fast flow, we have shown in Figs. 6(a) and 6(b) the illustrative examples of the phase portraits and the associated vector fields for $\kappa < \kappa_{SC}$ and $\kappa > \kappa_{SC}$, respectively. For $\kappa \in [-1, \kappa_{SC}]$, the fast flow possesses a limit cycle attractor, essentially derived from the local dynamics of the units, cf. the orbit indicated in red in Fig. 6(a). Apart from an attracting periodic orbit, one observes two additional types of closed orbits, namely, the homoclinic connections to the saddle point (SP), shown by blue and

green, as well as the periodic orbits around the center point (CP), an example of which is indicated in orange. For $\kappa > \kappa_{SC}$, the fast flow exhibits bistability between two oscillatory solutions, such that there is a coexistence of a limit cycle inherited from the local dynamics of units and the limit cycle associated with the former homoclinic orbits, cf. Fig. 6(b).

In the presence of noise, the described attractors of the fast flow turn to metastable states. Nevertheless, in contrast to the case of two adaptively coupled excitable units, the slow stochastic fluctuations here do not only involve switching between the metastable
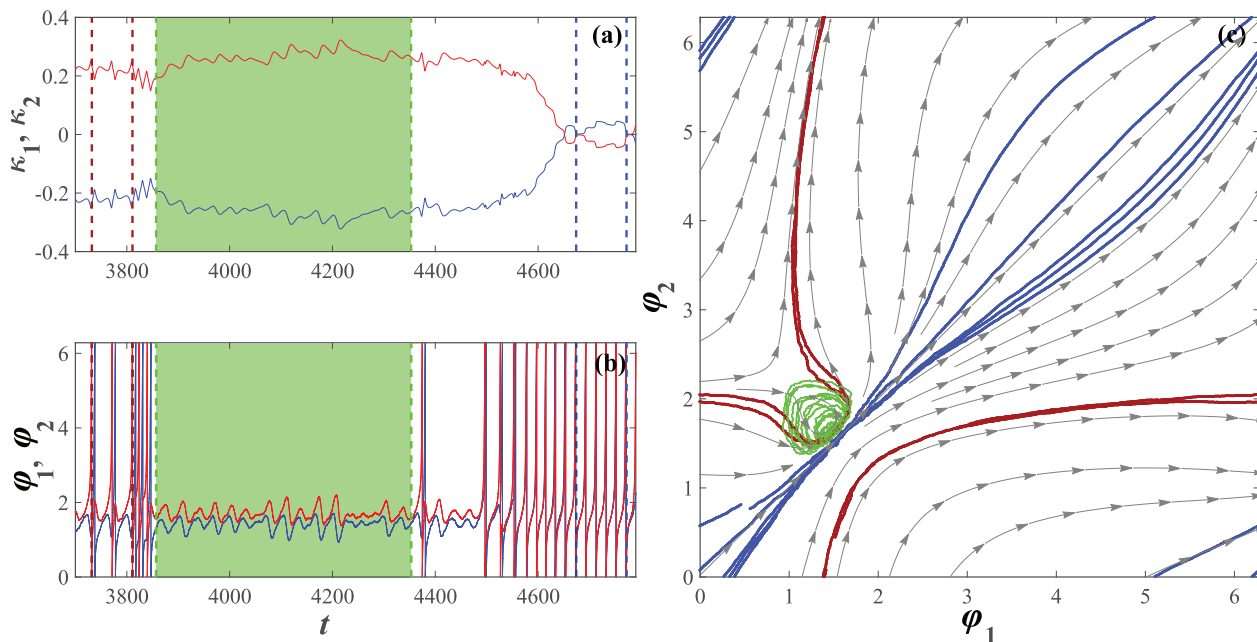
FIG. 7. (a) and (b) show the time traces of $\kappa_i(t)$ and $\varphi_i(t)$, respectively, with an episode where the system remains in the vicinity of an unstable fixed point highlighted in green. The parameters are $I_0 = 1.05$, $\varepsilon = 0.035$, $\beta = \pi$, $D = 10^{-4}$. (c) The orbits conforming to the two metastable states characterized by large-amplitude oscillations of phases are shown in red and blue, whereas the subthreshold oscillations are indicated in green. Superimposed is the vector field of the fast flow, corresponding to the limit $\varepsilon \to 0$.

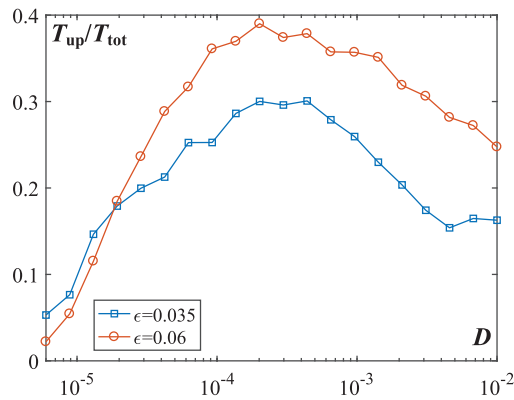**FIG. 8.** Numerically estimated fraction of time spent in the vicinity of the unstable fixed point T_{up}/T_{tot} as a function of noise for $\varepsilon = 0.035$ (squares) and $\varepsilon = 0.06$ (circles). Note that the positions of the maxima coincide with the corresponding resonant noise levels from Fig. 5. Remaining system parameters are $l_0 = 1.05, \beta = \pi$.

states but also comprise the *subthreshold oscillations* derived from the periodic orbits around the center point. These subthreshold oscillations provide for the trapping effect, which effectively leads to a reduced oscillation frequency. An example of the time series $\kappa_i(t)$ and $\varphi_i(t), i \in \{1, 2\}$ obtained for an intermediate $\varepsilon = 0.035$ in Figs. 7(a) and 7(b) indeed shows three characteristic episodes, including visits to two distinct oscillatory metastable states and an extended stay in the vicinity of the center, cf. the stochastic orbits

$(\varphi_1(t), \varphi_2(t))$ and the vector field of the fast flow in Fig. 7(c). In the case of finite scale separation, the trapping effect is manifested as the noise-enhanced stability of an unstable fixed point. The prevalence of subthreshold oscillations changes with noise in a non-monotone fashion, see the inset in Fig. 7(c), becoming maximal around the resonant noise level where the frequency dependence on noise exhibits a minimum, cf. Figs. 5 and 8. The fraction of time spent in the metastable state corresponding to subthreshold oscillations has been estimated by the numerical procedure analogous to the one already described in Sec. II.

IV. TWO MECHANISMS OF ISR IN CLASSICAL NEURONAL MODELS

So far, we have demonstrated the two paradigmatic scenarios for ISR considering the examples of coupled Type I units, whose local dynamics is close to a SNIPER bifurcation, be it in the excitable or the oscillatory regime. Nevertheless, the onset of ISR and the specific mechanisms of the phenomenon do not depend on the excitability class of local dynamics. In particular, we have recently demonstrated that a single Type II Fitzhugh–Nagumo relaxation oscillator exhibits qualitatively the same form of non-monotone dependence on noise,[30] with the mechanism involving noise-induced subthreshold oscillations that follow the maximal canard of an unstable focus. In that case, it has been established that the trapping effect and the related subthreshold oscillations are triggered due to a phase-sensitive excitability of a limit cycle. Moreover, we have verified that the same model of neuronal dynamics, set to different parameter regimes, may exhibit two different scenarios of ISR. In particular, by an appropriate selection of the system
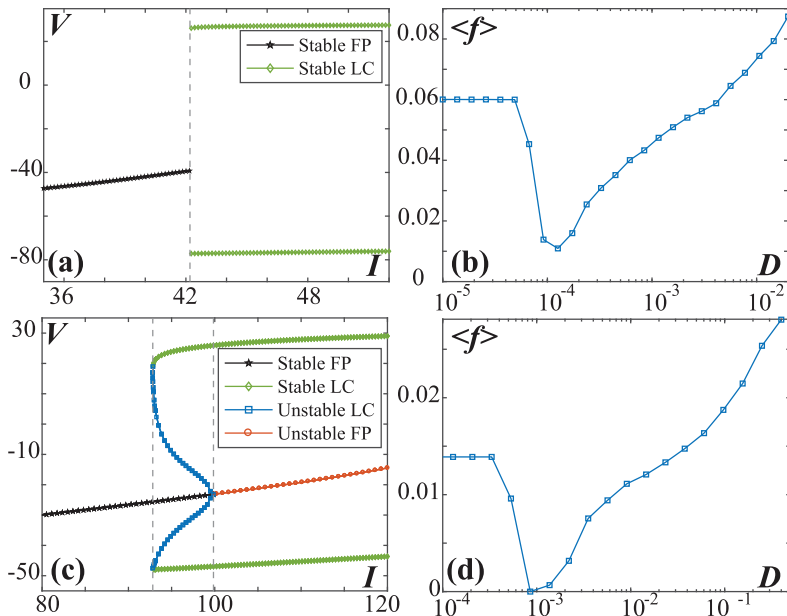

FIG. 9. (a) Bifurcation diagram showing the dependence of the amplitudes of the membrane potential V on the external bias current I for the version of Morris–Lecar model exhibiting a supercritical Hopf bifurcation. (b) illustrates the $\langle f \rangle (D)$ dependence for the Morris–Lecar neural oscillator in close vicinity of the supercritical Hopf bifurcation. (c) $V(I)$ bifurcation diagram for the setup where the Morris–Lecar model displays a subcritical Hopf bifurcation. (d) Characteristic non-monotone dependence $\langle f \rangle (D)$ for the Morris–Lecar model from (c), with the bifurcation parameter $I = 95$ set in the bistable regime. The two sets of parameters putting the Morris–Lecar model in the vicinity of a supercritical or a subcritical Hopf bifurcation are specified in the main text.

parameters, the Morris–Lecar neuron model

$$C\frac{dv}{dt} = -g_{fast}m(v)(v - E_{Na}) - g_{slow}W(v - E_K)$$
$$\qquad - g_{leak}(v - E_{leak}) + I,$$
$$\frac{dv}{dt} = \phi\frac{W_\infty(v) - W}{\tau(v)},$$
$$m(v) = 0.5\left[1 + \tanh\left(\frac{v - \beta_m}{\gamma_m}\right)\right], \qquad (8)$$
$$W_\infty(v) = \left[1 + \tanh\left(\frac{v - \beta_w}{\gamma_w}\right)\right],$$
$$\tau(v) = 1/\cosh\left(\frac{v - \beta_w}{2\gamma_w}\right),$$

where v and W, respectively, denote the membrane potential and the slow recovery variable, can be placed in the vicinity of a supercritical or a subcritical Hopf bifurcation,[53] with the external bias current I being the bifurcation parameter. In the first case, obtained for $E_{Na} = 50$ mV, $E_K = -100$ mV, $E_{leak} = -70$ mV, $g_{fast} = 20$ mS/cm², $g_{slow} = 20$ mS/cm², $g_{leak} = 2$ mS/cm², $\phi = 0.15$, $C = 2\,\mu$F/cm², $\beta_m = -1.2$ mV, $\beta_w = -13$ mV, $\gamma_m = 18$ mV, $\gamma_w = 10$ mV, the model is monostable under the variation of I, and the ISR is observed slightly above the Hopf bifurcation ($I = 43\,\mu$A/cm²) due to a noise-enhanced stability of an unstable fixed point, cf. Figs. 9(a) and 9(b). In the second case, conforming to the parameter set $E_{Na} = 120$ mV, $E_K = -84$ mV, $E_{leak} = -60$ mV, $g_{fast} = 4.4$ mS/cm², $g_{slow} = 8$ mS/cm², $g_{leak} = 2$ mS/cm², $\phi = 0.04$, $C = 20\,\mu$F/cm², $\beta_m = -1.2$ mV, $\beta_w = 2$ mV, $\gamma_m = 18$ mV, $\gamma_w = 30$ mV, the model displays bistability between a limit cycle and a stable equilibrium in a range of I just below the Hopf threshold. There, ISR emerges due to a mechanism based on biased switching, see the bifurcation diagram $V(I)$ in Fig. 9(c) and the dependence of the oscillation frequency on noise for $I = 95\,\mu$A/cm² in Fig. 9(d).

V. DISCUSSION AND OUTLOOK

Considering a model which involves the classical ingredients of neuronal dynamics, such as excitable behavior and coupling plasticity, we have demonstrated two paradigmatic scenarios for inverse stochastic resonance. By one scenario, the phenomenon arises in systems with multistable deterministic dynamics, where at least one of the attractors is a stable equilibrium. Due to the structure of the phase space, and, in particular, the position of the separatrices, the switching dynamics between the associated metastable states becomes biased at an intermediate noise level such that the longevity of the quasi-stationary states substantially increases or they may even turn into absorbing states. In the other scenario, an oscillatory system possesses a weakly unstable fixed point, whose stability is enhanced due to the action of noise. The latter results in a trapping effect such that the system exhibits subthreshold oscillations, whose prevalence is noise-dependent and is found to be maximal at the resonant noise level. Both scenarios involve classical facilitatory effects of noise, such as crossing the separatrices or stochastic mixing across the bifurcation threshold, which should warrant the

ubiquity of ISR. In terms of the robustness of the effect, we have demonstrated that the onset of ISR is independent on the excitability class of local dynamics, and moreover, that the same model of neuronal dynamics, depending on the particular parameters, may display two different scenarios for ISR.

Given that ISR has so far been observed at the level of models of individual neurons,[23,24,26,30] motifs of units with neuron-like dynamics[22,29] and neural networks,[27] it stands to reason that the phenomenon should be universal to neuronal dynamics, affecting both the emergent oscillations and systems of coupled oscillators. The explained mechanisms appear to be generic and should be expected in other systems comprised of units with local dynamics poised close to a bifurcation threshold. Inverse stochastic resonance should play important functional roles in neuronal systems, including the reduction of spiking frequency in the absence of neuromodulators, the triggering of stochastic bursting, i.e., of on–off tonic spiking activity, the suppression of pathologically long short-term memories,[14,24,26,28] and most notably, may contribute to generation of UP–DOWN states, characteristic for spontaneous and induced activity in cortical networks.[31,32]

REFERENCES

[1] B. Lindner, J. García-Ojalvo, A. Neiman, and L. Schimansky-Geier, Phys. Rep. **392**, 321 (2004).
[2] E. Forgoston and R. O. Moore, SIAM Rev. **60**, 969 (2018).
[3] B. Neiman and D. F. Russell, Phys. Rev. Lett. **88**, 138103 (2002).
[4] L. Ryashko and E. Slepukhina, Phys. Rev. E **96**, 032212 (2017).
[5] C. Zheng and A. Pikovsky, Phys. Rev. E **98**, 042148 (2018).
[6] I. Bačić, S. Yanchuk, M. Wolfrum, and I. Franović, Eur. Phys. J. Spec. Top. **227**, 1077 (2018).
[7] I. Franović and V. Klinshov, Chaos **28**, 023111 (2018).
[8] A. Fiasconaro, B. Spagnolo, and S. Boccaletti, Phys. Rev. E **72**, 061110 (2005).
[9] R. N. Mantegna and B. Spagnolo, Phys. Rev. Lett. **76**, 563 (1996).
[10] S. Ciuchi, F. de Pasquale, and B. Spagnolo, Phys. Rev. E **47**, 3915 (1993).
[11] N. V. Agudov, A. A. Dubkov, and B. Spagnolo, Physica A **325**, 144 (2003).
[12] G. Augello, D. Valentia, and B. Spagnolo, Eur. Phys. J. B **78**, 225 (2010).
[13] M. D. McDonnell and L. M. Ward, Nat. Rev. Neurosci. **12**, 415 (2011).
[14] B. A. Schmerl and M. D. McDonnell, Phys. Rev. E **88**, 052722 (2013).
[15] A. Destexhe and M. Rudolph-Lilith, *Neuronal Noise* (Springer, New York, 2012).
[16] A. S. Pikovsky and J. Kurths, Phys. Rev. Lett. **78**, 775 (1997).
[17] B. Lindner and L. Schimansky-Geier, Phys. Rev. E **60**, 7270 (1999).
[18] V. A. Makarov, V. I. Nekorkin, and M. G. Velarde, Phys. Rev. Lett. **86**, 3431 (2001).
[19] A. Zakharova, A. Feoktistov, T. Vadivasova, and E. Schöll, Eur. Phys. J. Spec. Top. **222**, 2481 (2013).
[20] N. Semenova, A. Zakharova, V. Anishchenko, and E. Schöll, Phys. Rev. Lett. **117**, 014102 (2016).
[21] L. H. Gammaitoni, P. Hänggi, P. Jung, and F. Marchesoni, Rev. Mod. Phys. **70**, 223 (1998).
[22] B. S. Gutkin, J. Jost, and H. C. Tuckwell, Eur. Phys. Lett. **81**, 20005 (2008).
[23] H. C. Tuckwell, J. Jost, and B. S. Gutkin, Phys. Rev. E **80**, 031907 (2009).

[24] M. Uzuntarla, J. R. Cressman, M. Ozer, and E. Barreto, Phys. Rev. E **88**, 042712 (2013).

[25] M. Uzuntarla, Phys. Lett. A **377**, 2585 (2013).

[26] M. Uzuntarla, J. J. Torres, P. So, M. Ozer, and E. Barreto, Phys. Rev. E **95**, 012404 (2017).

[27] M. Uzuntarla, E. Barreto, and J. J. Torres, PLoS Comput. Biol. **13**, e1005646 (2017).

[28] A. Buchin, S. Rieubland, M. Häusser, B. S. Gutkin, and A. Roth, PLoS Comput. Biol. **12**, e1005000 (2016).

[29] I. Bačić, V. Klinshov, V. I. Nekorkin, M. Perc, and I. Franović, Eur. Phys. Lett. **124**, 40004 (2018).

[30] I. Franović, O. E. Omel'chenko, and M. Wolfrum, Chaos **28**, 071105 (2018).

[31] T. T. G. Hahn, J. M. McFarland, S. Berberich, B. Sakmann, and M. R. Mehta, Nat. Neurosci. **15**, 1531 (2012).

[32] V. V. Vyazovskiy and K. D. Harris, Nat. Rev. Neurosci. **14**, 443 (2013).

[33] I. Franović and V. Klinshov, Eur. Phys. Lett. **116**, 48002 (2016).

[34] J. A. Kromer, R. D. Pinto, B. Lindner, and L. Schimansky-Geier, Eur. Phys. Lett. **108**, 20007 (2014).

[35] L. Lücken, O. V. Popovych, P. A. Tass, and S. Yanchuk, Phys. Rev. E **93**, 032210 (2016).

[36] D. Kasatkin, S. Yanchuk, E. Schöll, and V. Nekorkin, Phys. Rev. E **96**, 062211 (2017).

[37] P. O. Sporns and R. Kotter, PLoS Biol. **2**, e369 (2004).

[38] Y. L. Maistrenko, B. Lysyansky, C. Hauptmann, O. Burylko, and P. Tass, Phys. Rev. E **75**, 066207 (2007).

[39] T. Aoki and T. Aoyagi, Phys. Rev. Lett. **102**, 034101 (2009).

[40] T. Aoki and T. Aoyagi, Phys. Rev. E **84**, 066109 (2011).

[41] D. O. Hebb, *The Organization of Behavior: A Neuropsychological Approach* (John Wiley and Sons, New York, 1949).

[42] S. Song, K. D. Miller, and L. F. Abbott, Nat. Neurosci. **3**, 919 (2000).

[43] R. C. Froemke and Y. Dan, Nature **416**, 433 (2002).

[44] H.-X. Wang, R. C.Gerkin, D. W. Nauen, and G.-Q. Bi, Nat. Neurosci. **8**, 187 (2005).

[45] A. Morrison, M. Diesmann, and W. Gerstner, Biol. Cybern. **98**, 459 (2008).

[46] O. V. Popovych, S. Yanchuk, and P. A. Tass, Sci. Rep. **3**, 2926 (2013).

[47] P. Hänggi, P. Talkner, and M. Borkovec, Rev. Mod. Phys. **62**, 251 (1990).

[48] C. Kuehn, *Multiple Time Scale Dynamics* (Springer International Publishing, Switzerland, 2015).

[49] A. Shilnikov, Int. J. Bifurcat. Chaos **18**, 2141 (2008).

[50] N. Berglund and B. Gentz, *Noise-Induced Phenomena in Slow-Fast Dynamical Systems* (Springer, Berlin, 2006).

[51] *Stochastic Methods in Neuroscience*, edited by C. Laing and G. J. Lord (Oxford University Press, London, 2009).

[52] J. Touboul and G. Wainrib, Physica D **307**, 42 (2015).

[53] H. Wang, L. Wang, L. Yu, and Y. Chen, Phys. Rev. E **83**, 021915 (2011).

Igor Franović ⬤, Serhiy Yanchuk ⬤, Sebastian Eydam ⬤, Iva Bačić, and Matthias Wolfrum
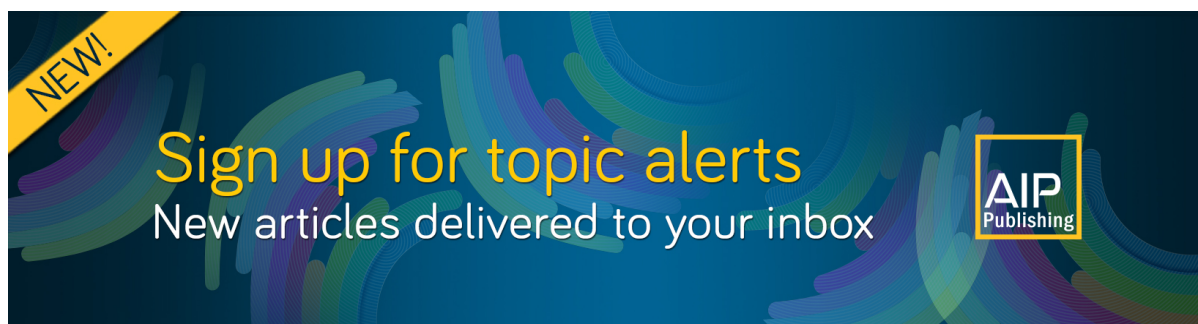
View Online   Export Citation   CrossMark

Dynamics of a stochastic excitable system with slowly adapting feedback

Igor Franović,[1,a)] Serhiy Yanchuk,[2,b)] Sebastian Eydam,[3,c)] Iva Bačić,[1,d)] and Matthias Wolfrum[3,e)]

AFFILIATIONS

[1]Scientific Computing Laboratory, Center for the Study of Complex Systems, Institute of Physics Belgrade, University of Belgrade, Pregrevica 118, 11080 Belgrade, Serbia
[2]Institut für Mathematik, Technische Universität Berlin, Straße des 17. Juni 136, 10623 Berlin, Germany
[3]Weierstrass Institute, Mohrenstrasse 39, 10117 Berlin, Germany

[a)]**Author to whom correspondence should be addressed:** franovic@ipb.ac.rs
[b)]**Electronic mail:** yanchuk@math.tu-berlin.de
[c)]**Electronic mail:** sebastian.eydam@gmail.com
[d)]**Electronic mail:** iva@scl.rs
[e)]**Electronic mail:** wolfrum@wias-berlin.de

ABSTRACT

We study an excitable active rotator with slowly adapting nonlinear feedback and noise. Depending on the adaptation and the noise level, this system may display noise-induced spiking, noise-perturbed oscillations, or stochastic bursting. We show how the system exhibits transitions between these dynamical regimes, as well as how one can enhance or suppress the coherence resonance or effectively control the features of the stochastic bursting. The setup can be considered a paradigmatic model for a neuron with a slow recovery variable or, more generally, as an excitable system under the influence of a nonlinear control mechanism. We employ a multiple timescale approach that combines the classical adiabatic elimination with averaging of rapid oscillations and stochastic averaging of noise-induced fluctuations by a corresponding stationary Fokker–Planck equation. This allows us to perform a numerical bifurcation analysis of a reduced slow system and to determine the parameter regions associated with different types of dynamics. In particular, we demonstrate the existence of a region of bistability, where the noise-induced switching between a stationary and an oscillatory regime gives rise to stochastic bursting.

Published under license by AIP Publishing. https://doi.org/10.1063/1.5145176

Recent years have witnessed a rapid expansion of stochastic models for a wide variety of important physical and biological phenomena, from sub-cellular processes and tissue dynamics, over large-scale population dynamics and genetic switching to optical devices, Josephson junctions, fluid mechanics, and climatology. These studies have demonstrated that the effects of noise manifest themselves on a broad range of scales but, nevertheless, display certain universal features. In particular, the effects of noise may generically be cast into two groups. On the one hand, the noise may enhance or suppress the features of deterministic dynamics, while on the other hand, it may give rise to novel forms of behavior, associated with the crossing of thresholds and separatrices or with stabilization of deterministically unstable states. The constructive role of noise has been evinced in diverse applications, from neural networks and chemical reactions to lasers and electronic circuits. Classical examples of stochastic facilitation in neuronal systems concern resonant phenomena, such as coherence resonance, where an intermediate level of noise may trigger coherent oscillations in excitable systems, as well as spontaneous switching between the coexisting metastable states. In the present study, we show how the interaction of noise and multiscale dynamics, induced by slowly adapting feedback, may affect an excitable system. It gives rise to a new mode of behavior based on switching dynamics, namely, the stochastic bursting and allows for an efficient control of the properties of coherence resonance.

I. INTRODUCTION

Multiscale dynamics is ubiquitous in real-world systems. In neuron models, for instance, the evolution of recovery or gating variables is usually much slower than the changes of the

membrane potential.[1,2] At the level of neural networks, certain mechanisms of synaptic adaptation, such as the spike timing-dependent plasticity,[3–5] are slower than the spiking dynamics of individual neurons. When modeling the dynamics of semiconductor lasers,[6–8] one similarly encounters at least two different timescales, one related to the carriers' and the other to the photons' lifetime, whereby their ratio can span several orders of magnitude. Investigating the dynamics of such multiscale systems has led to the development of a number of useful asymptotic and geometric methods, see Refs. 9–13, to name just a few.

Another ingredient inevitable in modeling real-world systems is noise, which may describe the intrinsic randomness of the system and the fluctuations in the embedding environment or may derive from coarse-graining over the degrees of freedom associated with small spatial or temporal scales.[14,15] For instance, neuronal dynamics is typically influenced by intrinsic sources of noise, such as the random opening of ion channels, and by external sources, like the synaptic noise.[16] In chemical reactions, noise comprises finite-size effects, while the stochasticity in laser dynamics reflects primarily quantum fluctuations. In general, the impact of noise can manifest itself by modification of the deterministic features of the system or by the emergence of qualitatively novel types of behavior, induced by the crossing of thresholds or separatrices.[17]

In the present paper, we study the effects of slowly adapting feedback and noise on an excitable system. Excitability is a general nonlinear phenomenon based on a threshold-like response of a system to perturbation.[1,15,18,19] An excitable system features a stable "rest" state intermitted by excitation events (firing), elicited by perturbations. In the absence of a perturbation, such a system remains in the rest state and a small perturbation induces a small-amplitude linear response. If the perturbation is sufficiently strong, an excitable system reacts by a large-amplitude nonlinear response, such as a spike of a neuron. When an excitable system receives additional feedback or a stochastic input or is coupled to other such systems, new effects may appear due to the self- or noise-induced excitations, as well as excitations from the neighboring systems. Such mechanisms can give rise to different forms of oscillations, patterns, propagating waves, and other phenomena.[15,20–28]

Our focus is on a stochastic excitable system subjected to a slow control via a low-pass filtered feedback

$$\dot{v}(t) = f(v(t), \mu(t)) + \sqrt{D}\xi(t), \qquad (1)$$

$$\dot{\mu}(t) = \varepsilon(-\mu(t) + \eta g(v(t))), \qquad (2)$$

where $\varepsilon \gtrsim 0$ is a small parameter that determines the timescale separation between the fast variable $v(t)$ and the slow feedback variable $\mu(t)$. The fast dynamics $\dot{v}(t) = f(v(t), 0)$ is excitable and is influenced by the Gaussian white noise $\xi(t)$ of variance D. Moreover, the slow feedback variable μ controls its excitability properties. The parameter η is the control gain such that for $\eta = 0$, one recovers a classical noise-driven excitable system.[15] An important example of a system conforming to (1) and (2) for $\eta \neq 0$ is the Izhikevich neuron model,[29] where the stochastic input to the fast variable would describe the action of synaptic noise.

Here, we analyze a simple paradigmatic example from the class of systems (1) and (2), where the excitable local dynamics is represented by an active rotator

$$\dot{\varphi}(t) = I - \sin\varphi(t) \quad \text{with} \quad \varphi \in [0, 2\pi).$$

The latter undergoes a saddle-node infinite period (SNIPER, sometimes also called SNIC – saddle node on invariant circle) bifurcation at $|I| = 1$, turning from excitable ($|I| \lesssim 1$) to oscillatory regime $|I| > 1$, see Ref. 30. The adaptation is represented by a positive periodic function $g(\varphi) = 1 - \sin\varphi$ such that the complete model reads

$$\dot{\varphi}(t) = I_0 + \mu(t) - \sin\varphi(t) + \sqrt{D}\xi(t), \qquad (3)$$

$$\dot{\mu}(t) = \varepsilon(-\mu(t) + \eta(1 - \sin\varphi(t))). \qquad (4)$$

In the presence of feedback, the noiseless dynamics of the active rotator depends now on $I = I_0 + \mu(t)$ involving the control variable $\mu(t)$, which can induce switching between the excitable equilibrium and the oscillatory regime. This adaptation rule provides a positive feedback for the spikes and oscillations, since $\mu(t)$ increases when $\varphi(t)$ is oscillating and drives the system toward the oscillatory regime, while in the vicinity of the equilibrium ($\sin\varphi \approx 1$) the control signal effectively vanishes.

We examine how the behavior of (3) and (4) is influenced by the noise level D and the control gain η, determining the phase diagram of dynamical regimes in terms of these two parameters. The first part of our results in Sec. II concerns the noise-free system $D = 0$, where we employ a combination of two multiscale methods, namely, adiabatic elimination in the regime where the fast subsystem has stable equilibrium and the averaging approach when the fast subsystem is oscillatory. As a result, we obtain a reduced slow system that is capable of describing both the slowly changing fast oscillations and the slowly drifting equilibrium, as well as the transitions between these regimes. The bifurcation analysis of this slow system reveals the emergence of bistability between the fast oscillations and the equilibrium for sufficiently large η.

The second part of our results, presented in Sec. III, addresses the multiscale analysis of the dynamics in the presence of noise ($D \neq 0$). Instead of deterministic averaging, we apply the method of *stochastic averaging*,[25,31–34] where the distribution density for the fast variable obtained from a stationary Fokker–Plank equation is used to determine the dynamics of the slow flow. In this way, we obtain a deterministic slow dynamics for which one can perform a complete numerical bifurcation analysis with respect to D and η. In Sec. IV, we investigate the effects of stochastic fluctuations on the slow dynamics, which vanish in the limit of infinite timescale separation $\varepsilon \to 0$ employed in Sec. III. The effect of a slowly adapting feedback on the coherence resonance is shown by extracting from numerical simulations the coefficient of variation of the spike time distribution in the excitable regime. In particular, we compare the results for small positive ε with the case of infinite time scale separation, where we use the stationary but noise dependent μ obtained in Sec. III. The noise-induced switching dynamics in the bistability region is demonstrated by numerical simulations showing an Eyring–Kramers type of behavior.

In terms of the different dynamical regimes, our study of stochastic dynamics reveals three characteristic (D, η) regions featuring noise-induced spiking, noise-perturbed spiking, and stochastic busting (see Fig. 1). We show that by varying the control gain
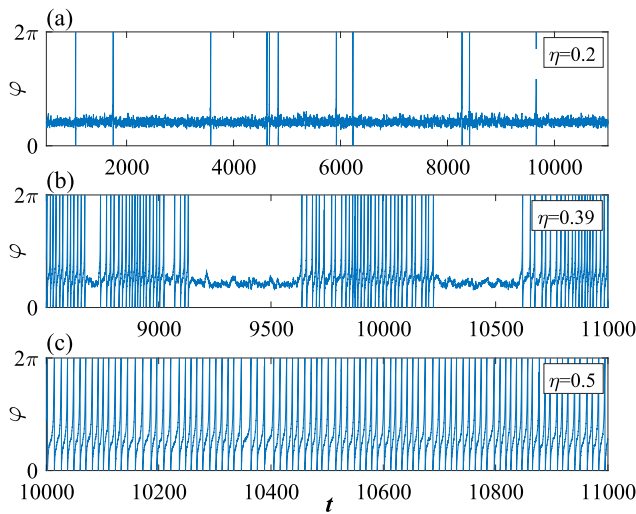
FIG. 1. Different dynamical regimes in the stochastic excitable system subjected to a slow control via a low-pass filtered feedback (3) and (4) with $\varepsilon = 0.005$, $D = 0.008$ and different choices of the control gain η: noise-induced spiking (a), stochastic bursting (b), and noise-perturbed spiking (c).
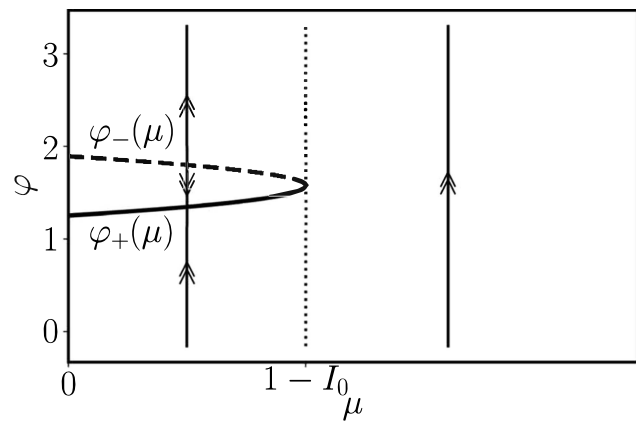

FIG. 2. Critical manifold and fast dynamics of systems (5) and (6). For $\mu < 1 - I_0$, the fast dynamics converges to the stable branch of the critical manifold, while for $\mu > 1 - I_0$, it is oscillatory with periodic rotation of the phase φ.

within the region of noise-induced spiking, one can enhance or suppress the coherence resonance, while within the bistability region, one can efficiently control the properties of stochastic bursting. Sections II–IV provide a detailed analysis of the described phenomena.

II. SLOW–FAST ANALYSIS OF THE DETERMINISTIC DYNAMICS

In this section, we analyze the systems (3) and (4) in the absence of noise ($D = 0$)

$$\dot{\varphi}(t) = I_0 - \sin \varphi(t) + \mu(t), \qquad (5)$$

$$\dot{\mu}(t) = \varepsilon \left(-\mu(t) + \eta \left(1 - \sin \varphi(t) \right) \right), \qquad (6)$$

considering the limit $\varepsilon \to 0$ within the framework of singular perturbation theory. The fast subsystem

$$\dot{\varphi}(t) = I_0 + \mu - \sin \varphi(t), \qquad (7)$$

often called a "layer equation" describes the dynamics on the fast timescale and is obtained from (5) and (6) by setting $\varepsilon = 0$, whereby μ acts as a parameter.

A. Dynamics for $\mu < 1 - I_0$: Adiabatic elimination

In the case $\mu < 1 - I_0$, the fast subsystem (7) possesses two equilibria

$$\varphi_+(\mu) = \arcsin(I_0 + \mu), \quad \varphi_-(\mu) = \pi - \varphi_+(\mu), \qquad (8)$$

where φ_+ is stable and φ_- is unstable. Considering them as functions of the parameter μ, the equilibria give rise to two branches, which

merge in a fold at $\mu = 1 - I_0$ (see Fig. 2). Equivalently, the set of equilibria of the fast subsystem

$$\{(\varphi, \mu) : \sin \varphi = I_0 + \mu\} \qquad (9)$$

comprises the critical manifold of (5) and (6), with the stable part $\varphi_+(\mu)$ and the unstable part $\varphi_-(\mu)$.

Hence, for $\mu < 1 - I_0$, the trajectories are rapidly attracted toward the stable branch of the critical manifold, along which for positive ε they slowly drift. In order to describe this slow dynamics, we rescale time $T = \varepsilon t$ and obtain

$$\varepsilon \varphi'(T) = I_0 + \mu(T) - \sin \varphi(T), \qquad (10)$$

$$\mu'(T) = -\mu(T) + \eta(1 - \sin \varphi(T)), \qquad (11)$$

where the prime denotes the derivative with respect to the slow time T. Setting $\varepsilon = 0$, we can directly eliminate the term $\sin \varphi(T) = I_0 + \mu(T)$ and obtain the equation for the slow dynamics on the critical manifold

$$\mu'(T) = -\mu(T) + \eta(1 - I_0 - \mu(T)). \qquad (12)$$

B. Dynamics for $\mu > 1 - I_0$: Averaging fast oscillations

For $\mu > 1 - I_0$, there is no stable equilibrium of the fast subsystem (7) (see Fig. 2). Instead, one finds periodic oscillations

$$\varphi_\mu(t) = 2 \arctan \frac{1 + \Omega(\mu) \tan \frac{t}{2} \Omega(\mu)}{I_0 + \mu}, \qquad (13)$$

with the μ-dependent frequency

$$\Omega(\mu) = \sqrt{(I_0 + \mu)^2 - 1}.$$

In this case, the fast oscillations $\varphi_\mu(t)$ should be averaged in order to obtain the dynamics of the slow variable $\mu(T)$, see Refs 35

and 36. A rigorous formal derivation is provided in Appendix A, finally arriving at

$$\mu'(T) = -\mu(T) + \eta(1 - I_0 - \mu(T) + \Omega(\mu(T))). \quad (14)$$

Here, we give a simplified explanation of the averaging procedure. First, we substitute the fast-oscillating solution $\varphi = \varphi_\mu(t)$ of the fast subsystem into the equation for the slow variable (11),

$$\mu'(T) = -\mu(T) + \eta(1 - \sin\varphi_\mu(t)).$$

Since the term $\sin(\cdot)$ is fast oscillating, the last equation can be averaged over the fast timescale t, which leads to

$$\mu'(T) = -\mu(T) + \eta\left(1 - \langle\sin\varphi_\mu(t)\rangle_t\right). \quad (15)$$

The average $\langle\sin\varphi_\mu(t)\rangle_t$ can be found by integrating (7) over the period, which gives

$$\langle\dot\varphi(t)\rangle_t = \Omega(\mu) = I_0 + \mu - \langle\sin\varphi_\mu(t)\rangle_t. \quad (16)$$

Hence, by substituting

$$\langle\sin\varphi_\mu(t)\rangle_t = I_0 + \mu(T) - \Omega(\mu(T))$$

into (15), we obtain the slow averaged dynamics (14).

C. Combined dynamics of the slow variable

Summarizing the results so far, Eq. (12) describes the dynamics of the slow variable for $\mu < 1 - I_0$, while Eq. (14) holds for $\mu > 1 - I_0$. These two equations can be conveniently combined into a single equation of the form (14) by extending the definition of the frequency $\Omega(\mu)$ as follows:

$$\Omega(\mu) = \begin{cases} 0, & \mu < 1 - I_0, \\ \sqrt{(I_0 + \mu)^2 - 1}, & \mu > 1 - I_0. \end{cases} \quad (17)$$

Hence, the slow dynamics is described by the scalar ordinary differential equation on the real line (14), and, as a result, the only possible attractors are fixed points, which are given by the zeros of the right-hand side as

$$\Omega(\mu) = \frac{\eta + 1}{\eta}\mu + I_0 - 1. \quad (18)$$

Geometrically, they are points of intersection of the frequency profile $\Omega(\mu)$ with the line $\frac{\eta+1}{\eta}\mu + I_0 - 1$ [see Fig. 3(a)]. In particular, one can check that there is always one fixed point

$$\mu_1 = \frac{\eta(1 - I_0)}{1 + \eta} < 1 - I_0, \quad (19)$$

for which $\Omega(\mu_1) = 0$ such that it corresponds to a pair of equilibria on the critical manifold (9). Since μ_1 is stable for the slow dynamics, the point $(\varphi_+(\mu_1), \mu_1)$ is also a stable equilibrium for original systems (5) and (6) with small ε. The other two fixed points of the slow
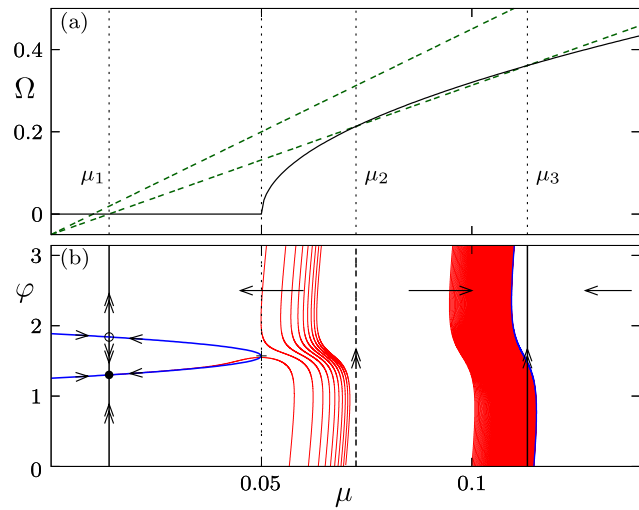

FIG. 3. (a) Graphical solution of the fixed point Eq. (18): $\Omega(\mu)$ according to (17) (black) and the right-hand side of (18) for different choices of η. One finds from one to three fixed points depending on η. (b) Scheme of the slow–fast dynamics of systems (5) and (6) with parameters $I_0 = 0.95$ and $\eta = 0.38$ and the numerical sample trajectories for $\varepsilon = 0.005$ (red). For $\mu < 1 - I_0$, trajectories are attracted to the stable branch of the slow manifold (blue curve) and subsequently slowly drift toward the stable fixed point $(\varphi_+(\mu_1), \mu_1)$ (black dot). For $\mu > 1 - I_0$, the sample trajectories show fast oscillations in φ with a slow average drift in μ in the direction indicated by the arrows.

equation

$$\mu_{2,3} = \frac{\eta\left(1 + \eta - I_0 \mp \sqrt{(\eta + I_0)^2 - 1 - 2\eta}\right)}{1 + 2\eta}, \quad (20)$$

with $\Omega(\mu_{2,3}) > 0$ appear in a saddle-node bifurcation at

$$\eta_{sn} = 1 - I_0 + \sqrt{2(1 - I_0)} \quad (21)$$

and correspond to a pair of periodic orbits of fast subsystem (7).

In Fig. 3(b) we show schematically the results of our slow–fast analysis for $I_0 = 0.95$ and $\eta = 0.38$. For the chosen parameter values there are two stable regimes: the fixed point $(\varphi_+(\mu_1), \mu_1)$ and a fast oscillation with $\langle\mu(t)\rangle_t \approx \mu_3$.

Finally, Fig. (4) presents the bifurcation diagram of the fixed points of the slow dynamics with respect to the control gain η. One observes that there is always one branch of stable fixed points corresponding to the steady state and two stable fixed points corresponding to fast oscillations for $\eta > \eta_{sn}$. For our choice of $I_0 = 0.95$, we obtain $\eta_{sn} \approx 0.3662$.

III. SLOW–FAST ANALYSIS OF THE DYNAMICS WITH NOISE

In this section, we consider the dynamics of systems (3) and (4) in the presence of noise ($D > 0$). In analogy to the noise-free case,
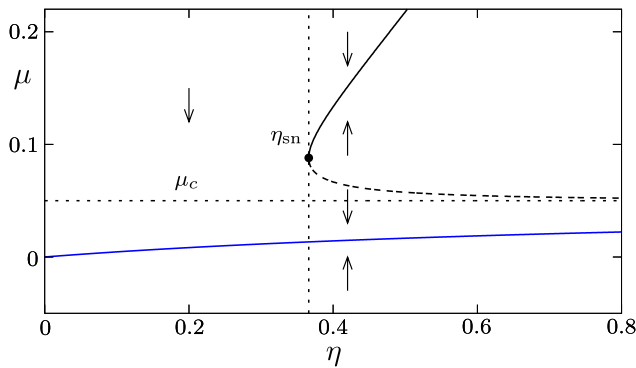
FIG. 4. Fixed points of the slow dynamics (14) for varying control gain η. The values $\mu_{2,3}$ on the upper branch (black curve) correspond to periodic orbits of the fast subsystem (7), while μ_1 (blue curve) is the branch of fixed points; solid and dashed lines indicate stable and unstable solutions, respectively. The direction of the motion in $\mu(T)$ is indicated by the arrows. The dotted lines indicate the onset of bistability for $\eta = \eta_{sn}$ and the transition at $\mu_c = 1 - I_0$ from equilibria to periodic orbits.

one can use the limit $\varepsilon \to 0$ and employ the *stochastic average*

$$\langle \sin \varphi(t) \rangle_t = \lim_{t \to \infty} \frac{1}{t} \int_0^t \sin \varphi(t) dt',$$

for solutions of the stochastic fast equation

$$\dot{\varphi}(t) = I_0 + \mu - \sin \varphi(t) + \sqrt{D} \xi(t) \tag{22}$$

to approximate the slow dynamics in (11) by

$$\mu'(T) = -\mu(T) + \eta(1 - \langle \sin \varphi(t) \rangle_t). \tag{23}$$

To this end, we consider the *stationary probability density distribution* $\rho(\varphi; \mu, D)$ for the fast noisy dynamics (3), which for fixed control μ and noise intensity D is given as a solution to the stationary Fokker–Planck equation

$$\frac{D}{2} \partial_{\varphi\varphi} \rho - \partial_\varphi [(I_0 + \mu - \sin \varphi)\rho] = 0, \tag{24}$$

together with the periodic boundary conditions $\rho(0) = \rho(2\pi)$ and the normalization

$$\int_0^{2\pi} \rho(\varphi; \mu, D) d\varphi = 1. \tag{25}$$

From this, we can calculate the average

$$\langle \sin \varphi(t) \rangle_t = \int_0^{2\pi} \rho(\varphi; \mu, D) \sin \varphi d\varphi \tag{26}$$

and obtain the mean frequency

$$\Omega_D(\mu) = I_0 + \mu - \langle \sin \varphi(t) \rangle_t, \tag{27}$$

which depends via (26) both on D and μ. Taking into account (23) and (27), the equation for the slow dynamics of $\mu(T)$ reads

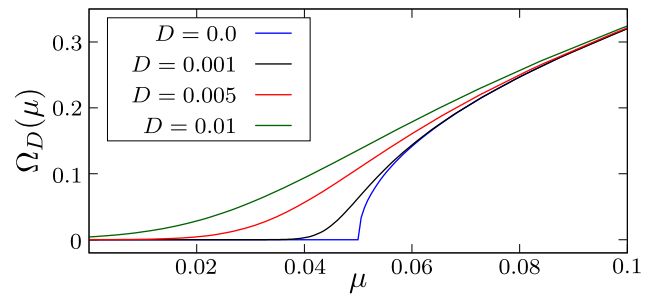$$\mu'(T) = -\mu(T) + \eta(1 - I_0 - \mu + \Omega_D(\mu(T))), \tag{28}$$

FIG. 5. Average frequency of the fast dynamics (3) given by (26) and (27) using numerical solutions of the stationary Fokker–Planck Eq. (24), where μ acts as a time independent parameter and fixed $I_0 = 0.95$.

i.e., it is of the same form as in the deterministic case (14). The corresponding fixed point equation for the stationary values of μ with respect to the slow dynamics is given by (18).

The stationary Fokker–Planck Eq. (24) can be solved directly by integral expressions [see Appendix B]. In particular, for $D = 0$, we readily recover the results for periodic averaging from Sec. II. However, for small non-vanishing D, the integrals become difficult to evaluate numerically, and we preferred to solve (24) as a first-order ODE boundary value problem with software AUTO,[37] which provides numerical solutions to boundary value problems by collocation methods together with continuation tools for numerical bifurcation analysis.

In Fig. 5 are shown the numerically obtained effective frequencies $\Omega_D(\mu)$ for different noise levels D. Solving the stationary Fokker–Planck Eq. (24) together with the fixed point equation for $\mu(T)$ (18), we obtain for fixed values of D and varying control gain η branches of stationary solutions $(\mu^*, \rho(\varphi; \mu^*, D))$ [see Fig. 6(a)]. For small noise intensities, these branches are folded, which indicates the coexistence of up to three stationary solutions, similarly as in the noise-free case. Alternatively, we can also fix η and obtain branches for varying D [see Fig. 6(c)]. For small η they are monotonically increasing, while for larger η they are folded. For $\eta_{sn} < \eta$ there are two separate branches, emanating from the three solutions of (18) at $D = 0.6$

Numerical continuation of the folds in the (η, D) parameter plane provides the curves outlining the boundaries of the bistability region. Figure 6(b) shows that the two branches of folds meet at a cusp point (η_{cu}, D_{cu}). One of the branches approaches for $D \to 0$ the value $\eta = \eta_{sn}$, which we have calculated in (21), while the other one diverges to infinite values of η. From our numerics for different values of I_0, we observe that closer to the critical value $I_0 = 1$, the cusp point shifts to a smaller noise intensity D such that the region of bistability decreases.

Note that for $D > 0$, all the average frequencies satisfy $\Omega_D > 0$ such that a clear distinction between the stationary and the oscillatory regime of the fast dynamics is no longer possible. However, one can compare the critical value of the deterministic fast dynamics
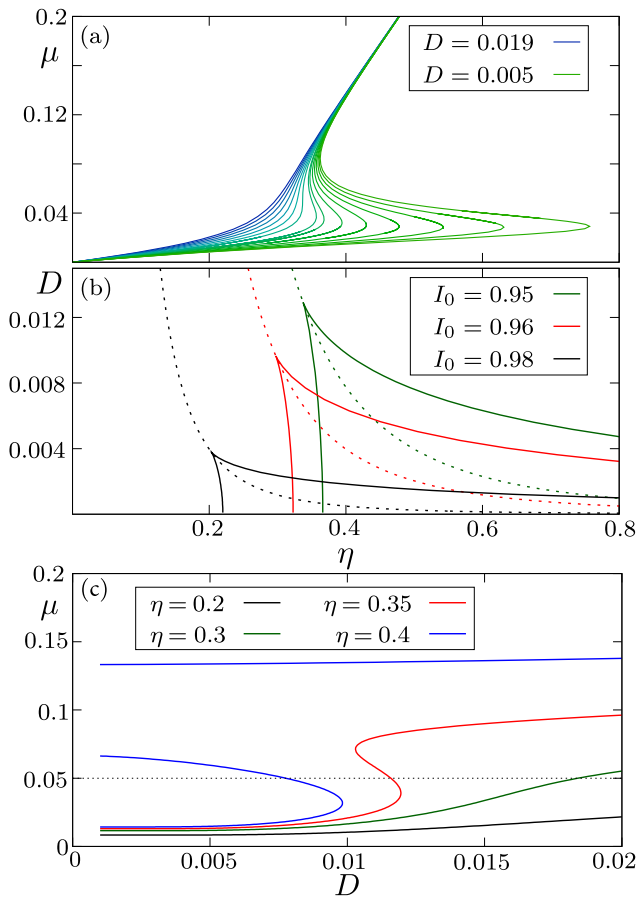
$$\mu_c = 1 - I_0, \tag{29}$$

FIG. 6. Panels (a) and (c): Branches of fixed points μ^* of the slow dynamics (28) calculated at $I_0 = 0.95$ from (18) together with the stationary Fokker–Planck Eq. (24). (a) Branches $\mu^*(\eta)$ for noise values $D = 0.005, 0.006, \ldots, 0.019$ and (b) two-dimensional bifurcation diagrams in terms of η and D for three different values of I_0 show the curves of fold bifurcations, which meet at the cusp point. Dashed curves indicate the case where $\mu^* = \mu_c = 1 - I_0$. (c) Branches $\mu^*(D)$ for control gain values $\eta \in \{0.2, 0.3, 0.35, 0.4\}$.

with the corresponding stationary value μ^* of the slow variable from (28) to distinguish between the regime of $\mu^* < \mu_c$, where the oscillations are induced by the noisy fluctuations of $\mu(t)$ and have the form of rare spikes [see Fig. 1(a)], and the regime $\mu^* > \mu_c$ where the oscillatory behavior is already induced by the stationary value of μ^* [see Fig. 1(c)].

Our numerical bifurcation analysis shows that the curves where the stationary values of μ satisfy the condition $\mu = \mu_c$, shown as dashed line in Fig. 6(b), pass exactly through the corresponding cusp points and inside the bistability region refer to the unstable solutions given by the middle part of the S-shaped curves in Fig. 6(a). From this, we conclude that changing the parameters across this line outside the bistability region results in a gradual transition between the regime of fluctuation-induced oscillations and the oscillations induced by the stationary value of μ^*, while at the boundary of the

bistability region, a hysteretic transition between the two regimes is obtained. Moreover, for finite timescale separation $\varepsilon > 0$, there can also be transitions between the two stable regimes within the bistability region, which are induced as well by the stochastic fluctuations. In Sec. IV, we study in detail how the region of bistability found for the singular limit $\varepsilon \to 0$ also affects the dynamics of the original system in the case of finite timescale separation.

IV. EFFECTS OF FLUCTUATIONS AND FINITE TIMESCALE SEPARATION

The two basic deterministic regimes of the fast dynamics, which are the excitable equilibrium, and the oscillations induce in a natural way the two corresponding states of the system with noise and small $\varepsilon > 0$, namely,

- noise-induced spiking, characterized by a Poisson-like distribution of inter-spike intervals (ISIs) [see Fig. 7(a)] and
- noisy oscillations, involving a Gaussian-like distribution of the ISIs, centered around the deterministic oscillation period [see Fig. 7(b)].

These states are found for sufficiently small or large values of η, respectively, where only a corresponding single branch of the deterministic system is available and the fluctuations of μ around its average value have no substantial impact on the dynamics, cf. the blue and orange distributions in Fig. 7. For sufficiently large noise levels above the cusp ($D > D_{cu}$) and intermediate values of η, one observes a gradual transition between these two regimes. However, for smaller noise $D < D_{cu}$, allowing for the existence of the region

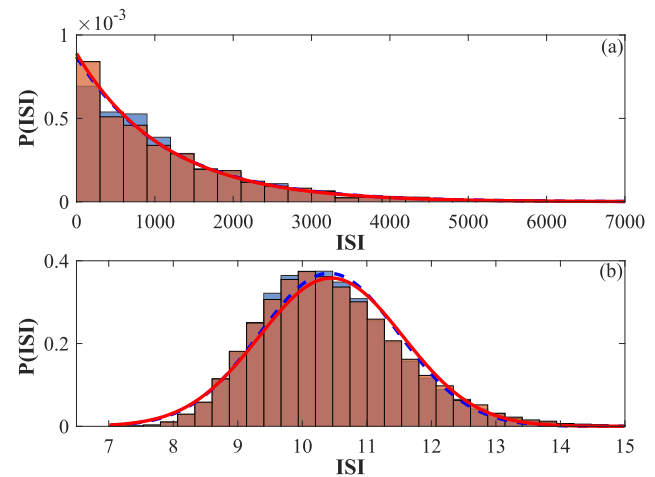**FIG. 7.** Histograms of inter-spike intervals of the phase variable for control gain $\eta = 0.2$ (top panel) and $\eta = 0.5$ (bottom panel) obtained from numerical simulations of full systems (3) and (4) with $\varepsilon = 0.005$ (orange) and in the limit of infinite timescale separation (blue), using (22) with the stationary $\mu(T) \equiv \mu_D$ determined from the stationary Fokker–Planck Eq. (24). Solid red and dashed blue curves represent fits to an exponential decay (a) and a Gaussian (b) for the histograms concerning the full system and the limit of infinite scale separation, respectively.

of bistability [cf. Fig. 6(b)], new regimes of stochastic dynamics can emerge, namely,

- enhanced coherence resonance, where a noise-induced dynamical shift of the excitability parameter $I_0 + \mu_D$ is self-adjusted close to criticality and
- noise-induced switching between the two coexisting regimes in the bistability region [see Fig. 1(b)].

A. Enhanced coherence resonance

The phenomenon of coherence resonance,[20,38,39] where the regularity of noise-induced oscillations becomes maximal at an intermediate noise level, is well-known for noisy excitable systems such as the fast Eq. (22) without adaptation, i.e., for $\eta = 0$ and therefore also $\mu = 0$. For values of the control gain $0 < \eta < \eta_{\text{cu}}$ below the region of bistability, the control leads to a substantially enhanced coherence resonance. This effect can be quantified by studying the noise dependence of the coefficient of variation of the inter-spike intervals. For a given noisy trajectory of (22), the spiking times t_k are defined as the first passage times $\varphi(t_k) = 2\pi k, k \in \mathbb{N}$ with corresponding inter-spike intervals $\tau_k = t_k - t_{k-1}$. The coefficient of variation of their distribution is defined as

$$R(D) = \frac{\sqrt{\langle \tau_k^2 \rangle - \langle \tau_k \rangle^2}}{\langle \tau_k \rangle}. \tag{30}$$

For (22) with a fixed μ, the latter can be determined from direct numerical simulations. However, inserting for μ the corresponding stochastic averages $\mu^*(D; \eta)$ obtained in the section shows a strong nonlinear dependence both on η and D [see also Figs. 6(a) and 6(c)]. In particular, the strong nonlinear dependence on D for η slightly below the cusp value η_{cu} has a substantial impact on the resonant behavior reflected in the form of $R(D)$. In Fig. 8, we show the $R(D)$ dependence for different values of the control gain η, comparing the numerical results for the fast subsystem (22) with inserted stationary values $\mu^*(D; \eta)$ to numerical simulations of (3) and (4) for $\varepsilon = 0.005$. For $0 < \eta < \eta_{cu}$, one finds that the coherence resonance can be substantially enhanced, cf., for example, the $R(D)$ dependencies for $\eta = 0$ and $\eta = 0.3$. On the other hand, introducing negative values of the control gain η, the resonant effect can be readily suppressed. This implies that the adaptive feedback we employ provides an efficient *control of coherence resonance*. Such an effect has already been demonstrated in Refs. 40, 41, and 42 by using a delayed feedback control of Pyragas type. However, this control method requires the feedback delay time as an additional control parameter to be well adapted to the maximum resonance frequency.

B. Bursting behavior due to noise-induced switching

For parameter values (η, D) within the bistable region and finite timescale separation $\varepsilon > 0$, the coexisting states of excitable equilibrium and fast oscillations turn into metastable states of full systems (3) and (4). Based on our slow–fast analysis, the corresponding dynamics can be understood as follows. The noisy fluctuations of $\varphi(t)$ around its average distribution, given by the stationary Fokker–Planck Eq. (24), induces fluctuations of $\langle \sin \varphi(t) \rangle_t$, and hence also of μ, around their stationary average values calculated
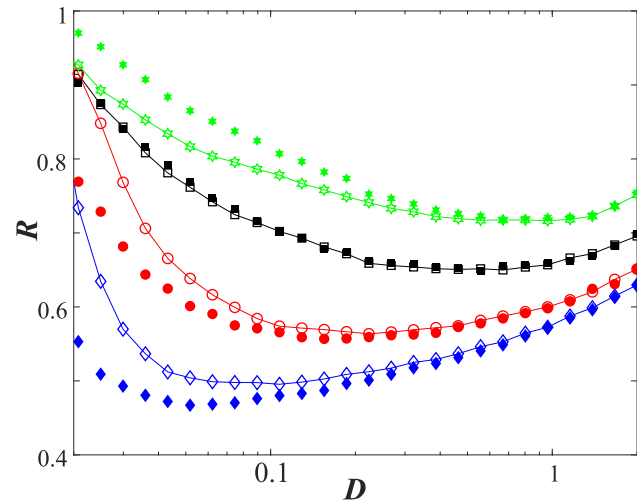

FIG. 8. Enhancement or suppression of coherence resonance by a slowly adapting feedback control. The connected lines with empty symbols refer to $R(D)$ dependencies for full systems (3) and (4) at different values of the control gain: $\eta = -0.2$ (green hexagonals), $\eta = 0$ (black squares), $\eta = 0.2$ (red circles), and $\eta = 0.3$ (blue diamonds), having fixed $I_0 = 0.95, \varepsilon = 0.005$. The unconnected filled symbols indicate the corresponding $R(D)$ dependencies obtained from numerical simulations of the fast subsystem 22 with stationary $\mu^*(D)$.

above. For small ε, the corresponding distribution of μ is centered in narrow peaks at the stable stationary values. However, with increasing ε, the nonlinear filtering induces a strong skewness of each peak in the distribution, and their overlapping indicates the possibility of noise-induced transitions between the two metastable states. Figure 9 shows the distribution for $\varepsilon = 0.005$ and different values of the η within the bistability region. These transitions can be understood in analogy to the Eyring–Kramers process in a double well potential. In the generic case of different energy levels for the two potential wells, transitions in one of the directions occur at a higher rate and the system stays preferably in the state associated with the global minimum of the potential. Such behavior of biased switching is very pronounced closed to the boundaries of the bistability region, where a switching to the state close to the fold has a much lower probability than switching back.

In Fig. 10 are shown the numerical time averages $\langle \mu(T) \rangle$ for varying control gain η. One can see that for most values of η, the long-time behavior is dominated by one of the two metastable states, which indicates a biased switching process. Nevertheless, at an intermediate value of η, we find a balanced switching, where transitions in both directions occur at an almost equal rate. A corresponding time trace is shown in Figs. 11 and 1(b). For $\varepsilon \to 0$, the switching rate decreases to zero exponentially and the switching bias in the unbalanced regime increases. This leads to the characteristic steplike behavior of the averages observed in Fig. 10 for smaller ε.

The noise-induced switching shown in Figs. 11 and 1(b) resembles the regime of bursting in neuronal systems. Here, it emerges by an interplay of slow adaptation and noise. In the present setup,
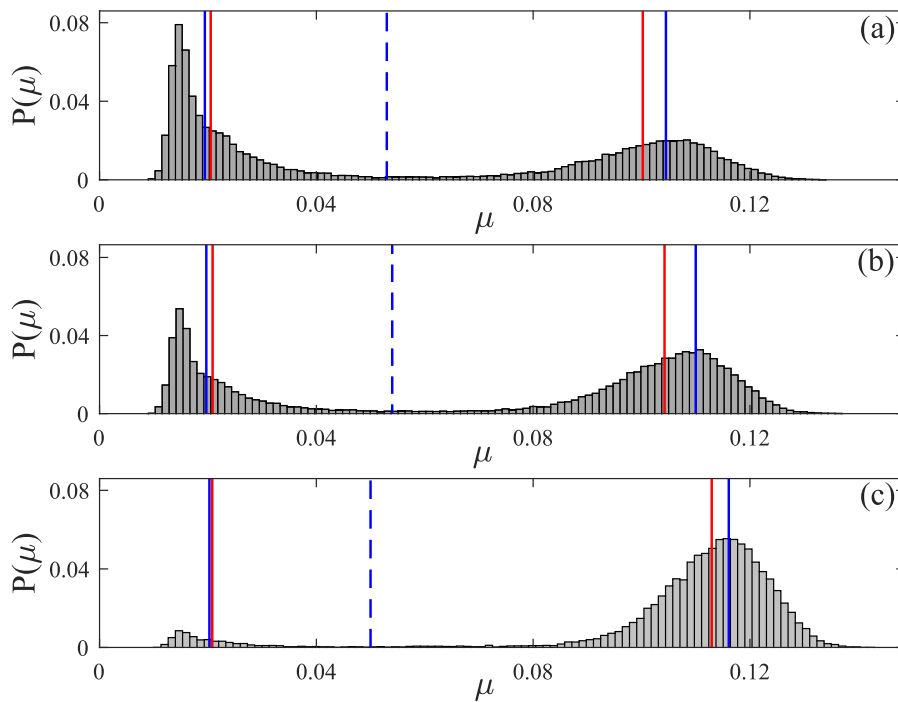
FIG. 9. Stationary distributions $P(\mu)$, sampled from numerical simulations of (3) and (4) with $\varepsilon = 0.005$. Parameters $\eta = 0.37$ in (a), $\eta = 0.373$ in (b) and $\eta = 0.38$ in (c) and fixed noise level $D = 0.009$ lie inside the bistability region from Fig. 6(b). Blue vertical lines indicate the fixed points of μ from the stationary Fokker–Planck Eq. (24) together with the fixed point Eq. (18) of the slow dynamics. Red vertical lines indicate the mean values of all μ in $P(\mu)$ below and of all μ above the unstable fixed point in the middle (dashed blue lines).

the bursts are triggered just by the stochastic fluctuations. However, in regime $\eta > \eta_{cu}$, the system is also quite susceptible to external inputs, which could initiate the bursts even without any intrinsic noise.

V. DISCUSSION AND OUTLOOK

Our model provides a novel perspective on how the dynamics of an excitable system is influenced by the interaction of a slowly adapting feedback and noise. The feedback is taken from a low-pass
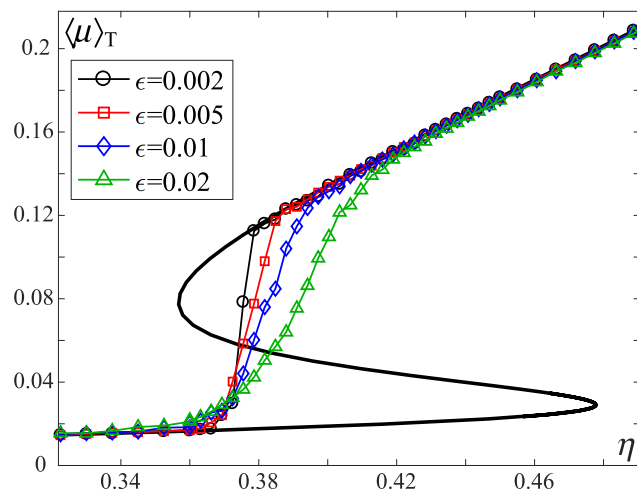
FIG. 10. Long-time averages $\langle\mu\rangle_T$ from numerical simulations of (3) and (4) with fixed noise intensity $D = 0.008$ and varying control gain η at different values of $\varepsilon \in \{0.002, 0.005, 0.01, 0.02\}$. The black curve represents the corresponding result for the infinite timescale separation [cf. Fig. 6(a)].
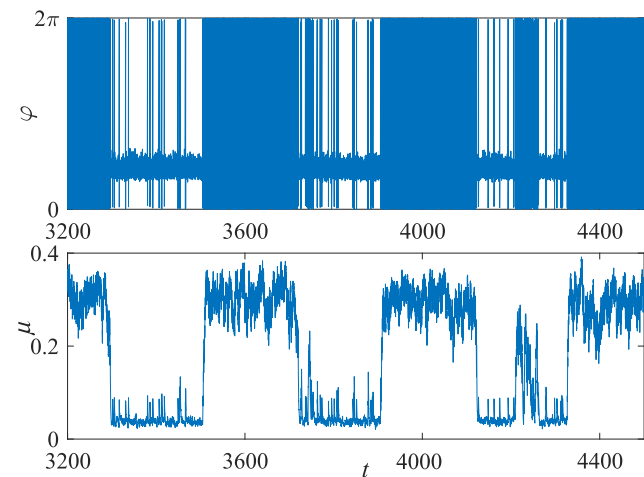
FIG. 11. Time series $\varphi(t)$ (top panel) and $\mu(t)$ (bottom panel) illustrating the regime of balanced switching. The system parameters are $\eta = 0.38$, $D = 0.008$, $l_0 = 0.95$, $\varepsilon = 0.01$.
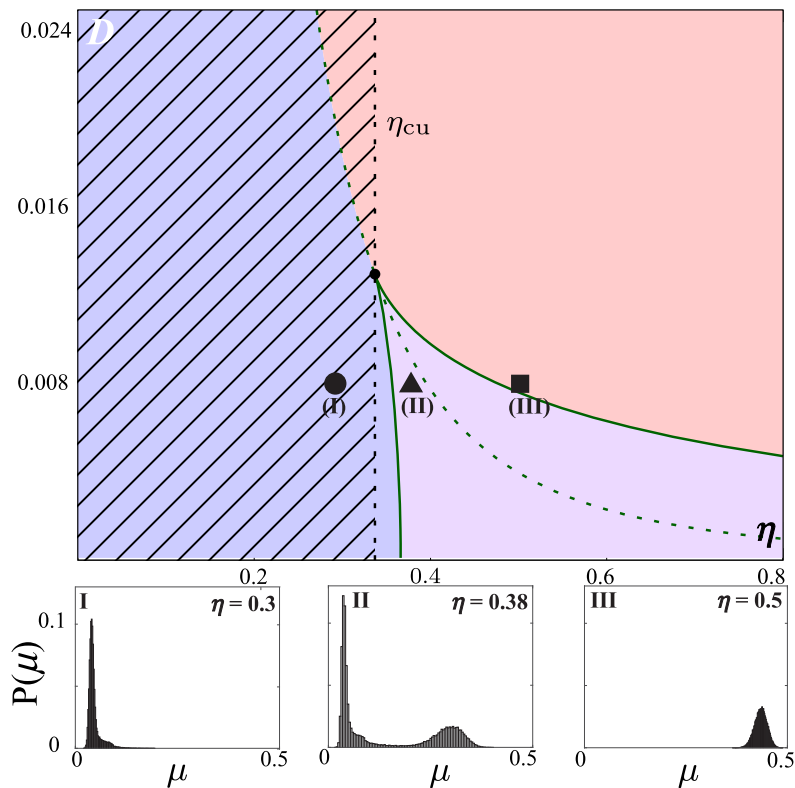
FIG. 12. Upper panel: parameter regions for different dynamical regimes: noise-induced spiking (blue), noise-perturbed oscillations (red), and noise-induced bursting (violet). Enhanced coherence resonance can be found in the hatched region. Symbols indicate the parameter values associated with the histograms $P(\mu)$ shown below. Lower panels: sampled distributions of $\mu(T)$ from numerical solutions with $\varepsilon = 0.005$, $D = 0.008$, and $\eta \in 0.3, 0.38, 0.5$.

filter of a function that gives a positive feedback to the oscillations by pushing the excitability parameter toward the oscillatory regime. Since excitability, feedback, and noise are typical ingredients of neural systems, we believe that the application of our results to a specific neural model would be a next natural step, aiming to gain a deeper understanding of the onset of different dynamical regimes, as well as the means of controlling their properties and the emerging resonant effects. In Fig. 12 are summarized our main results. In particular, the multiple timescale analysis for the limit of infinite timescale separation has allowed us to perform a numerical bifurcation analysis providing the parameter regions for the different dynamical regimes illustrated in Fig. 1. Numerical simulations for finite values of ε (lower panels in Fig. 12) show that the slowly varying control variable $\mu(T)$ is distributed around the stationary values from the limiting problem $\varepsilon = 0$ [see also Fig. 9]. Moreover, we have demonstrated that the filtered feedback in our model provides an efficient control of the effect of coherence resonance, which can be substantially enhanced or suppressed by a corresponding choice of the feedback gain. In the regime where the limiting problem $\varepsilon = 0$ indicates bistability between the equilibrium and a fast oscillation, the stochastic fluctuations at finite values of ε give rise to switching between the associated metastable states. However, our analysis shows that for sufficiently high noise intensity, this bistability vanishes and the two different deterministic states can no longer be distinguished.

From the point of view of the theory of multiscale systems, the deterministic part of the presented model provides one of the simplest examples combining the regimes of stable equilibrium and oscillations within the fast subsystem. A rigorous mathematical treatment of the dynamical transitions between the two regimes and the corresponding reductions by the standard adiabatic elimination and the averaging technique is still missing. Also, our approach to analysis of stochastic dynamics in multiscale systems by introducing a stationary Fokker–Planck equation for the fast dynamics leads to important questions concerning the limiting properties of the trajectories and the specific implications of the fluctuations. Nevertheless, we have considered only the case when the noise acts in the fast variable. An open problem is to study how the obtained results are influenced by the noise in the slow variable, where interesting new effects can be expected.[43]

APPENDIX A: MULTISCALE AVERAGING IN THE REGIME OF FAST OSCILLATIONS

In this appendix, we provide a rigorous formal derivation of the slow averaged Eq. (14) for the case of periodic dynamics in the fast layers.

We apply the following general multiscale ansatz:

$$\varphi = \bar{\varphi}(t, \varepsilon t) + \varepsilon \hat{\varphi}(t, \varepsilon t),$$
$$\mu = \bar{\mu}(t, \varepsilon t) + \varepsilon \hat{\mu}(t, \varepsilon t).$$

Substituting this ansatz into (3) and (4), one obtains up to the terms of the order ε,

$$\partial_1 \bar{\varphi} + \varepsilon \partial_2 \bar{\varphi} + \varepsilon \partial_1 \hat{\varphi} = I_0 - \sin(\bar{\varphi} + \varepsilon \hat{\varphi}) + \bar{\mu} + \varepsilon \hat{\mu},$$
$$\partial_1 \bar{\mu} + \varepsilon \partial_2 \bar{\mu} + \varepsilon \partial_1 \hat{\mu} = \varepsilon \left(-\bar{\mu} - \varepsilon \hat{\mu} + \eta \left(1 - \sin(\bar{\varphi} + \varepsilon \hat{\varphi})\right)\right),$$

where subscripts 1 and 2 refer to partial derivatives with respect to t and εt, respectively. Collecting the terms of order $\mathcal{O}(1)$, one finds

$$\partial_1 \bar{\varphi} = I_0 - \sin \bar{\varphi} + \bar{\mu}, \tag{A1}$$

$$\partial_1 \bar{\mu} = 0. \tag{A2}$$

Equation (A2) implies that $\bar{\mu} = \bar{\mu}(\varepsilon t)$ depends only on the slow time and acts as a parameter in (A1). For $\bar{\mu} > 1 - I_0$, Eq. (A1) has the oscillating solution $\bar{\varphi} = \varphi_{\bar{\mu}}(t)$ given by (13). Note that the parameters of this solution can depend on the slow time.

As a next step, we consider the terms of order ε,

$$\partial_2 \bar{\varphi} + \partial_1 \hat{\varphi} = -\hat{\varphi} \cos \bar{\varphi} + \hat{\mu},$$
$$\partial_2 \bar{\mu} + \partial_1 \hat{\mu} = -\bar{\mu} + \eta \left(1 - \sin \bar{\varphi}\right). \tag{A3}$$

We rewrite Eq. (A3) as

$$\partial_2 \bar{\mu} + \bar{\mu} = -\partial_1 \hat{\mu} + \eta \left(1 - \sin \bar{\varphi}\right), \tag{A4}$$

where the left-hand side depends only on the slow time. Hence, the solvability condition for (A4) is the requirement that its right-hand side is independent on the fast time t, i.e.,

$$-\partial_1 \hat{\mu} + \eta \left(1 - \sin \bar{\varphi}\right) = u(T), \tag{A5}$$

with some function $u(T)$, where $T = \varepsilon t$ is the slow time. By integrating (A5) with respect to the fast time, we obtain

$$\hat{\mu}(t) = \hat{\mu}(0) + \eta \left(t - \int_0^t \sin \bar{\varphi} \, dt\right) - t u(T). \tag{A6}$$

The integral in (A6) can be computed using (A1),

$$\int_0^t \sin \bar{\varphi} \, dt = t I_0 + t \bar{\mu} - \bar{\varphi}(t) + \bar{\varphi}(0),$$

such that

$$\hat{\mu}(t) = \hat{\mu}(0) + t \left[\eta \left(1 - I_0 - \bar{\mu} + \frac{\bar{\varphi}(t) - \bar{\varphi}(0)}{t}\right) - u(T)\right].$$

Taking into account that

$$\frac{\bar{\varphi}(t) - \bar{\varphi}(0)}{t} = \Omega(\bar{\mu}) + \mathcal{O}\left(\frac{1}{t}\right),$$

we obtain the expression for $\hat{\mu}$,

$$\hat{\mu}(t) = \hat{\mu}(0) + t \left[\eta \left(1 - I_0 - \bar{\mu} + \Omega(\bar{\mu})\right) - u(T)\right] + \mathcal{O}(1),$$

where the linearly growing term must vanish for $\hat{\mu}(t)$ to be bounded. Setting such a secular term to zero (even without computing explicitly $\hat{\mu}$), we have

$$u(T) = \eta \left(1 - I_0 - \bar{\mu} + \Omega(\bar{\mu})\right)$$

and, hence, taking into account (A4) and (A5), the equation for the leading order approximation of the slow variable reads

$$\partial_2 \bar{\mu} + \bar{\mu} = \eta \left(1 - I_0 - \bar{\mu} + \Omega(\bar{\mu})\right).$$

Since $\bar{\mu}$ is the function of the slow time only, we have $\partial_2 \bar{\mu} = \bar{\mu}'$, which results in the required averaged Eq. (14).

APPENDIX B: EXPLICIT SOLUTION OF THE STATIONARY FOKKER–PLANCK EQUATION

Here, we present the analytic solution of the stationary Fokker–Planck Eqs. (24) and (25). By integrating Eq. (24) once, one obtains

$$\frac{D}{2} \partial_\varphi \rho - (I_0 + \mu - \sin \varphi) \rho = C, \tag{B1}$$

with a constant C to be determined. Solving (B1), and taking into account the normalization (25) and the boundary condition $\rho(0) = \rho(2\pi)$, we arrive at

$$\rho(\varphi; \mu, D) = \frac{1}{g_\Lambda} \Lambda(\varphi),$$

where

$$\Lambda(\varphi) = \int_0^{2\pi} \frac{\Psi(\varphi)}{\Psi(\varphi + \xi)} d\xi,$$

$$g_\Lambda = \int_0^{2\pi} \Lambda(\varphi) d\xi,$$

$$\Psi(\varphi) = \exp\left\{\frac{2}{D} \left[(I_0 + \mu)\varphi + \cos \varphi - 1\right]\right\}.$$

DATA AVAILABILITY

The data that support the findings of this study are available from the corresponding author upon reasonable request.

REFERENCES

[1] E. M. Izhikevich, *Dynamical Systems in Neuroscience: The Geometry of Excitability and Bursting* (The MIT Press, 2007), ISBN: 9780262090438.

[2] W. Gerstner, W. M. Kistler, R. Naud, and L. Paninski, *Neuronal Dynamics: From Single Neurons to Networks and Models of Cognition* (Cambridge University Press, 2014), ISBN: 9781107447615.

[3] L. F. Abbott and P. Dayan, *Theoretical Neuroscience* (The MIT Press, 2005).

[4] C. Clopath, L. Büsing, E. Vasilaki, and W. Gerstner, Nat. Neurosci. **13**, 344 (2010).

[5] O. Popovych, S. Yanchuk, and P. A. P. Tass, Sci. Rep. **3**, 2926 (2013).

[6] R. Lang and K. Kobayashi, IEEE J. Quantum Electron. **16**, 347 (1980).

[7] K. Lüdge, *Nonlinear Laser Dynamics* (Wiley-VCH Verlag GmbH & Co. KGaA, Weinheim, 2011), ISBN: 9783527639823.

[8] M. C. Soriano, J. García-Ojalvo, C. R. Mirasso, and I. Fischer, Rev. Mod. Phys. **85**, 421 (2013).

[9] M. Krupa, B. Sandstede, and P. Szmolyan, J. Differ. Equ. **133**, 49 (1997).

[10] M. Lichtner, M. Wolfrum, and S. Yanchuk, SIAM J. Math. Anal. **43**, 788 (2011).

[11] M. Desroches, J. Guckenheimer, B. Krauskopf, C. Kuehn, H. M. Osinga, and M. Wechselberger, SIAM Rev. **54**, 211 (2012).

[12] C. Kuehn, *Multiple Time Scale Dynamics* (Springer-Verlag GmbH, 2015), Vol. 191, ISBN: 978-3-319-12315-8.

[13] H. Jardon-Kojakhmetov and C. Kuehn, arxiv.org/abs/1901.01402 (2019).

[14] H. Haken, *Advanced Synergetics* (Springer, Berlin, 1985).

[15] B. Lindner, J. García-Ojalvo, A. Neiman, and L. Schimansky-Geier, Phys. Rep. **392**, 321 (2004).

[16] A. Destexhe and M. Rudolph-Lilith, *Neuronal Noise* (Springer, New York, 2012).

[17] E. Forgoston and R. O. Moore, SIAM Rev. **60**, 969 (2018).

[18] J. D. Murray, *Mathematical Biology*, Biomathematics Vol. 19 (Springer, New York, 1989), ISBN: 0-387-19460-6 (New York), 3-540-19460-6 (Berlin).

[19] A. T. Winfree, *The Geometry of Biological Time* (Springer, 2001), Vol. 12, ISBN: 978-1-4419-3196-2

[20] A. S. Pikovsky and J. Kurths, Phys. Rev. Lett. **78**, 775 (1997).

[21] V.-C. Oriol, M. Ronny, R. Sten, and L. Schimansky-Geier, Phys. Rev. E **83**, 036209 (2011).

[22] G. B. Ermentrout and D. Kleinfeld, Neuron **29**, 33 (2001).

[23] L. Lücken, D. P. Rosin, V. M. Worlitzer, and S. Yanchuk, Chaos **27**, 13114 (2017).

[24] I. Franović, O. E. Omel'chenko, and M. Wolfrum, Chaos **28**, 071105 (2018).

[25] I. Bačić, S. Yanchuk, M. Wolfrum, and I. Franović, EPJ ST **227**, 1077 (2018).

[26] I. Franović, K. Todorović, M. Perc, N. Vasović, and N. Burić, Phys. Rev. E **92**, 062911 (2015).

[27] I. Franović, M. Perc, K. Todorović, S. Kostić, and N. Burić, Phys. Rev. E **92**, 062912 (2015).

[28] S. Yanchuk, S. Ruschel, J. Sieber, and M. Wolfrum, Phys. Rev. Lett. **123**, 053901 (2019).

[29] E. M. Izhikevich, IEEE Trans. Neural Netw. **15**, 1063 (2004).

[30] S. H. Strogatz, *Nonlinear Dynamics and Chaos: With Applications to Physics, Biology, Chemistry, and Engineering* (Addison-Wesley, 1994).

[31] A. Shilnikov and M. Kolomiets, Int. J. Bifurc. Chaos **18**, 2141 (2008).

[32] G. Pavliotis and A. Stuart, *Multiscale Methods: Averaging and Homogenization* (Springer, Berlin, 2008).

[33] M. Galtier and G. Wainrib, Phys. Rev. E **2**, 13 (2012).

[34] L. Lücken, O. V. Popovych, P. A. Tass, and S. Yanchuk, Phys. Rev. E **93**, 32210 (2016).

[35] A. I. Neishtadt, J. Appl. Math. Mech **48**, 133 (1984).

[36] J. Guckenheimer and P. Holmes, *Nonlinear Oscillations, Dynamical Systems and Bifurcations of Vector Fields* (Springer-Verlag, New York, 1983).

[37] E. J. Doedel, R. C. Paffenroth, A. R. Champneys, T. F. Fairgrieve, Y. A. Kuznetsov, B. Sandstede, and X. Wang, *AUTO-07p: Continuation and Bifurcation Software for Ordinary Differential Equations* (Concordia University, Canada, 2007).

[38] B. Lindner and L. Schimansky-Geier, Phys. Rev. E **60**, 7270 (1999).

[39] V. A. Makarov, V. I. Nekorkin, and M. G. Velarde, Phys. Rev. Lett. **86**, 3431 (2001).

[40] R. Aust, P. Hövel, J. Hizanidis, and E. Schöll, Eur. Phys. J. Spec. Top. **187**, 77 (2010).

[41] N. Kouvaris, L. Schimansky-Geier, and E. Schöll, Eur. Phys. J. Spec. Top. **191**, 29 (2010).

[42] N. B. Janson, A. G. Balanov, and E. Schöll, Phys. Rev. Lett. **93**, 010601 (2004).

[43] P. H. Dannenberg, J. C. Neu, and S. W. Teitsworth, Phys. Rev. Lett. **113**, 020601 (2014).

Inverse stochastic resonance in a system of active rotators with adaptive coupling

Iva Bačić

Institute of Physics Belgrade

Inverse stochastic resonance is a phenomenon where an oscillating system shows a nonlinear response to noise, displaying a minimal oscillation frequency at an intermediate noise level. Such an effect has been indicated to play important functional roles in neuronal systems, contributing to reduction of spiking frequency in the absence of neuromodulators or to triggering of the on-off tonic spiking activity. We demonstrate a novel generic scenario for such an effect in a multi-timescale system, considering the example of emergent oscillations in two adaptively coupled active rotators with excitable local dynamics. The fast-slow analysis we carry out indicates that the plasticity plays a facilitatory role by guiding the fast-flow dynamics to parameter domains where the stable equilibria change character from nodes to focuses, which ultimately enhances the influence of noise. The described scenario persists for different plasticity rules, underlying its robustness in light of potential application to neuronal systems.

Gas-phase X-ray action spectroscopy of protonated nanosolvated substance P peptide around O K-edge

I. Bačić[1], M. Lj. Ranković[1], F. Canon[2], V. Cerovski[1], C. Nicolas[3], A. Giuliani[3,4] and A. R. Milosavljević[1]

[1] *Institute of Physics Belgrade, University of Belgrade, Pregrevica 118, 11080 Belgrade, Serbia*
[2] *INRA, UMR1324 Centre des Sciences du Goût et de l'Alimentation, F-21000 Dijon, France*
[3] *SOLEIL, l'Orme des Merisiers, St Aubin, BP48, 91192 Gif sur Yvette Cedex, France*
[4] *INRA, UAR1008, CEPIA, Rue de la Géraudière, BP 71627, 44316 Nantes, France*

We report preliminary results from unprecedented near edge X-ray absorption fine structure action spectroscopy of a gas-phase nanosolvated peptide ion. Doubly protonated substance P (Arg-Pro-Lys-Pro-Gln-Gln-Phe-Phe-Gly-Leu-Met-NH2) cations have been isolated in a linear ion trap and submitted to soft X-ray synchrotron radiation by means of coupling a commercial quadrupole ion trap mass spectrometer (Thermo Finningan LTQ XL) to the PLEIADES beamline at the SOLEIL synchrotron radiation facility (France) [1]. X-ray activation tandem mass spectra have been recorded for different photon energies, scanned over C, N and O K-edge ionization thresholds.

Figure 1 shows the photofragment ions yield corresponding to a total water loss (a normalized integral yield of all fragments corresponding to the loss of one or more water molecules) from the doubly protonated substance P cation nanosolvated with 11 water molecules $[M+2H+11H_2O]^{2+}$ upon soft X-ray irradiation. We observed that a resonant excitation of an O 1s electron to an unoccupied molecular orbital, following by a resonant Auger decay, induces an increased water detachment from the precursor.
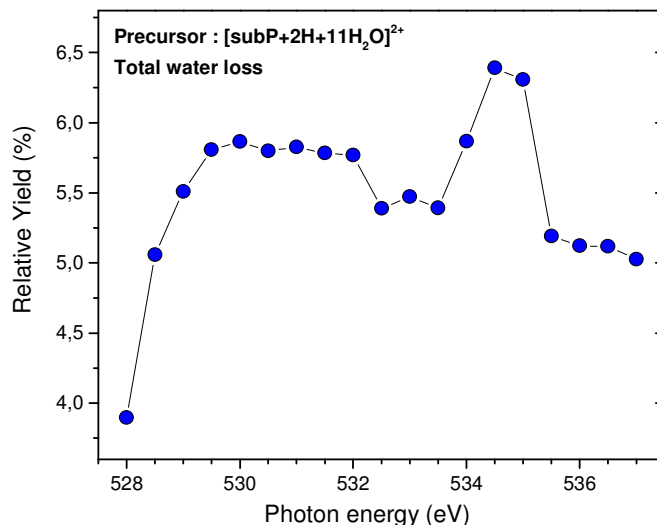

Fig.1. Photofragment ions yield that corresponds to a range m/z 674-766 (an integral yield of all fragments corresponding to the loss of one or more water molecules) from a doubly protonated nanosolvated substance P cation precursor $[M+2H+11H_2O]^{2+}$ (m/z 773.5).

REFERENCES

[1]   A. R. Milosavljević et al., J. Phys. Chem. Letters 3, 1191 (2012).

Disordered Configurations of the Glauber Model on Two-Dimensional Networks

I. Bačić[a], I. Franović[a] and M. Perc[b, c, d]

[a]Scientific Computing Laboratory, Center for the Study of Complex Systems, Institute of Physics Belgrade - Belgrade, Serbia
[b]Faculty of Natural Sciences and Mathematics, University of Maribor - Maribor, Slovenia
[c]Center for Applied Mathematics and Theoretical Physics, University of Maribor - Maribor, Slovenia
[d]Complexity Science Hub - Vienna, Austria

Abstract. We analyze the ordering efficiency and the structure of disordered configurations for the zero-temperature Glauber model on Watts-Strogatz networks obtained by rewiring 2D regular square lattices. In the small-world regime, the dynamics fails to reach the ordered state in the thermodynamic limit. Due to the interplay of the perturbed regular topology and energy neutral stochastic state transitions, the stationary state consists of two intertwined domains, manifested as multi-cluster states on the original lattice. Moreover, for intermediate rewiring probabilities, one finds an additional source of disorder due to the low connectivity degree, which gives rise to small isolated droplets of spins. We also examine the ordering process in paradigmatic two-layer networks with heterogeneous rewiring probabilities. Comparing the cases of a multiplex network and the corresponding network with random inter-layer connectivity, we demonstrate that the character of the final state qualitatively depends on the type of inter-layer connections.
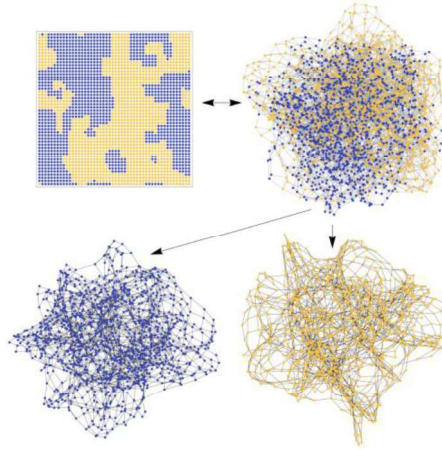
FIGURE 1. A disordered configuration with two domains comprises a multi-cluster state on the lattice.

REFERENCES

1. Bačić I., Franović I., and Perc M., *EPL* **120**, 68001 (2017).

Committee

Meeting chairs

Aleksandar Milosavljević *(Institute of Physics Belgrade, University of Belgrade, Serbia)*

Paola Bolognesi *(CNR-Istituto di Struttura della Materia, Roma, Italy)*

Scientific Committee

Paola Bolognesi *(CNR-Istituto di Struttura della Materia, Roma, Italy)*

Alicja Domaracka *(CIMAP, Caen, France)*

Henning Zettergren *(Stockholm Univeristy, Stockholm, Sweden)*

Aleksandar Milosavljević *(IPB, Belgrade, Serbia)*

Manuel Alcami *(Universidad Autónoma de Madrid, Departamento de Quimica, Spain)*

Local Organising Committee *(IPB, Belgrade, Serbia)*

Aleksandar Milosavljević

Nenad Simonović

Sanja Tošić (meeting secretary)

Andrej Bunjac

Miloš Ranković

Iva Bačić

Beatriz Martin, COST XLIC Local Science Manage

Partners

COST is supported by the EU Framework Programme Horizon 2020

Highlights from the previous volumes

Disordered configurations of the Glauber model on two-dimensional networks

The Glauber model provides a paradigm for modeling ordering processes in complex systems. The question that we answer is: How is the efficiency of the ordering process in the Glauber model affected if we rewire the links of the two-dimensional host lattice? Our research reveals that the fraction of disordered configurations exhibits a nonlinear dependence on the rewiring probability. In the small-world regime, the Glauber dynamics remains trapped in a metastable configuration that is disordered. In fact, we have observed a stationary state that consists of two intertwined domains of similar size, as shown in the figure below. For higher rewiring probabilities, we observe isolated droplets of spins, which emerge due to poorly connected nodes in the network. We have also studied what happens to the ordering process on two-layer networks, in particular comparing outcomes on a multiplex network and on the corresponding network with random interlayer connections. We have shown that, in this case, the properties of the stationary state are strongly affected by the type of inter-layer connections.
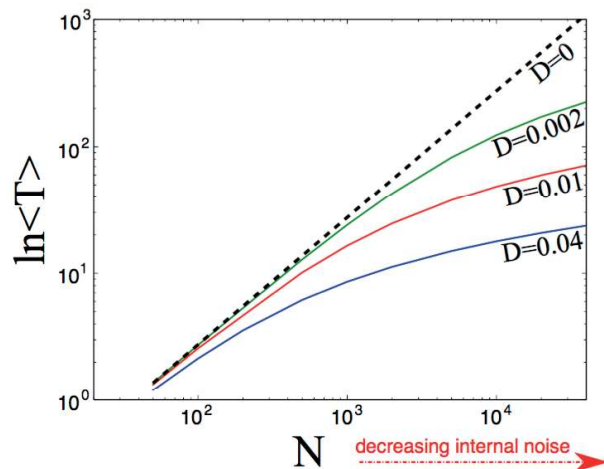
Rare events in "noisy" networks

Bringing diseases to extinction and mitigating the effects of human-caused environmental changes which accelerate the rate of species extinction are issues of worldwide importance. Both phenomena are typically rare events, relying on the interplay between network topology, nonlinear dynamics, and random fluctuations from the environment and interactions. However, the prediction of such rare events, in general stochastic networks, was an unsolved problem, despite extensive work in network dynamics. Here we solve the problem of predicting rare events as large fluctuations from metastable states with a general theory that combines mean-field approximations, large-deviation techniques and network topology. A benefit of our approach is its flexibility in describing the effects of multiple sources of different continuous and discrete noise. Using our theory, we demonstrate that networks with both internal interaction noise and external parameter noise exhibit a crossover where the familiar exponential scaling of rare-event times with the number of nodes in the network is lost, and parametric noise dominates.

A disordered configuration with two domains comprizes a multiclustered state on the lattice.

The average extinction time, $\langle T \rangle$, for a regular network *vs.* the number of nodes, N, and several amplitudes of external noise, D.

Original article by BAČIĆ IVA *et al.*
EPL, **120** (2017) 68001

Original article by HINDES J. and SCHWARTZ I. B.
EPL, **120** (2017) 56004

edp sciences   Journals   Books   Conferences   👤 EDPS Account

europhysicsnews

The magazine of the European Physics Community
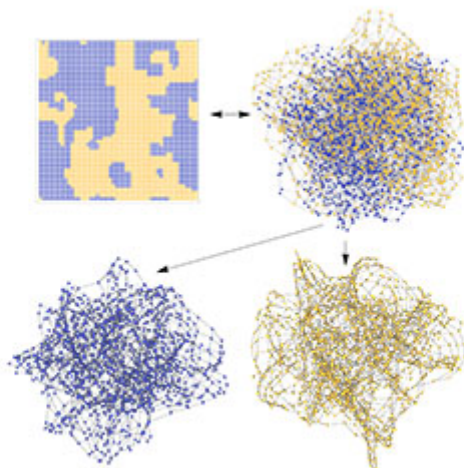
FEATURES   HIGHLIGHTS   NEWS   JOBS/CLASSIFIED   EVENTS

BOOKS   ABOUT US   COMPANY DIRECTORY   🔍 SEARCH   ☰ MENU

DISORDERED CONFIGURATIONS OF THE GLAUBER MODEL ON TWO-DIMENSIONAL NETWORKS (VOL. 49, NO. 3)

The

A disordered configuration with two domains comprises a multiclustered state on the lattice.

Glauber model provides a paradigm for modeling ordering processes in complex systems. The question that we answer is: How is the efficiency of the ordering process in the Glauber model affected if we rewire the links of the two-dimensional host lattice? Our research reveals that the fraction of disordered configurations exhibits a nonlinear dependence on the rewiring probability. In the small-world regime, the Glauber dynamics remains trapped in a metastable configuration that is disordered. In fact, we have observed a stationary state that consists of two intertwined domains of similar size, as shown in the figure. For higher rewiring probabilities, we observe isolated droplets of spins, which emerge due to poorly connected nodes in the network. We have also studied what happens to the ordering process on two-layer networks, in particular comparing outcomes on a multiplex network and on the corresponding network with random inter-layer connections. We have shown that, in this case, the properties of the stationary state are strongly affected by the type of inter-layer connections.

OK

I. Baćić, I. Franović and M. Perc , Disordered configurations of the Glauber model in two-dimensional networks, *EPL*, **120**, 68001 (2017)

Isidora Majkić

Karakteristike mreže poznanstava u populaciji sa izraženim podgrupama

U ovom radu predstavljamo model rasta društvene mreže motivisan međusobnim upoznavanjem polaznika različitih seminara u Petnici, koju čine dve interagujuće podgrupe pojedinaca. U okviru modela, najpre generišemo mreže početnih podgrupa koristeći dva algoritma: Watts-Strogatz i Barabási-Albert. U prvom slučaju, rezultujuća mreža ima small-world strukturu, koju karakterišu kratak srednji put i visok koeficijent klasterovanja; u drugom slučaju se dobija mreža sa scale-free strukturom, za koju je karakteristično prisustvo dobro povezanih pojedinaca i čiji je koeficijent klasterovanja jednak nuli. Rast mreže se potom realizuje putem postepenog povezivanja pojedinaca iz različitih grupa, pri čemu smo dodatno razmatrale i efekat ostvarivanja novih poznanstava među pojedincima unutar početnih podgrupa logikom preferencijalnog povezivanja, što znači da čvorovi koji imaju više linkova lakše ostvaruju nove veze. Cilj rada je određivanje osobina mreža koje nastaju simulacijom ovih modela. Karakteristike koje se računaju uključuju koeficijent klasterovanja (broj koji opisuje koliko često su susedi prosečnog čvora i međusobno povezani), srednji najkraći put, srednji betweenness centrality (za svaki čvor broj najkraćih puteva koji prolazi kroz taj čvor). Na osnovu rezultata zaključujemo da struktura početnih podgrupa ne utiče na topološke karakteristike rezultujuće mreže u dugovremenskom limesu, već je važan samo ukupan broj ostvarenih veza.

Uvod

Mreže poznanstva su sastavni deo naših života. Mnogobrojni primeri uključuju škole, on-line društvene mreže, mreže citiranosti naučnika, saradnje glumaca, i dr. (Albert i Barabási 2002). Kod analize socijalnih mreža se kroz pristup zasnovan na teoriji kompleksnih mreža proučavaju interakcije među individuama od kojih se mreža sastoji. Pored analize podataka, važno je razviti matematičke modele kojim se te mreže mogu opisati. Razvoj pojednostavljenog modela za cilj ima uspostavljanje kontrolne mreže sa kojim bi realni podaci o društvenim mrežama mogli da se porede u budućnosti.

Iako različite socijalne mreže imaju različite strukture, mogu se primetiti karakteristike koje su zajedničke za neke klase mreža. Tako se, na primer, mogu uočiti mreže kod kojih se izdvajaju grupe prijatelja koji su unutar sebe bolje povezani nego sa ostatkom mreže. Ovakvu strukturu mreže poznanstva imaju, između ostalog, škole u kojima se kao podgrupe izdvajaju odeljenja, ili Istraživačka stanica Petnica u kojoj su polaznici podeljeni po seminarima. Kod ovakvih populacija je velika verovatnoća da ćemo poznavati osobu ukoliko sa njom imamo puno zajedničkih prijatelja, ali pored toga svako ima dodatne prijatelje koji ne poznaju nikoga iz naše podgrupe (npr. prijatelji iz drugog mesta). Na nivou cele mreže, pojedinci interaguju kako sa pojedincima iz svoje grupe, tako i sa pojedincima iz drugih grupa, pri čemu pravila ostvarivanja linkova unutar i izvan grupe nisu nužno ista.

Isidora Majkić (2002), Pančevo, učenica 2. razreda Matematičke gimnazije u Beogradu

MENTORI:

Aleksandra Alorić, Institut za fiziku u Beogradu

Iva Bačić, Institut za fiziku u Beogradu

Fizika

Konferencija polaznika srednjoškolskih programa Istraživačke stanice Petnica "Korak u nauku"

## Ispitivanje Pottsovog modela na prepovezanim rešetkama

Nina Jakovljević (2001)
učenica 4. razreda Gimnazije Kruševac, Kruševac

Mentorstvo:
dr Iva Bačić, Institut za fiziku Beograd, Beograd

Pottsov model opisuje sistem sačinjen od N interagujućih spinova gde se svaki spin može naći u jednom od q stanja. U ovom radu je ispitano kako narušavanje regularnosti topologije utiče na proces uređivanja Pottsovog modela za q=3 stanja pri temperaturi od T=0K. Simulirana je dinamika Pottsovog modela na dvodimenzionalnoj kvadratnoj rešetki čiji su linkovi prepovezani s verovatnoćom p u skladu sa Watts-Strogatzovim algoritmom,pri čemu je p je fiksan na ansamblu i variran u opsegu p ∈ [0, 0.95]. Pokazuje se da je za verovatnoće prepovezivanja p ∈ [0, 0.2] proces uređivanja manje efikasan u odnosu na onaj na regularnoj rešetki (p=0). Ipak, s povećanjem p (p>0.2) i kako topologija teži nasumičnoj (p->1), uređivanje sistema se izrazito pospešuje. U većini slučajeva, konačna, neuređena stanja sadrže takozvane blinker spinove na granicama rešetke koji beskonačno dugo mogu menjati svoje stanje.
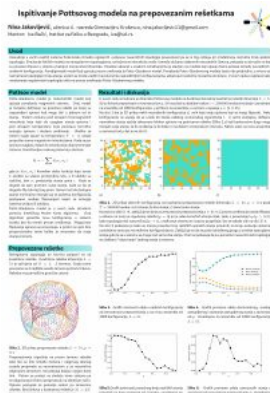
Kvantna tomografija nasumičnih uvezanih stanja

Isidora Majkić (2002)
učenica 3. razreda Matematičke gimnazije, Beograd
Nina Zdravković (2001)
učenica 4. razreda Gimnazije "Bora Stanković", Niš

Mentorstvo:
dr Aleksandra Dimić, Fizički fakultet, Univerzitet u Beogradu

U ovom radu predstavljamo kvantnu tomografiju koja služi za rekonstrukciju kvantnog stanja nakon što je ono dobijeno nekim procesom pripreme. Kroz tomografiju želimo da proverimo da li je kroz pripremu dobijeno odgovarajuće stanje koje će nam služiti za dalje kvantno računanje. Motivacija je proizašla iz želje za istraživanje quantum supremacy i izvrsnog napretka koje bi kvantno računarstvo donelo. Nauka se trenutno susreće sa problemom koji dekoherencija donosi. Bavile smo se tomografijom nasumično generisanih uvezanih stanja pri prisustvu šuma, ali i metodom uklanjanja istog. Rezultati koje smo mi dobile pokazuju da uspešnost tomografije, izražen preko vernosti (eng. *fidelity*) i konkurentnosti, polinomnom regresijom opada sa porastom šuma. Zaključile smo da broj qubita utiče na preciznost metode, ali da broj dvokubitnih logičkih kapija ne utiče. Model za eliminisanje šuma uspeva da gotovo potpuno umanji šum, ali se preciznost smanjuje porastom šuma, a i brojem qubita.

Dear Ms. Bačić,

Thank you for your review of the manuscript referenced below, which we have safely received:

Title: ███████████████████████████████
Author: ██████████████████████
[Manuscript #CHA20-AR-████1],

A copy of this review is attached for your reference. If you uploaded your review - that exact file is attached.

Sincerely,

Kristen Overstreet
Peer Review Manager
Chaos Editorial Office
AIP Publishing
1305 Walt Whitman Road
Suite 300
Melville, NY 11747-4300
phone: +1-516-576-2372
e-mail: cha-edoffice@aip.org

Dear Ms. Bačić,

Thank you for your review of the manuscript referenced below, which we have safely received:

Title: ████████████████████████████████████

Author: ████████████████████████

[Manuscript #CHA20-AR-█████2],

A copy of this review is attached for your reference. If you uploaded your review – that exact file is attached.

If you would like to have a record of this review sent to your ORCID account, click on the link below:

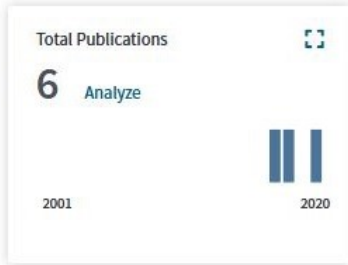https://chaos.peerx-press.org/cgi-bin/main.plex?el=████████████████████

Sincerely,

Kristen Overstreet
Peer Review Manager
Chaos Editorial Office
AIP Publishing
1305 Walt Whitman Road
Suite 300
Melville, NY 11747-4300
phone: +1-516-576-2372

Web of Science

Citation report for 6 results from Web of Science Core Collection between [1900 ▾] and [2021 ▾] [Go]
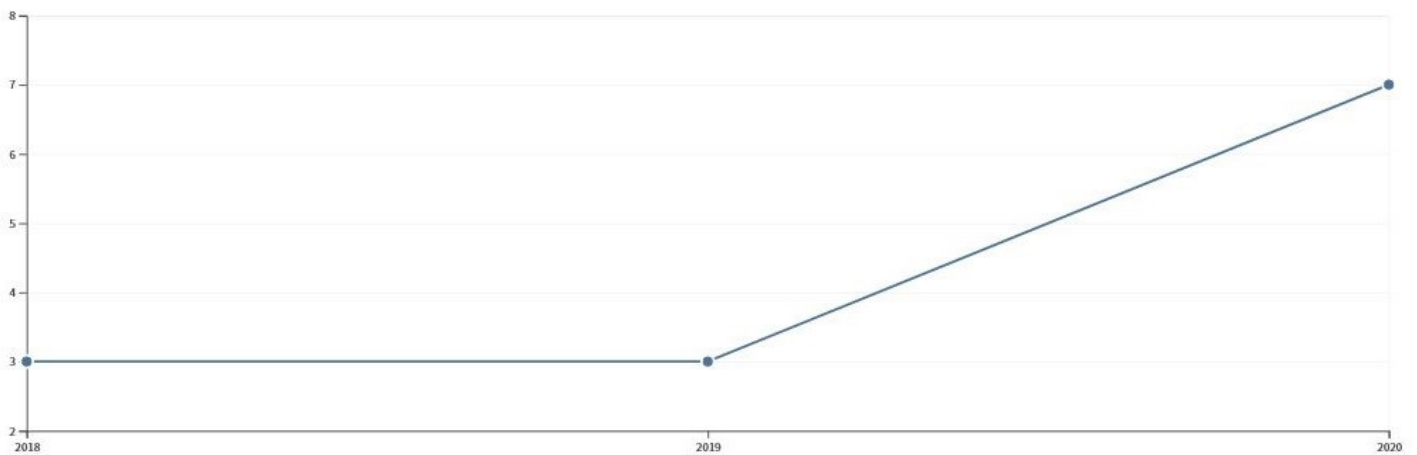
You searched for: **AUTHOR:** (bacic, Iva) ...**More**

This report reflects citations to source items indexed within Web of Science Core Collection. Perform a Cited Reference Search to include citations to items not indexed within Web of Science Core Collection.

Export Data: [Save to Excel File   ▾]   ⊹

Total Publications	h-index	Sum of Times Cited	Citing articles
6 Analyze	**3**	**13**	**13** Analyze
	Average citations per item	Without self citations	Without self citations
2001 — 2020	**2.17**	**12**	**12** Analyze

Sum of Times Cited per Year

Use the checkboxes to remove individual items from this Citation Report

0	3	3	7	0	13	4.33

or restrict to items published between [1900 ▼] and [2021 ▼] [Go]

1. Inverse stochastic resonance in a system of excitable active rotators with adaptive coupling

By: Bacic, Iva; Klinshov, Vladimir; Nekorkin, Vladimir; et al.
EPL   Volume: 124   Issue: 4   Article Number: 40004   Published: NOV 2018

0	0	1	4	0	5	1.67

2. Noise-induced switching in two adaptively coupled excitable systems

By: Bacic, Iva; Yanchuk, Serhiy; Wolfrum, Matthias; et al.
EUROPEAN PHYSICAL JOURNAL-SPECIAL TOPICS   Volume: 227   Issue: 10-11   Pages: 1077-1090   Published: NOV 2018

0	2	2	0	0	4	1.33

3. Mean-field dynamics of a population of stochastic map neurons

By: Franovic, Igor; Maslennikov, Oleg V.; Bacic, Iva; et al.
PHYSICAL REVIEW E   Volume: 96   Issue: 1   Article Number: 012226   Published: JUL 27 2017

0	1	0	2	0	3	0.75

4. Disordered configurations of the Glauber model in two-dimensional networks

By: Bacic, Iva; Franovic, Igor; Perc, Matjaz
EPL   Volume: 120   Issue: 6   Article Number: 68001   Published: DEC 2017

0	0	0	1	0	1	0.25

5. Dynamics of a stochastic excitable system with slowly adapting feedback

By: Franovic, Igor; Yanchuk, Serhiy; Eydam, Sebastian; et al.
CHAOS   Volume: 30   Issue: 8   Article Number: 083109   Published: AUG 2020

0	0	0	0	0	0	0.00

6. Two paradigmatic scenarios for inverse stochastic resonance

By: Bacic, Iva; Franovic, Igor
CHAOS   Volume: 30   Issue: 3   Article Number: 033123   Published: MAR 2020

0	0	0	0	0	0	0.00

☐ Select Page   🖶 ✉   [Save to Excel File ▼]

Sort by: **Times Cited** ↓≡   Date   More ▼   ◀   1   of 1 ▶

---

6 records matched your query of the 78,249,728 in the data limits you selected.
Key: 🧬 *= Structure available.*

Clarivate
Accelerating innovation

Sign up for the Web of Science newsletter   Follow us   🐦 f

УНИВЕРЗИТЕТ У БЕОГРАДУ
ФИЗИЧКИ ФАКУЛТЕТ

Бр. 162/11
27. 11. 2020
БЕОГРАД, СТУДЕНТСКИ ТРГ 12-16
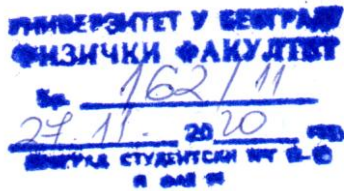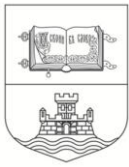
На основу члана 29 Закона о општем управном поступку («Службени гласник РС» број 18/2016 и 95/2018), и члана 149 Статута Универзитета у Београду - Физичког факултета, по захтеву ИВЕ БАЧИЋ, мастер физичара, издаје се следеће

У В Е Р Е Њ Е

ИВА БАЧИЋ, мастер физичар, дана 27. новембра 2020. године, одбранио је докторску дисертацију под називом

„SELF-ORGANIZATION IN COUPLED EXCITABLE SYSTEMS: INTERPLAY BETWEEN MULTIPLE TIMESCALE DYNAMICS AND NOISE" (Самоорганизација у спрегнутим екситабилним системима: садејство вишеструких временских скала и шума)

пред Комисијом Универзитета у Београду - Физичког факултета и тиме испунио све услове за промоцију у ДОКТОРА НАУКА – ФИЗИЧКЕ НАУКЕ.

Уверење се издаје на лични захтев, а служи ради регулисања права из радног односа и важи до промоције, односно добијања докторске дипломе.

Уверење је ослобођено плаћања таксе.

ДЕКАН ФИЗИЧКОГ ФАКУЛТЕТА
Проф. др Иван Белча